Theresa Merl, BSc

Ammonia Imaging in Biological Systems – Sensor Development and Application

MASTER'S THESIS

to achieve the university degree of

Diplom-Ingenieur (Dipl.-Ing.)

Master's degree programme: Technical Chemistry

submitted to

Graz University of Technology

Supervisors

Assoc.Prof. kand. Sergey Borisov

Institute of Analytical Chemistry and Food Chemistry

Graz University of Technology

Asst.Prof. Klaus Koren

Center for Water Technology, Department of Biology

Aarhus University

Graz, August 2020

Straight ahead you can't go very far.

Antoine de Saint-Exupéry

Abstract

Ammonia (NH_3) is a participant in several important processes andapplications. In fact, one of the areas it plays the greatest role in is agriculture and its livestock management as it is used to fertilize soils by applying manure onto fields. This results in ammonia emission and it is considered the biggest source of NH_3 in the atmosphere. But heavy ammonia emissions can have a negative effect on the environment and as a result harm the health of humans and animals too. Even though such emissions can occur on a large scale the driving forces take place in the chemical microenvironment and the biological processes within the soil.
So far, no technique was utilized to elucidate the local activities and spatial heterogeneity of the soil air interphase concerning the parameter ammonia.
In this regard, a novel optical ammonia sensor able to measure within the ppm concentration range was developed, characterized and applied in this thesis.
The specifically designed ammonia optode is based on the deprotonation of a pH sensitive fluorophore immersed in a polymer matrix, coupled with a reference dye to enable ratiometric imaging, and protected against protons and ions by covering the sensor layer with a proton impermeable membrane. This way ammonia can diffuse through this protective layer to then deprotonate the pH indicator dye and induce a change in fluorescence emission, generating a signal. The NH_3 optode shows fast response times, full reversibility, a detection limit of 2.11 ppm and a broad dynamic range of up to 1800 ppm and is well suited for NH_3 volatilization studies.
The application of this newly developed optical sensor combined with two other optical sensors for pH and O_2 were used to monitor the NH_3 emission from a soil surface upon manure addition. This combined and ratiometric imaging approach enables simultaneous measurements in real time and a spatial resolution of <100 µm. As these parameters are interconnected with each other and within the microenvironment influencing ammonia emission, two-dimensional imaging and visualization of such allows to enhance the understanding on a microscale. Therefore, NH_3 dynamics can be investigated on a more detailed scale and this new sensor is able to emerge as an indispensable tool for further environmental studies regarding ammonia.

Kurzfassung

Ammoniak (NH_3) ist an mehreren wichtigen Prozessen und Anwendungen auf dieser Erde beteiligt. Einer der Bereiche, in denen es die größte Rolle spielt, ist die Landwirtschaft und ihre Viehhaltung, da es zur Düngung der Böden durch Aufbringen von Gülle verwendet wird. Dies führt zu Ammoniakemissionen und ist die größte Quelle von Ammoniak in der Atmosphäre, was sich sowohl negativ auf die Umwelt als auch auf die Gesundheit von Mensch und Tier auswirkt. Obwohl solche Emissionen in großem Umfang auftreten können, finden die treibenden Kräfte in der chemischen Mikroumgebung und den biologischen Prozessen im Boden statt.
Bislang wurde keine Technik eingesetzt, um die lokalen Aktivitäten und die räumliche Heterogenität der Grenzflächen von Boden und der darüber liegenden Luft bezüglich des Parameters Ammoniak zu veranschaulichen.
In diesem Zusammenhang wurde ein neuartiger optischer Ammoniaksensor entwickelt, der in der Lage ist, im ppm-Konzentrationsbereich zu messen, charakterisiert und in dieser Arbeit angewendet. Die speziell entwickelte Ammoniak-Optode basiert auf der Deprotonierung eines pH-sensitiven Fluorophors, das gemeinsam mit einem Referenzfarbstoff in eine Polymermatrix eingebettet ist, um die ratiometrische
Ansatz zu ermöglichen. Die Sensorchemie ist gegen Protonen und Ionen geschützt, indem die Sensorschicht mit einer protonenundurchlässigen Membran bedeckt ist. Auf diese Weise kann Ammoniak durch diese Schutzschicht diffundieren, um dann den pH-Indikator zu deprotonieren und eine Änderung der Fluoreszenzemission zu induzieren, wodurch ein Signal erzeugt wird. Die NH_3-Optode zeigt schnelle Ansprechzeiten, volle Reversibilität, eine Nachweisgrenze von 2,11 ppm und einen breiten dynamischen Bereich von bis zu 1800 ppm und eignet sich daher gut für NH_3-Emissionsstudien.
Die Anwendung dieses neu entwickelten optischen Sensors in Kombination mit den beiden anderen optischen Sensoren, pH und O_2, wurde zur Überwachung der NH_3-Emission von einer Bodenoberfläche nach der Zugabe von Gülle verwendet. Dieser kombinierte und ratiometrische Imaging-Ansatz ermöglicht simultane Messungen in Echtzeit und eine räumliche Auflösung von <100 µm. Da diese Parameter miteinander verbunden sind und innerhalb der Mikroumgebung die Ammoniakemission beeinflussen, ermöglicht die zweidimensionale Abbildung und Visualisierung solcher Parameter ein besseres Verständnis im Mikromaßstab. Daher kann die NH_3-Dynamik auf einer detaillierteren Skala untersucht werden, und dieser neue Sensor kann sich als unverzichtbares Hilfsmittel für weitere Umweltstudien in Bezug auf Ammoniak erweisen.

AFFIDATIV

I declare that I have authored this thesis independently, that I have not used other than the declared sources/resources, and that I have explicitly indicated all material which has been quoted either literally or by content from the sources used. The text document uploaded to TUGRAZonline is identical to the present master‘s thesis.

EIDESSTATTLICHE ERKLÄRUNG

Ich erkläre an Eides statt, dass ich die vorliegende Arbeit selbstständig verfasst, andere als die angegebenen Quellen/Hilfsmittel nicht benutzt, und die den benutzten Quellen wörtlich und inhaltlich entnommenen Stellen als solche kenntlich gemacht habe. Das in TUGRAZonline hochgeladene Textdokument ist mit der vorliegenden Masterarbeit identisch.

Date/ Datum	Signature/ Unterschrift

Danksagung

An erster Stelle möchte ich mich bei Sergey bedanken, der es mir ermöglicht hat die Masterarbeit in Dänemark zu absolvieren, mit dem nötigen Projektlabor und den vielen Unterschriften, die dafür notwendig waren und das alles, ohne mich wirklich zu kennen. Danke für dein Vertrauen und besonders für deine ständige Bereitschaft bei Fragen und Problemen im Labor und die Hilfsbereitschaft und Ideen.

Als nächstes und genauso wichtig ist es mich bei Klaus zu bedanken. Auch du hast mir eigentlich blindes Vertrauen geschenkt und die Freiheit geboten mich an dieses Thema in meiner Art und Zeit heranzutasten. Zusätzlich hat es auch nie an Unterstützung und aufbauenden Worten gefehlt von deiner Seite, was nicht selbstverständlich ist. Tusintak!

Natürlich gehören liebe und hilfsbereite Arbeitsgruppen zu jeder Arbeit dazu, vielen Dank an die Arbeitsgruppe in Graz, die alle meine Fragen während dem Projektlabor beantwortet und mir im Labor unter die Arme gegriffen hat.
Und danke auch an die super Arbeitsgruppe in Aarhus, sowohl Group Klaus (Klaus, Fabi, Silvia), als auch die Institutsleute von Bioscience, besonders die hilfreichen Labtechnicians (Lars, Mette, Ronni)! Fabi und Silvia, ohne eure Hilfe wäre ich bei vielen Sachen nur halb so schnell und gut vorangekommen und man weiß man kann euch alles fragen und das ist so viel wert.

Und natürlich unersetzlich, liebe Alkürbisten/ChemistFwiends: ohne euch hätte ich diese letzten Jahre sowohl unitechnisch als auch lebenstechnisch nicht so durchgezogen/überstanden. Die zahlreichen Lern-/Protokollschreib-Nächte, Kaffeepausen, Weihnachts- und Geburtstagsfeiern und eigentlich noch öfter, Ein- und Auszugsparties gehören zu den besten Erinnerungen, die ich aus der Studienzeit habe und die Freundschaften, die daraus entstanden sind, sind einfach unbezahlbar. Also nochmal danke an: Jakob (beste Meme-quelle), Anna (zache Prüfungs- und Kaffeepausenpartnerin), Vici (Motivations- und Schnapsqueen), Feri (Sport- und Glühweinqueen), Fabe-star (Lauftrainer und Fragebuch einfach immer), Valen (meine Medizinerin des chemischen Vertrauens/für meine Nerven), Flo (sexy Witzereißer).

Jakob, QUEEN, ich bin so froh, dass es dich gibt und sich diese Freundschaft entwickelt hat. Danke für deine emotionale und, für dich immer selbstverständliche, Unterstützung und unendlich viele Stunden gefüllt mit Memes und Lachen.

Kathi, beste on-off Mitbewohnerin, die ich mir wünschen hätte können, danke dafür, dass du meinen Horizont immer miterweitert hast mit all deinen Auslandsaufenthalten, aber auch mit deiner Offenheit und Akzeptanz anderen und mir gegenüber.

Ohne die proof-reading Hilfe und Vereinfachung von meinen super langen und verschachtelten Sätzen von Marko, Jakob und Kathi, wäre jeder Leser so aufgeschmissen wie die drei es beim Durchlesen oft genug waren, super großes Danke an euch, da meine Sätze keine einfachen sind.

Marlene und Anna, ihr seid die besten Schwestern in allen aber besonders in den wichtigsten Hinsichten, ihr wart so verständnisvoll in den letzten Jahren, habt meine Stressphasen ausgehalten und mich sogar runtergeholt und wart wirklich die beste Unterstützung im Studium und eigentlich immer, ihr seid so cool!

Mama, Papa, Christa, Oma und Opa danke für eure offenen Ohren, euer Verständnis, eure Motivation aber auch für eure finanzielle Unterstützung. Ihr habt mir ein sorgenfreies Leben in Graz und generell egal wo ich war ermöglicht, danke.

Theresa Merl, BSc Graz, August 2020

Contents

I. Introduction

1. Biological Relevance and Environmental Impact of Ammonia

This section is based on the according literature [1-2] and other sources will be cited independently.

The element nitrogen is an indispensable element on earth as it makes up 80% of the atmosphere and is crucial for life on our planet. There are several forms of N with one of them being NH_3: a colourless, obtrusively smelling gas. Ammonia and its protonated counterpart ammonium (NH_4^+) alternate dependant on the pH (pK_a 9.24) within an aqueous environment. In order to gather information about the amount of nitrogen resulting from either of the two forms the sum of NH_3 and $NH_4^+$is used and describes the total ammonia nitrogen (TAN). Ammonia together with nitrate (NO_3^-) and nitrogen gas (N_2) make up the majority of nitrogen accessible to the environment. There are different types of microorganisms like bacteria and archaea involved in the processes for the incorporation or transformation of nitrogen and the various forms of the element in nature. Moreover, the compound that can be utilized by all prokaryotes as nitrogen source is NH_3, some can use $NO_3^-$and only a few can draw from N_2 via nitrogen fixation. Nitrogen fixation results in ammonia and this is only one of several pathways within the nitrogen cycle in which NH_3 plays a key role. The nitrogen cycle with the respective pathways is illustrated in Figure 1.

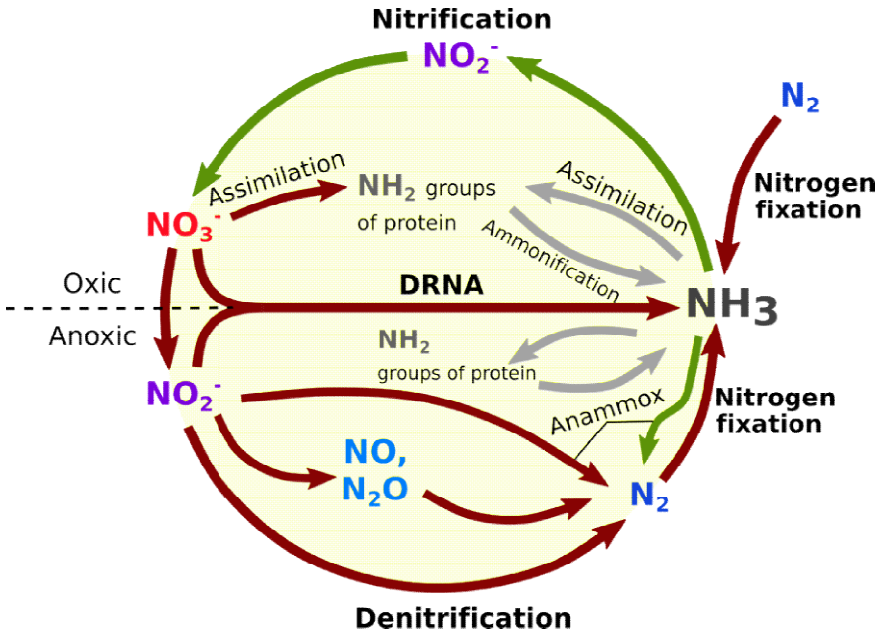

Figure 1: Nitrogen cycle, in which oxidation reactions are illustrated by the green arrows and reductions by the red arrows. The reactions without redox change are shown in grey. DRNA stands for dissimilative reduction to ammonia.

Nitrogen cycle

Other reactions in addition to nitrogen fixation are nitrification, anammox, denitrification, dissimilative reduction of nitrate to ammonia (DRNA), ammonification and the assimilation of N compounds by plants (Figure 1). Nitrification is the aerobic oxidation of NH_3 to nitrite (NO_2^-) conducted by nitrifying bacteria consuming O_2 and then via a different specific group of bacteria NO_2^- is oxidized to NO_3^-. In contrast, anammox is the oxidation of NH_3 with nitrite under anoxic circumstances resulting in N_2. Then there is the reduction of nitrate, also occurring under anoxic conditions, leading to NO_2^-. From there two processes are possible to happen, either denitrification forming the gaseous N end products N_2O, NO, N_2 or the dissimilative process in which nitrite is further reduced to ammonia. Furthermore, the breakdown of N containing organic matter, hence, proteins or nucleotides is called ammonification, in which microorganisms produce NH_3.

Environmental impact of ammonia

Although ammonia already naturally participates in a number of microbiological processes within soils and other biological systems anthropogenic distribution of the compound additionally intervenes within the nitrogen cycle.[3] This is due to the importance ammonia and ammonium (NH_4^+) have to soils and plants. In addition to the supply via ammonification and

nitrification these compounds are added in form of manure or synthetic fertilizers to agricultural fields to enhance crop yields. Upon manure addition one of the processes occurring is ammonification, through which organic nitrogen compounds such as urea are metabolically disintegrated to form NH_3 and NH_4^+. These ammonia and ammonium releases are then reused and transformed into amino acids by microorganisms and plants. Hence, ammonia concentrations are depleted or increased via the various processes within the nitrogen cycle but also by agricultural actions. Also, the influence of other parameters needs to be considered, such as pH, which plays a dominant role in the ruling over what form of NH_3 or NH_4^+ is apparent and can lead to volatilization of ammonia at high pH values.[4] Oxygen shows a great influence too as the pathways within the microenvironments do depend on the availability of oxygen and the following anoxic or oxic conditions.[5]

Even though it is widely used and indispensable ammonia can have a detrimental impact on the environment. For example, it displays toxicity towards different organisms including fish, other marine species as well as towards human health.[6,7] For fish merely the concentration of ammonia starting at 25 ppb is enough in order to be harmful. When it comes to human health the gas-to-particle transformation between NH_3 and acid gases in the atmosphere leading to small particles polluting the air provokes health impacting exposures.[8]

Some of the main contributors to ammonia emission into the atmosphere are agricultural activity and its handling of livestock manure. In addition, this entails the release of other gases (e.g. N_2O and NO), the deterioration of ozone (O_3), acidification of soils and the facilitation of algal growth. A leading role within these negative effects plays nitrification. Nitrification describes a stepwise oxidation of NH_3 resulting in nitrate, which further impacts plant agriculture. Even though nitrate is also gladly assimilated by plants, redundant quantities of the highly water-soluble compound can leach into water bodies causing eutrophication and subsequently harming marine organisms. This mainly happens when the soil becomes waterlogged or an excess of fertilizer was applied. In a next step the abundance of nitrate paired with a lack of oxygen enables denitrification removing fixed nitrogen as well as producing nitrous oxide (N_2O) and nitric oxide (NO) amongst other gaseous N products. N_2O is a greenhouse gas and is about 300 times more impactful on global warming than CO_2. Furthermore, N_2O can be converted to NO within the atmosphere and NO can decompose O_3 via reacting with it forming nitrite, which renters into the environment as nitric acid in acid rain.

Even though agriculture is considered the main contributor to the worldwide ammonia in the atmosphere, with 30 Tg N $year^{-1}$ from a total release of 40 Tg N $year^{-1}$, there are some others too.[3] Ammonia is emitted from and cycled within oceans, seas and their sediments as well as from biomass burning. In addition, more NH_3 enters the environment via human activities such as fossil fuel combustion, resulting from motor vehicles, and the chemical industry. The latter supplying both: fertilizer production and refrigerator systems.

Application areas of ammonia detection

These sources of ammonia also constitute the areas in which monitoring of the levels of this compound are required in both gas phase and aqueous environments. In addition to environmental, automotive and chemical industry measurement applications in medicine are of high interest. Due to the differences in ammonia distribution within these sectors, the levels of ammonia that need to be detected vary accordingly, ranging from sub-ppb levels up to high concentrations within the range of ppm. These areas and some of the concentration levels in pursuit are discussed below.

Environment

Ammonia levels in the air rise noticeably close to farming regions and stables. The amount of manure used as fertilizer as well as the applied technique impact these levels too. In general, if ammonia concentrations exceed certain limits it can affect human and animal health but as already discussedalso the environment in several ways. Hence, in this case gas phase measurements are conducted by using various sensors. These need to be able to measure in the ppm range as ammonia levels can reach up to 25 ppm in stables and 200 ppm when ammonia is released from soils.[9,10] Monitoring of low ammonia concentrations in the ppb range within aqueous surroundings are used in the area of fish farming due to the lethal effect NH_3 can have on this species.

Automotive Industry

Atmospheric pollution from ammonia needs to be monitored because of the following reasons. Due to ammonia exhaust, air pollution via particulate matter is increased especially close to and around cities, with levels rising up to 20-30 ppb.[11]The detection of air quality concerning ammonia is crucial for enclosed areas. For example, it is important to ensure good air quality inside a car as air conditioning uses fresh air from outside. But as soon as air quality suffers from agricultural sites, fires or other sources of ammonia the uptake of polluted

air should be hindered by switching the air inlet valve. Furthermore, exhaust systems and their gases need to be controlled as ammonia or urea are injected in order to reduce NO_x within diesel engines. This is called the selective catalytic reduction (SCR) of NO_x with NH_3. The addition of too much NH_3 needs to be avoided otherwise emission further worsens the air pollution. In this regard levels from 1-100 ppm can be detected.[12]

Chemical Industry

The production of explosives, in which nitric acid is a main constituent, needed a cheap source of nitrogen. This was assured with the ammonia production via the Haber-Bosch process, which became the main technique. However, these days the main implementation of the produced ammonia is within fertilizers, chemical production, pharmaceutical production and refrigeration systems. In all of these fields nearly pure ammonia is utilized, thus, it is necessary to have certain safety measures implemented as a sudden surge in ammonia can put worker's health into danger. As the exceedance of the established workspace long-term maximum of 20 ppm is to be avoided. A sensor with the possibility to measure levels in the range of this value is desirable.

Biomedical applications

The possibility to tackle certain diseases through detecting elevated concentrations of ammonia in the breath is one of many operational areas within medicine. Diseases that showcase higher levels of NH_3 are asthma, infections via bacteria within the lungs and the stomach and chronic kidney disorder.[13,14] Ammonia levels of healthy humans normally are within 30-1800 ppb but can rise to 1-15 ppm when a chronic kidney diseases is displayed.[13,15] For this particular application of human breatha bioelectronic ammonia sensor using protein nanowires that operates in a range of 10 to 10^6 ppb has recently been developed, which can be used in industrial or environmental settings too.[14] Additionally, ammonia concentration within the blood are of relevance in sports medicine. Where expired ammonia that transitioned from the blood to the lungs upon exercise can amount to 0.1 to 10 ppm.[16]

2. Solute Imaging

This section is based on literature [17-18] and other sources will be cited accordingly.

The diverse concentration levels discussed originating or in need of observation from the mentioned areas demand for different ammonia sensors. Some of the most common ammonia detectors are detectors based on amperometric read out, spectrophotometric sensors, potentiometric ion selective electrodes (ISEs), etc. and are described in more detail in section 3 together with the basics of chemical sensors. Even though, these are widely used methods and made it possible to gather important information they do come with certain drawbacks such as the need of sample pretreatment, a diminished stability or the consumption of analyte or reagents. Furthermore, as it is described above the chemical microenvironment in terrestrial systems, sediments and wetlands together with emissions from soils, which employ ammonia but other solutes as well, are of analytical interest. So far, ammonia gas phase assessments were conducted with the disadvantage of only offering bulk analysis. This way no information about the soil/air interface of ammonia can be obtained. Especially high spatial and temporal resolution of NH_3 in soils can be of great help to gain better knowledge about the biogeochemical processes. Spatial and temporal monitoring in heterogeneous sediments and soils of solutes such as O_2, pH, H_2S and others were performed using microsensors[19], diffusive equilibration in thin films (DET)[20] and diffusive gradients in thin films (DGT)[21,22]. Microsensors are very fragile and only provide one-dimensional measurements.[21] Even though DET and DGT can resolve 1D profiles as well as 2D concentration images they are complex in their handling and analysis processes, thus, time consuming.[18] Therefore, in regard to the disadvantages of the previous methods, the planar optode technique is the answer to these shortcomings due to its ability of high spatial and time resolution, fine scale, non-invasive, two-dimensional, real time and reversible analyte imaging. Principles of optical sensors are again discussed in more detail in section 4.

Moreover, a goodnumber of O_2[23] and pH [24] planar optodes has been employed thus far, especially within soils and sediments concerning biogeochemical processes. Though in a lesser degree, planar optodes for other analytes, for example H_2S in sediment[25] and NH_4^+ upon manure amendment in soil[26] have also been implemented. There has also been simultaneous monitoring of several parameters. This is possible via composite planar optodes for which the combination of O_2 and pH is one of many examples.[27] Another possibility to measure multiple

analytes at the same time is the pairing of the sensing layer of a planar optode with a DGT binding gel. Here, imaging of trace metals together with either pH or O_2 was enabled.[28,29]
These arrangements showed that it is of great importance to concurrently measure the spatial distribution of several solutes in order to understand the chemical microenvironment.
Hence, the already discussed role of oxygen and pH played within marine and terrestrial systems and the impact these two have on the processes within the nitrogen cycle led to the idea of simultaneous spatial as well as temporal quantification of O_2 and pH along with ammonia.

3. Chemical Sensors

3.1. What is a chemical sensor?

This section elucidates the principle of chemical sensors, which is premised on references[30–33] and others will be cited independently.

The term chemical sensor describes a self-reliantdevice, which is small in its size and gathers information about one or several chemical species. In other words, as it was stated by IUPAC in 1991:“A chemical sensor is a device that transforms chemical information, ranging from the concentration of a specific sample component to total composition analysis, into an analytically useful signal. The chemical information, mentioned above, may originate from a chemical reaction of the analyte or from a physical property of the system investigated.“[34]

The principle of such sensor is that it holds a recognition element, a transduction element as well as a signal processor that can steadily monitor a chemical concentration. In addition to that, more requirements for sensors are reversibility, robustness, cost effectiveness, selectivity for the investigated chemical speciesand sensitivity in a broad dynamic and relevant range. Also, fast response times must be given together with an easily understandable calibration approach as well as simple handling of the sensor. The already mentioned recognition element, also called receptor, interacts with components of the sample towards which affinity is displayed. This interplay of receptor and analyte can lead to alterations of physical or chemical characteristics of the recognition element. The transduction element, or transducer, translates the physiochemical variations produced by the receptor into a measurable electrical signal such as voltage or current.

The classification of chemical sensors follows a variation of principles. One of those principles relies on the operating principle of the transducer, others are the mode of application (in vitro/vivo), the analysed species, form of stimulus (e.g. magnetic, optical, electric, etc.) or the method utilized for monitoring the effect. More frequently used is the transducer principle in order to classify chemical sensors, again defined by IUPAC [34]:

Optical sensors display an alteration of optical phenomena upon interaction between the analyte and the receptor. The different optical properties involved are absorbance, reflectance, fluorescence, luminescence, reflective index, optothermal effect and light scattering.

Electrochemical sensors convert the outcome of the electrochemical analyte-electrode interaction into suitable signal. This comprises voltammetric, potentiometric, field-effect transistor based sensors that are chemically sensitized as well as potentiometric solid electrolyte gas sensors.

Electrical sensors show signals due to changes of electrical properties initiated by the interaction of the analyte with no electrochemical processes occurring. Examples for such are different semiconductor sensors, electrolytic conductivity as well as electric permittivity sensors.

Mass sensitive sensors are premised on the mass change at a specially altered surface due to accumulation of analyte. These make up piezoelectric and surface acoustic wave sensors.

Magnetic sensors gather the signal when alterations of paramagnetic properties of a gas sample take place (e.g. oxygen).

Thermometric sensors rely on measuring heat effects of chemical reactions or adsorption comprising the analyte.

Sensors based on other physical properties are premised on for example nuclear radiation if utilized for the identification of chemical composition.

3.2. Different methods used for ammonia

The following section is based on previous literature[2], which is complemented by other references that will be cited accordingly.

Metal-Oxide Gas Sensors function according to the adsorption and interaction of gas molecules at the metal-oxide surface, which is the sensing layer, and result in a change of conductance. The majority of such sensors consists of SnO_2 but since they lack in selectivity towards one specific gas, the use of other metals or additives demonstrating a higher selectivity towards NH_3 were sought for.[35] An example for thatis WO_3, and in combination with additives such as Au and MoO_3 even a minimum of 1 ppm as detection limit was realized.[36] The detection limits in general vary from 1 to 1000 ppm in that kind of sensors. Their main utilization is within combustion gas detectors or gas alarm systems in order to be informed about an ammonia loss within refrigeration systems.[37,38]

Catalytic Ammonia Sensors involve catalytic metals and their alteration of the charge carrier concentration upon concentration change of the analysed gas. The determination of such charge carriers' changes can be monitored with a field effect device, such as a capacitor or transistor.[39]Furthermore, the combination of this interplay between gas and a catalytic metal with a solid-state ion conducting material results in a chemical cell in which the potentiometric change towards varying gas concentrations is measured.[40]

Ion selective electrodes are another example for potentiometric sensing. In this system an electrochemical cell makes up two half cells. The principle of this is the determination of the potential difference between the ion selective electrode and a reference electrode upon $NH_4^+$is selectively bound by an ionophore within a membrane and the thereby introduced concentration change.[41]These sensors are simple in handling, are cheap and mainly used in freshwater but also suffer in reduced stabilities.[42]

Conducting Polymer Gas Detectors gather the change of the polymer conductivity dependant on amperometric read out. The conductivity is altered when the polymer interacts with gaseous ammonia. An example for such polymer is polypyrrole and since one of the reactions between the polymer and ammonia is irreversible the sensitivity of this sensor

decreases continuously.[43,44]Another polymer for this set up is polyaniline with which a detection limit of about 1 ppm is possible.[45]

Spectrophotometric Ammonia Analysers are one of the main optical principle methods to sense ammonia, in which the coloration of the analyte takes place. The detection of dissolved ammonia can be conducted following various coloration reactions. One of these is the so called Nessler reaction, which can be used in flow injection analysis.[46] The reagent of this comprises dipotassium tetraiodomercurate(II) in a dilute alkaline solution, e.g. sodium hydroxide. However, this reagent displays one main drawback being the toxicity of such. An additional coloration process used to elucidate the ammonia concentration is the Berthelot reaction.[47,48]The sensing is based on a resulting blue coloration upon mixing ammonia, phenol and hypochlorite.[47]The biggest disadvantage of this method is the slow kinetics it shows, which can be improved by incorporating this reaction within a microfluidic device.[48]

Optical sensors make up the other part taking advantage of optical principles in order to detect ammonia. This method uses light from different sources, which interacts with the sensor layer. Upon alterations of optical characteristics due to the interaction with ammonia the light then arriving at the detector shows a changed spectrum. One of the sensors comprised within this subcategory are optical absorption ammonia detectors but also other optical characteristics such as fluorescence can be utilized. The principle of such fluorescent optical sensorsis described in detail within the next section (section 4). As the majority of optical sensors detect NH_3 via the deprotonation of a pH sensitive fluorescent dye, which can take place upon the diffusion of ammonia through a gas permeable membrane.

4. Optical Sensors based on Fluorescence

This section is based on the literature[32,49–52]and other references used will be cited accordingly.

In general, the importance of fluorescence sensing methods is given due to thestrong application demands within analytical chemistry, the environment, medicine and others. Moreover, the possibility of identifying a great variety of analytes along with other qualities they offer, like their temporal and spatial resolution, sensitivity, selectivity and response times, make them a great alternative to other detectors. Some of the detectable analytesare

cations (H^+, Na^+, K^+, Ca^{2+}, NH_4^+), anions (halide ions, citrates, phosphates), gases (O_2, CO_2, NH_3) and neutral molecules (sugars). On top of that they can be used asfibre optic chemical sensors (FCOS), enabling sensing in inaccessible locations, but also two-dimensional imaging as planar waveguide-based chemical sensors (PWCS) is possible, offering observations of e.g. microenvironments.

However, fluorescent molecular sensors consist of a fluorophore, which can be a small molecule (fluorescent indicator dye). The fluorophore takes up the role of the signal transducer as it indicates the presence of an analyte by altering its photophysical properties. These alterations are the optical signal that can further be interpreted as information about the analyte concentration present. Other components are the polymer matrix, within which the fluorophore (indicator dye) is immobilized, the solid support material onto which the polymer containing the indicator dye is deposited as well as possible membranes (e.g. able to exclude protons) or optical insulation layers, the light source to excite the fluorophore and the light detector coupled with the electronics to elucidate the signal. Only then when all components are taken into consideration it is feasible to talk about an optical sensor.

For fluorescent molecular sensors three classes can be identified and these are illustrated in Figure 2 as well:

- The 1st class comprises fluorophores that experience quenching after colliding with the analyte. This is used in measuring O_2 for example, or ions such as Cl^-.
- In the 2nd class fluorophores are able to bind an analyte, but reversibly. An example for such is the fluorescent pH indicator when the analyte is a proton. If the analyte is an ion though, they are called fluorescent chelating agent. Moreover, further distinction is possible via the enhancement of the fluorescence upon binding (CEF: Chelation/Complexation Enhancement of Fluorescence) or when the fluorescence is quenched (CEQ: Chelation/Complexation Enhancement of Quenching).
- In the 3rd class fluorescent molecular sensors depend on an additional feature in order to generate a signal. This feature is a receptor, which recognizes the specific analyte. The signal transduction is conducted or in other words the change in photophysical characteristics of the fluorophoreare quenched or enhanced if the receptor interacts with e.g. an ion, in that case an ionophore is involved and linked to the fluorophore. The whole molecular sensor is then characterized as fluoroionophore.

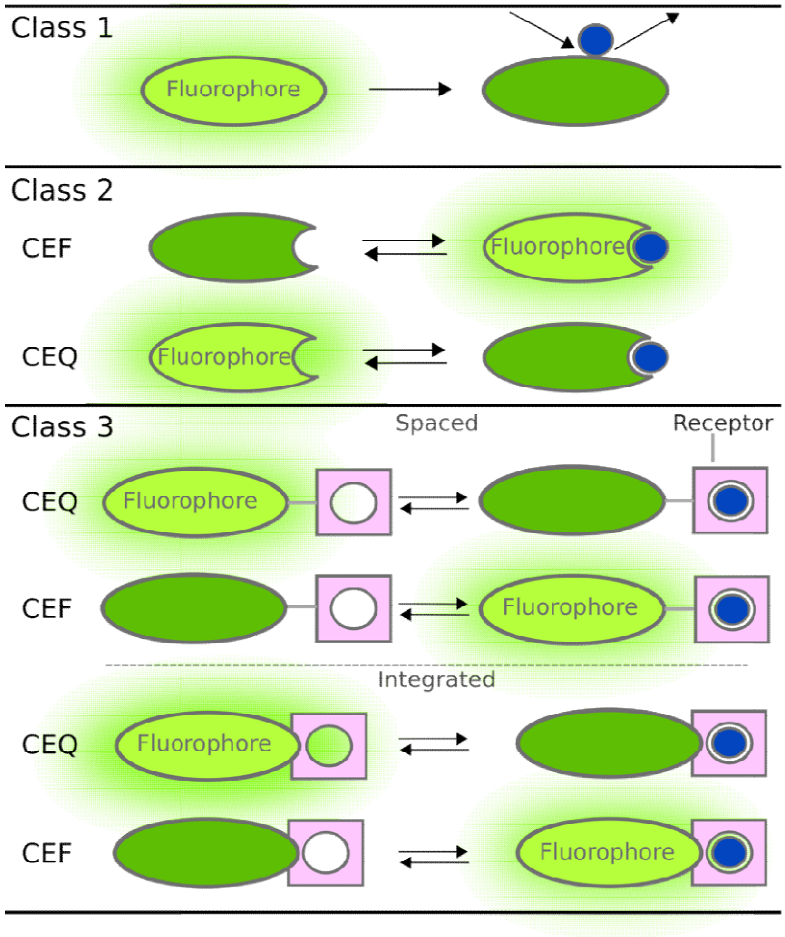

Figure 2: The three classes of fluorescent molecular sensors, where class 1 comprises fluorophores that undergo quenching upon colliding with the analyte. Class 2 fluorophores can reversibly bind the analyte and class 3 fluorophores are linked to a receptor either in a spaced or in an integrated manner. CEF: Chelation/Complexation Enhancement of Fluorescence. CEQ: Chelation/Complexation Enhancement of Quenching.

4.1. pH Optical Sensors

Fluorescence based optical pH sensors can be assigned to the already discussed class 2 sensors within the previous section4. The principle of this method relies on the interaction of the indicator dye with protons and the then varying concentration of acidic and basic forms of this indicator, which can optically be detected. The relationship between the protonated (acidic) and deprotonated (basic) form can be outlined with the help of the Henderson-Hasselbalch (equation 4.1.1). In addition, the equation shows the importance the pK_a has for the sensitivity of a pH indicator as it is highest at pH = pK_a. This way sensors employing a pH indicator are restricted to the pK_a and the possible pH range due to the limitation of pH = $pK_a \pm 2$.

$$\boldsymbol{pH = pK_a + \log\frac{A^-}{HA}} \qquad (\mathbf{4.1.1})$$

The changes in fluorescence induced by different pH values can depend on the following processes that occur and upon which three classes are established:

- Class A: Fluorophores experiencing a photoinduced proton transfer and only showcasing changes in the excitation spectrum but the fluorescence spectrum remaining unchanged. This is due to the lower pK (higher acidity) of such fluorophores when in the excited state compared to when in the ground state. Thus, emission is mainly displayed by the basic form as the protonated form follows immediate excited-state deprotonation.
- Class B: Fluorophores not experiencing either of the possible processes (photoinduced proton transfer or photoinduced electron transfer) and the course of both the absorption and the fluorescence spectra against the pH should resemble one another. This is taking place in the form of a decline in acidic absorption and emission bands with rising pH together with an increase of the absorption and emission bands of the basic part.
- Class C: Fluorophores experiencing a photoinduced electron transfer, where the fluorescence is being quenched due to the electron transfer when the fluorophore is deprotonated. In contrast, the fluorescence is increased when the fluorophore is protonated as this condition hinders electron transfer.

However, it is important to note that optical pH sensors are influenced by some parameters with the most important ones being temperature and ionic strength.

Also, the signals obtained from fluorescence can fluctuate due topossible drawbacks such as the indicator concentration that can cause an inner filter effect, leaching and bleaching of the indicator, irregular excitation light, the sensitivity of the instruments, aggregation and some others. The desired signal can become inert to these interferingeffects, which are analyte concentration independent, by implementing various referencing methods. Since one of the possibilities is already feasible without the need of any additional components this is the first one to be mentioned.

Ratiometric referencing can be conducted by measuring the excitation or emission bands at two spectrally separated wavelengths. The result of this is a referenced parameter called ratio, which can be used for examining the referenced changes in intensity. Since there do exist fluorophores able to display two emission bands induced by protonation or deprotonation (Class B fluorophores) these are well suited for the ratiometric referencing approach (Figure 3). On the other hand, fluorophores without the ability of emitting at two wavelengths but only at a single one need a supplementary fluorophore (reference fluorophore) that preferably is excitable at the same wavelength but shows a distinguishable emission band compared to the sensitive fluorophore (Figure 4, left). Furthermore, the reference fluorophore has to be analyte insensitive in order to be considered.

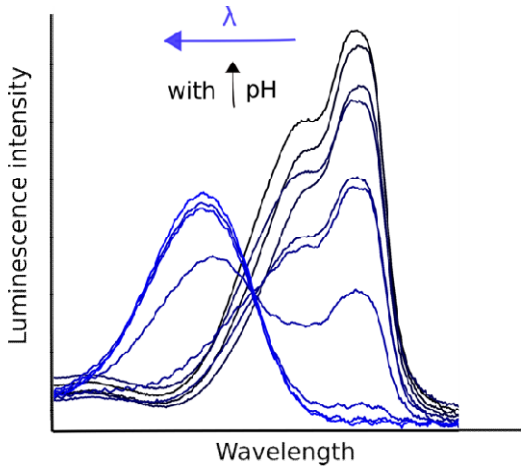

Figure 3: Example of a pH sensitive fluorophore (Class B) changing its emission bands upon deprotonation, showcasing a hypsochromic shift, and suited for self-referencing.

An additional method to reference the fluorescence intensities of indicator dyes is the **dual lifetime referencing (DLR)** (Figure 4, right). In this method a different fluorescence parameter called the decay time is employed. The decay time together with anisotropy are intrinsically referenced and do not suffer from instabilities of the fluorescence intensity. Also, this approach utilizes a sensitive indicator dye paired with an analyte insensitive fluorophore. Since the pH sensitive dyes display rather short decay times (nanosecond range) the reference dye is expected to offer longer decay times (micro- or millisecond range) for measurement simplification purposes. A ratio is generated here as well from the luminescence intensities; however, this is then transformed into a phase shift resulting from the deviating decay times of the used fluorophores. Moreover, there are two domains that can be used to assess the ratio, either a time or a frequency domain.

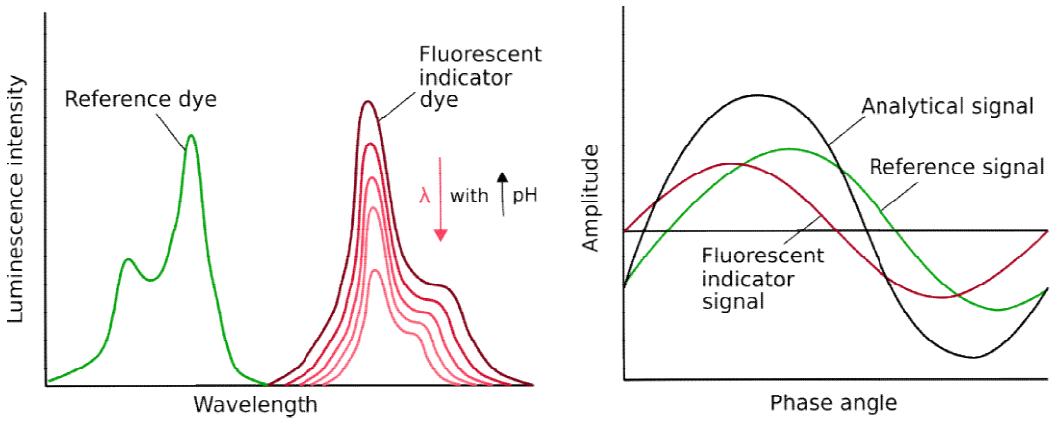

Figure 4: Illustration of two-wavelength ratiometric referencing (left) and dual-lifetime referencing in the frequency domain (right).

4.2. NH_3 Optical Sensors

There are different concepts used in order to conduct optical ammonia detection. The simplest of such isenabling ammonia diffusion through a proton and ion impermeable membrane to then deprotonate apH indicator, these indicators already are well studied as discussed in section 4.1. Hence, the same principles apply for NH_3 optical sensors as they do for pH sensitive fluorophores with the only difference of employing a gas permeable membrane, put on top of the immobilized pH sensitive dye. This way interferences of protons and ions with the pH sensitive indicator are avoided. The fluorescent pH indicator concept can be seen in Figure 5. So far a wide range of pH indicator dyes were applied for optical ammonia sensors, to name some: fluorescein[53], aza-BODIPYs[54], Oxazine[55] and coumarin dyes[56]. A variety of indicators was tested as the sensitivity of such an ammonia sensor depends on the pK_a value of the used pH indicator dye as the lower the pK_a the easier deprotonation via ammonia can take place.[54]And even though low limits of detection of 0.11 ppb[54] can be achieved with this simple approach the main drawback is the selectivity due to displayed cross-sensitivity towards other volatile alkaline gases, such as trimethylamine and other amines.[57] These gases can also diffuse through the hydrophobic membrane and therefore deprotonate the pH indicator. Another concept, which happens to be similar, is the addition of an ionophore to the immersed pH indicator (Figure 5 b). The selectivity towards ammonia is enhanced due to the ability of the ionophore to bind the generated NH_4^+ molecule behind the hydrophobic membrane. But still no eradication of the cross-sensitivity towards volatile amines is obtained by this only a diminishment of such.[58]However, a concept able to completely overcome this problem of cross-sensitivity is the one utilizing a fluoroionophore together with an internal buffer (Figure 5 c) and not being in need of a pH indicator.[59] In this concept NH_3 is converted to NH_4^+ with the help of the buffer and can then be detected by the ion selective receptor unit (the ionophore), which is connected to the transducer unit (the fluorophore). So far this is not the optimal solution since further research has to go into this concept to improve the binding constant with ammonium as well as further investigate possible pK_a alterations.[59]

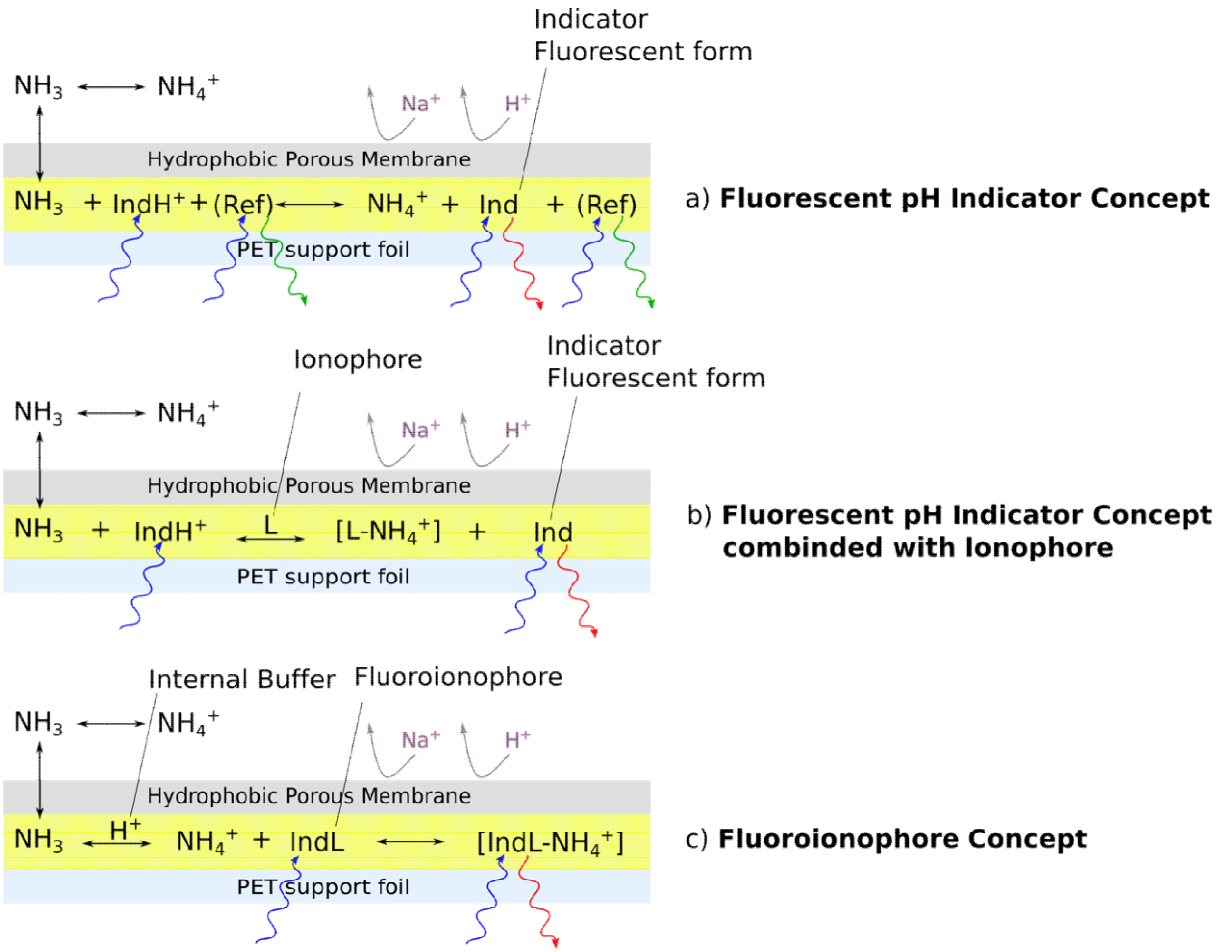

Figure 5: The main optical ammonia sensing concepts. a) the protonated pH indicator dye ($IndH^+$) is deprotonated (Ind) by NH_3 upon diffusion of NH_3 through a proton impermeable membrane. b) similar concept to a) with the addition of an ionophore (L), which can bind the generated ammonium (NH_4^+) ion and by doing so enhances the selectivity for the analyte NH_3. c) a fluoroionophore that is selective towards ions, specifically towards NH_4^+, which is generated with the help of an internal acidic buffer when NH_3 reaches the sensor layer.

II. Theoretical Background

5. Fundamentals of Luminescence

This section is based on literature [49,60] and other sources will be cited accordingly.

Luminescence is described as the emission of light, which can be in the form of ultraviolet, visible or infrared photons, derived from a species that is electronically excited. Compounds displaying luminescence are organic compounds (aromatic hydrocarbons, coumarins, oxazines, fluorescein, amino acids, etc.), inorganic compounds (lanthanide ions, crystals, doped glasses, etc.) and organometallic compounds (complexes with fluorogenic chelating agents, complexes with lanthanide ions, ruthenium complexes, etc.). There are different types of luminescence, which originate from various modes of excitation, hence, these types are assigned according to the respective excitation process. In general, the interaction of light with matter leads to various excitations, which are physical effects (Figure 6). One of the excitation and energy harvesting modes is the absorption of photons, elevating the absorbing compound to an electronically excited state. The then following de-excitation joined by emission of photons is a particular event of luminescence, namely photoluminescence and further entails fluorescence, phosphorescence and delayed fluorescence. In this thesis the emphasis is placed on the absorption of light, photoluminescence and the associated processes.

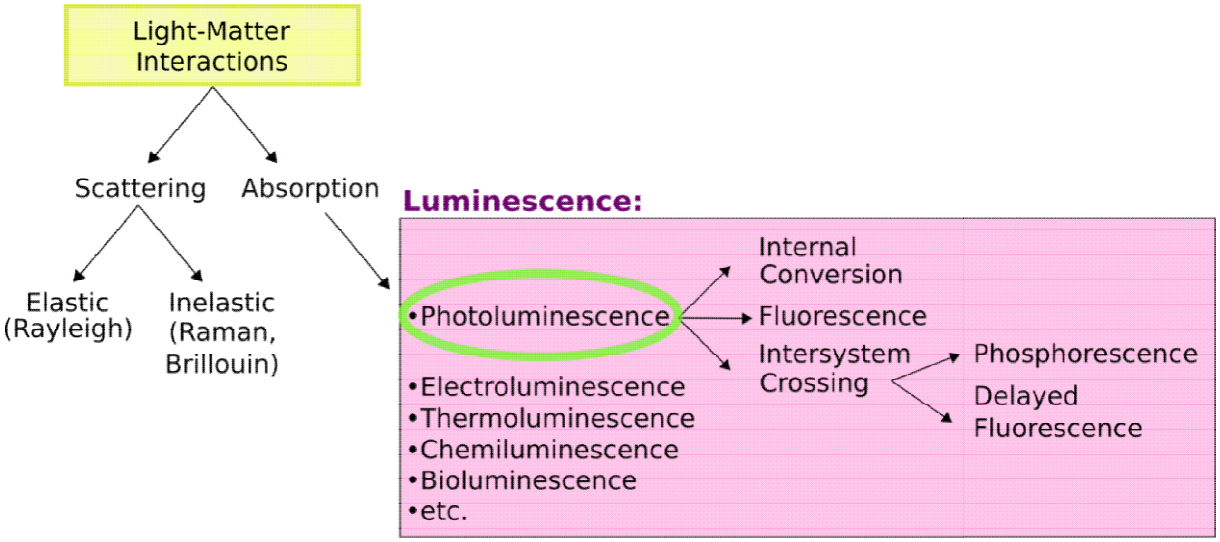

Figure 6: Light matter interactions and the various ways of de-excitation entailed in luminescence.

5.1. Absorption

When a photon is absorbed by a molecule an electron is promoted from the orbital in the ground state of this molecule up to an unoccupied orbital resulting in an excited state molecule. As there are different molecular orbitals depending on the linkage of the atoms within a molecule, different appropriate energies of the absorbed photons are required to excite electrons to antibonding orbitals. In the case of ethylene (CH_2=CH_2) for example the carbon atoms are coupled via one σ bond and one π bond. And upon excitation one π electron can be transferred to an antibonding orbital with the expression π^*. This would then be a $\pi \rightarrow \pi^*$ transition. Other transitions exist too involving the electrons from σ molecular orbitals as well as non-bonding electrons from lone pairs from the so-called n orbitals. In order to get a better understanding of the energy levels of the orbitals and possible transitions, these transitions are explained/illustrated exemplarily for formaldehyde in Figure 7. The facilitation of excitation depends on the difference in energy between the respective molecular orbitals, thus, the required energy for the various electronic transitions follow an order from the lowest to the highest energy needed:

$$n \rightarrow \pi^* < \pi \rightarrow \pi^* < n \rightarrow \sigma^* < \sigma \rightarrow \pi^* < \sigma \rightarrow \sigma^*$$

The main transitions taking place, especially in fluorescence spectroscopy, are $n \rightarrow \pi^*$and $\pi \rightarrow \pi^*$. This is because the other transitions are observed at higher energies, therefore they would only occur at lower wavelengths. Also, a decline in energy needed for the $\pi \rightarrow \pi^*$ transition is achieved by extending the conjugated π-system (conjugated cyclic and linear systems). Hence, the decreased energy demand results in a shift to higher wavelengths within the absorption band.

Furthermore, the orbitals of highest importance are the highest occupied molecular orbital (HOMO) and the lowest unoccupied molecular orbital (LUMO) and both are referring to the ground state. This is because the transition of one electron out of two with opposite spins takes place from the HOMO to the LUMO. The spin of this electron usually stays unaltered; thus, the total spin quantum number equals zero. When that is the case also the multiplicity remains unchanged, that means both the ground state as well as the excited state equal one and both are then named singlet state. Hence, the related transition is a singlet-singlet

transition. In addition to that there also exists a triplet state. This occurs when an electron changes its spin and the molecule then finds itself in a somewhat converted state instead of a singlet excited state. In that case the electrons showcase parallel spins, which leads to a total spin quantum number of one and also to a multiplicity of three. In accordance with Hund's Rule, the triplet state has a lower energy compared to the singlet state of the same formation.

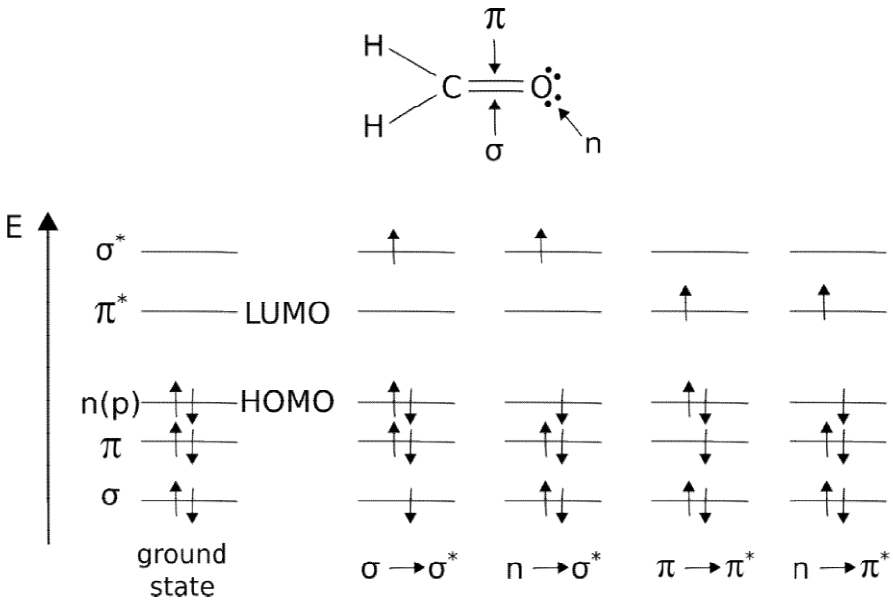

Figure 7: The respective energy levels and their possible transitions of the example formaldehyde.

In order to experimentally control the efficiency of light absorption by a medium at a specific wavelength λ either the absorbance A(λ) or the transmittance T(λ) can be used, which are defined as:

$$\boldsymbol{A(\lambda) = \log \frac{I_\lambda^0}{I_\lambda} = -\log T(\lambda)} \qquad \boldsymbol{(5.1.1)}$$

I_λ^0 … *light intensity of the beam entering absorbing medium*

I_λ … *light intensity of the beam leaving absorbing medium*

In most cases, the absorption process follows the Beer-Lambert law (equation 5.1.2):

$$\boldsymbol{A(\lambda) = \log \frac{I_\lambda^0}{I_\lambda} = \varepsilon(\lambda) * l * c} \qquad (\mathbf{5.1.2})$$

$\varepsilon(\lambda)$ … $molar\ decadic\ absorption\ coefficient$ $[L\ mol\ cm^{-1}]$
l … $absorption\ path\ length\ of\ the\ medium$ $[cm]$
c … $concentration\ of the\ dye\ solution$ $[mol\ L^{-1}]$

If the linear dependence of the absorbance on concentration cannot be determined, according to the Beer-Lambert law, then this can be a result of aggregate formation at high concentrations or the presence of other absorbing compounds.

5.2. Franck-Condon Principle

The Franck-Condon principle is based on the Born-Oppenheimer approximation, which states that upon excitation the promotion of an electron to a higher, antibonding molecular orbital takes less time (10^{-15} s) than molecular vibrations (10^{-10}-10^{-12} s). In other words, the movements of electrons are faster compared to the ones of the nuclei. Therefore, there is not enough time for the nuclei to undergo modifications in its position when an electronic transition occurs. Hence, vertical electron transitions occur. This can be seen in Figure 8 together with the potential energy curve representing the internuclear distance (in case there are two atoms). So, if an electron is vertically transitioning from the ground state to an excited state, termination of such is reached as soon as the vertical line intersects the potential energy curve at the lowest excited state. When the transition is finished, the molecule, now excited, starts to vibrate at a frequency analogous to the energy at the intersection location (excited state). Moreover, the intensities of numerous vibrational transitions rely on the shape as well as the relative position of the potential energy curves. One of those transitions is the 0-0 one and is considered as the classic electronic transition.

Furthermore, absorption band widths are the outcome of two events: homogenous and inhomogeneous broadening. The first event is the result of the continuous occurrence of a number of vibrational sublevels in each electronic state whereas the latter takes place due to the variations of the structure of the solvation shell enclosing the chromophore.

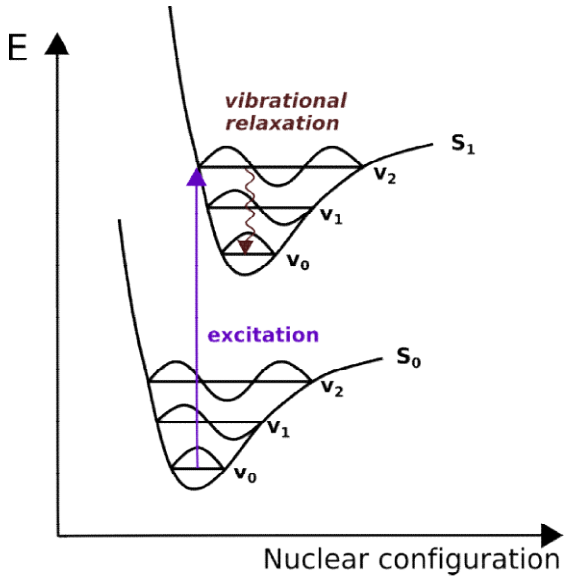

Figure 8: Frank-Condon Principle.

5.3. Transitions between Electronic States and Perrin-Jablonski Diagram

There are several electronic energy levels an electron can be promoted to. Each electronic energy level associates with specific vibrational energy levels. Therefore, a variety of possible de-excitation processes for an excited electron exist. These transitions together with the energy states are exhibited in the Perrin-Jablonski diagram (Figure 9).

The ground state of a molecule is characterized as $S_0$and the excited singlet electronic states as S_1, S_2, etc. and likewise the triplet electronic states as T_1, T_2, etc. The various ways an excited electron can return to the ground state and the characteristic times of these processes are further described in the subsequent sections.

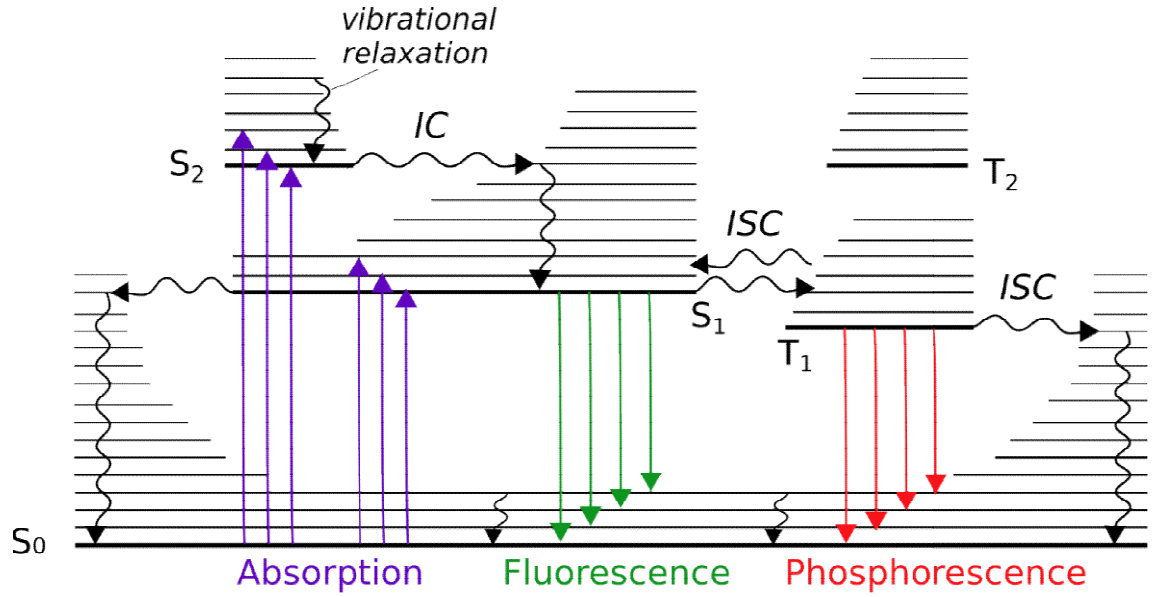

Figure 9: The Perrin-Jablonski diagram elucidating the processes ranging from excitation to the following de-excitation possibilities, radiative as well as non-radiative.

5.3.1. Internal conversion (IC)

If a non-radiative transition between two electronic states takes place, and these states are of same spin multiplicity, this is described as internal conversion (IC). Moreover, vibrational relaxation to the lowest vibrational level of the definite electronic state may follow in solution. It may occur that excess vibrational energy is transmitted to the solvent molecules in close proximity. The time scale for these processes leading an excited molecule from a higher energy level to the lowest vibrational level of the first singlet state is between 10^{-13}-10^{-11} s. Even though there is the possibility of internal conversion from S_1 to S_0, the great energy gap between those energy levels presented leads to a lower efficiency of this relaxation. However, IC from S_1 to S_0 can compete with emission of photons (fluorescence) and emission of photons upon intersystem crossing to the triplet state can take place (phosphorescence).

5.3.2. Fluorescence

Fluorescence is the process when relaxation from the excited state S_1 to the ground state S_0 with concomitant emission of photons proceeds. This process of fluorescence emission is mostly independent of the excitation wavelength as, apart from some exemptions, the transition commences from S_1. Since variations between the vibrational levels in the ground as well as in the excited state are analogous to each other, the fluorescence spectrum mirrors the spectrum of the S_0 to S_1 absorption bands ('mirror image' rule). But the fluorescence bands are moved to higher wavelengths (lower energy) compared to the absorption bands due to the energy loss in the excited state upon vibrational relaxation. This occurrence of fluorescence emission at higher wavelengths, as opposed to the absorption bands within the spectrum, should be present at all times, as the Stokes rule states. Hence, the Stokes shift describes the difference between the maxima of the absorption band and the emission band. In general, there mostly is a slight overlap between the absorption spectrum and that of fluorescence, which then means that a fragment of light is emitted at shorter wavelengths than the light absorbed. Nevertheless, since at room temperature a small number of molecules is in a higher vibrational level than the lowest ones of S_0 and S_1, this energy defect can be described but also be compensated for. Thus, the lower the temperature the higher the possibility to avoid the deviation from the Stokes law.

Furthermore, the time scale for fluorescence is comparable with the time absorbing a photon takes (10^{-15} s). After all, the excited molecule though remains in the S_1 state for some time, ranging from tens of 10^{-11} s (picoseconds) to hundreds of 10^{-9} s (nanoseconds), before

fluorescence emission or other excitation processes set in. This stay in the S_1 excited state is also characterized as fluorescence lifetime of the molecule.

5.3.3. Intersystem crossing (ISC)

Intersystem crossing is another non-radiative de-excitation process starting from S_1 toward T_n, which depicts electronic states of diverging multiplicities. This movement of an excited molecule happens between the two iso-energetic vibrational levels of the S_1 excited singlet state and the T_n triplet state and entails the subsequent vibrational relaxation of that molecule to the 0 vibrational level of T_1. Moreover, with a time of 10^{-7}-10^{-9} s intersystem crossing may be able to content with other de-excitation processes commencing from S_1, such as fluorescence and internal conversion. Even tough, inter-electronic states crossing between states of different multiplicity is forbidden spin-orbit coupling can enable it, in which the orbital magnetic as well as the spin magnetic moment are involved. However, this is dependent on the participating singlet and triplet states. Additionally, the presence of heavy atoms (e.g. Pb, Br) enhances spin-orbit coupling and through this intersystem crossing is preferred.

5.3.4. Phosphorescence

Phosphorescence, the radiative de-excitation from the triplet state T_1 to the S_0 state, is usually a forbidden transition. Additionally, this spin prohibition is the case for the non-radiative de-excitation pathways between those two states. But due to spin-orbit coupling these processes are possible. Even though, the prohibited transition can take place, a slow radiative rate constant is generated in solution at room temperature in the case of phosphorescence. Since this enables frequent collisions with solvent molecules non-radiative de-excitation such as intersystem crossing or vibrational relaxation is favoured over radiative de-excitation (phosphorescence). In contrast, when the conditions change to low temperatures or when enclosed in a rigid medium and collision numbers drop, observation of phosphorescence dominates together with a long-lasting lifetime of the triplet state able to reach a time scale of up to seconds and even minutes.

Also, the lower lying 0 vibrational level of the triplet state T_1 compared to the one of the excited singlet state S_1 results in a lower energy of T_1, which is expressed in higher wavelengths of the phosphorescence emission than the fluorescence emission.

5.3.5. Delayed fluorescence

The transition from T_1 to S_1, also called reverse intersystem crossing, then followed by emission makes up delayed fluorescence. In fact, this type is one of two possibilities, namely, thermally activated delayed fluorescence (E-type), which depends on a small energy difference between S_1 and T_1 as well as on a prolonged lifetime of T_1. When temperature rises, efficiency of this fluorescence emission increases. Since this is the delayed fluorescence, spectral properties resemble the ones of normal fluorescence with the only difference of longer decay times (lifetimes). These decay times are comparable to the ones of phosphorescence as the molecules reside in T_1 before de-excitation from S_1 takes place.

The other possibility of this process is the triplet-triplet annihilation (P-type). In this case enough energy is generated by the collision of two molecules in the excited triplet state T_1 enabling one of the molecules to transition to the S_1 state. This occurs in concentrated solutions. The product of these events is delayed fluorescence due to the previous stay of electrons in the triplet state T_1.

5.4. Lifetime

The absorption of photons promotes a distinct number of molecules to the excited singlet state S_1 and a measure of the time the molecules spent remaining in this state S_1 is described as the lifetime of this excited state. After staying in the S_1 state for a certain time these molecules rebound to the ground state S_0, through radiative and non-radiative de-excitation pathways. In this excited state the average lifetime is given by:

$$\boldsymbol{\tau_S = \frac{1}{k_r^S + k_{nr}^S}} \tag{5.4.1}$$

$k_r^S \ldots rate\ constant\ for\ radiative\ de-excitation\ from\ S_1 \rightarrow S_0\ (fluorescence)$
$k_{nr}^S \ldots rate\ constant\ for\ overall\ non-radiative\ de-excitation$ from S_1

Furthermore, the de-excitation paths discussed, both radiative and non-radiative despite triplet-triplet annihilation, follow first-order kinetics which, when integrated, leads to the following equation:

$$[\boldsymbol{A}^*] = [\boldsymbol{A}^*]_{\boldsymbol{0}} \cdot \boldsymbol{e}^{-\frac{\boldsymbol{t}}{\tau_S}} \tag{5.4.2}$$

$[A^*]$ … $time\ evolution\ of\ the\ concentration\ of\ excited\ molecules$
$[A^*]_0$ … $time\ evolution\ of\ the\ concentration\ of\ excited\ molecules\ at\ time\ 0$

Whilst organic molecules demonstrate a lifetime of the excited S_1 state varying from tens of 10^{-11} s (picoseconds) to hundreds of 10^{-9} s (nanoseconds), they exhibit even longer triplet lifetimes (phosphorescence) from microseconds to seconds. Although, this fact could be an easy way to identify either fluorescence or phosphorescence due to the difference in lifetimes, it is not feasible as there are compounds, inorganic or organometallic, yielding longer lifetimes.

5.5. Quantum yields

The fluorescence quantum yield represents the ratio between the number of emitted photons and absorbed photons (equation 5.5.1). It is an important parameter describing the brightness of a molecule since an increase in fluorescence quantum yield results in increased fluorescence emission.

$$\boldsymbol{\Phi_F} = \frac{\boldsymbol{emitted\ photons}}{\boldsymbol{absorbed\ photons}} = \frac{\boldsymbol{k_r^S}}{\boldsymbol{k_r^S + k_{nr}^S}} = \boldsymbol{k_r^S} \cdot \boldsymbol{\tau_S} \tag{5.5.1}$$

k_r^S … $rate\ constant\ for\ radiative\ de-excitation\ from\ S_1 \rightarrow S_0\ (fluorescence)$
k_{nr}^S … $rate\ constant\ for\ overall\ non-radiative\ de-excitation$ from S_1
τ_S … $lifetime\ of\ the\ excited\ state$

Events such as dynamic quenching and static quenching of excited species can have an influence on either both the quantum yields and the lifetime of the excited state by decreasing both in the case of the former (dynamic quenching). But in the case of the latter (static quenching) only a decrease in quantum yields without impacting the lifetime is caused. In addition, the quantum yields and lifetimes can also be affected by other parameters like temperature, polarity, viscosity, pH, etc. As an example, higher temperatures lead to a decrease in fluorescence quantum yields and lifetimes due to the preference of non-radiative processes (intramolecular vibrations, collisions with solvent molecules etc.).

5.6. Luminescence Quenching

The possibilities of intrinsic de-excitation an excited molecule (M^*) can experience were outlined within section 5.3, which involved the various transitions between electronic states. Additionally, there is another option for de-excitation competing with the intrinsic processes. That process is called quenching and involves the intermolecular interaction between one excited molecule (M^*) and a quenching molecule (Q) resulting in decreased or even inhibited fluorescence emission. There a number of different photophysical processes taking place between molecules, which can lead to fluorescence quenching, such as collision with heavy atoms, photoinduced electron transfer (PET), photoinduced proton transfer (PPT), excimer or exciplex formation as well as energy transfer. Here, two types of quenching, which comprise some of the mentioned processes, will be described: dynamic and static quenching.

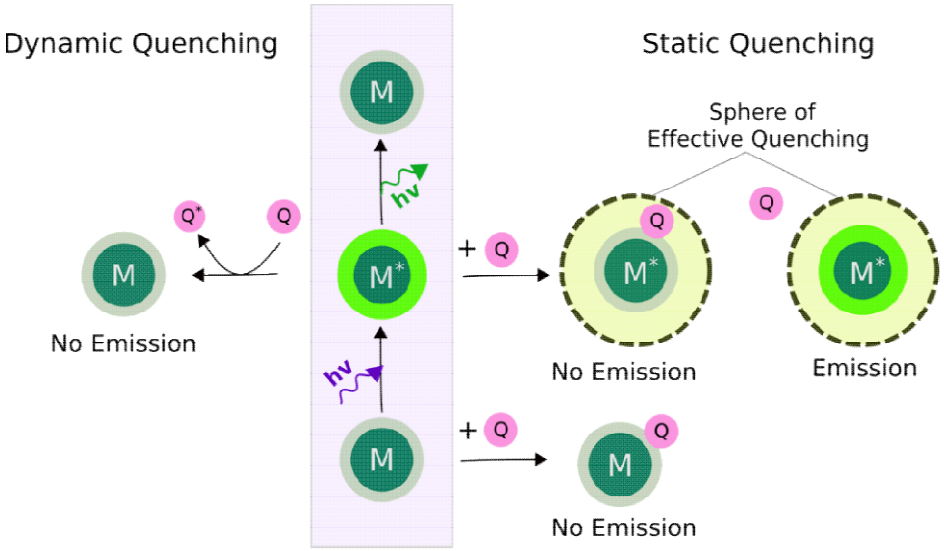

Figure 10: Illustration of two types of quenching: dynamic and static quenching.

Dynamic quenching is the diffusion-controlled and time-dependent collision between the excited molecule (M^*) and a quencher molecule (Q) and takes place during the lifetime of S_1. Such quencher molecules can be oxygen, acrylamide, iodide, succinimide, etc. When the excited molecule and the quencher molecule collide a non-radiative energy transfer occurs. Hence, M^* is forced to revert to the ground state. The likelihood of this process is higher at increased excited state lifetimes.

Furthermore, dynamic quenching influences luminescence intensity as well as the lifetime and is, as already mentioned, diffusion controlled. Thus, the time-dependency comes with the

importance of the quenching rate constant k_q for this process, which can be depicted with the help of these facts and by the Stern-Volmer equation:

$$\frac{\Phi_0}{\Phi} = \frac{I_0}{I} = 1 + k_q \tau_0 [Q] = 1 + K_{SV}[Q] \quad (5.6.1)$$

In this equation (5.6.1) the steady-state fluorescence intensities I_0 and I describe the quencher absence or presence, respectively. This I_0/I ratio is in a proportional relation to the ratio τ_0/τ of the lifetimes. The quenching rate constant k_q together with the non-quenched excited state lifetime τ_0 make up the Stern-Volmer constant K_{SV} and Q stands for the quencher molecule concentration. In a Stern-Volmer plot the ratio I_0/I is then plotted against the quencher concentration. If a linear behaviour is depicted, the slope can define the Stern-Volmer constant.

Static quenching entails two possibilities which either is the development of a ground-state non-emitting complex or the presence of a sphere of effective quenching. The former occurs as soon as quencher molecules are added and due to that the fluorescence intensity experiences a decrease. However, no impact is observed on the excited-state lifetime. Some formations of these complexes can be demonstrated by observing alterations in the absorption spectrum as soon as complexation took place. If this observation is not the case, a non-specific interaction could be the explanation, and therefore the model of an effective sphere of quenching may provide a better justification. In this model it is assumed that an excited molecule M^* is enclosed in an active sphere (or quenching sphere) and if a quencher (Q) is located inside this sphere the fluorescence intensity of M^* is quenched. Hence, M^* is not affected by Q if the quencher is situated outside the quencher sphere. The idea of the sphere should explain the eventuality of a viscous media or rigid matrices in which M^* and Q are unable to modify their positions in space, especially towards one another, while the excited-state lifetime of M^* remains.

III. Experiments for Optode Development

6. Materials and Methods

6.1. Materials

Table 1: List of Chemicals.

Chemical	Supplier
Hydrochlorid acid	Merck
Sodium hydroxide	Merck
Sodium dithionite	Sigma Aldrich
Sodium Chloride	Sigma Aldrich
Ammonium chloride	Bie&Bernsten
Trimethylamine hydrochloride	Merck
Sodium phosphate monobasic monohydrate	Sigma Aldrich
Sodium phosphate dibasic dihydrate	Sigma Aldrich
Oxazin 170 perchlorate	Sigma Aldrich
Macrolex® fluorescence yellow 10GN	Lanxess
Macrolex® fluorescence red G	Lanxess
Bromophenol blue	Sigma Aldrich
Platinum(II)-meso(2,3,4,5,6-pentafluoro)phenyl-porphyrin	Frontier Scientific
1-Hydroxypyrene-3,6,8- tris-bis(2-ethylhexyl)sulfonamide	Dr. Sergey Borisov, Graz University of Technology, Austria
Perylene	Sigma Aldrich
4', 4''(5'')-Di-tert-butyldibenzo-18-crown-6	Sigma Aldrich
Ethyl eosin	Sigma Aldrich
Methane sulfonic acid	Sigma Aldrich

Table 2: List of Polymers.

Polymer	**Supplier**
Hydromed D4	AdvanSource Biomaterials
Polystyrene MW 192,000 g mol^{-1}	Sigma Aldrich
Ethyl cellulose	Merck
Cellulose acetate propionate	Sigma Aldrich
Poly[4,5-difluoro-2,2-bis(trifluoromethyl)-1,3-dioxole-*co*-tetrafluoroethylene] (Teflon AF)	Sigma Aldrich
PDMS (Silicone Elastomer Kit, Sylgard 184)	DOW Europe

Table 3: List of Solvents.

Solvent	**Supplier**
Chloroform	Merck
Tetrahydrofuran	Sigma Aldrich
Isopropanol	Sigma Aldrich
Ethanol	Sigma Aldrich
Hexane	Merck
Perfluorocyclohexane	Sigma Aldrich

Table 4: List of other Chemicals and Materials.

Other chemicals or materials	**Supplier**
Monocrystalline diamond powder	Microdiamant
Silicone glue (Elastosil E43)	Wacker
UV curing glue (Loctite 3494)	Henkel Adhesives
Isolation tape (Super 33+ Vinyl electrical tape)	Scotch ™Brand
Film applicator	Byk Gardner
Polyethylene terephthalate foil	PuetzFolien
PTFE Fluoropore membrane filter	Advantec
Microscope glass slides	Hounisen
Tissue culture test plates (12 wells)	TPP Techno Plastic Products
pH meter (PHM 210)	Meterlab, Radiometer Analytical
FireSting GO_2	PyroScience
SLR camera (EOS 1300D)	Canon
Macro objective lens (Macro 100 F2.8 D)	Tokina
BlueLED(470 nm)	r-s components, Copenhagen
UV LED (405 nm)	r-s components, Copenhagen
Orange 530 nm longpass filter (OG530 SCHOTT, 52 mm x 2 mm)	Schott
Yellow 455 nm long-pass filter (GG455 SCHOTT, 52 mm x 2 mm)	Schott
#10 Medium Yellow Plastic Filter	Leefilters

6.2. Methods

6.2.1. Optical Characterization

Absoprtion Spectra

Absorption Spectra of the Oxazine perchlorate 170 dye, which was immersed in Hydromed D4 and knife coated onto a polyethylene terephthalate (PET) foil and covered with a layer of 9 µm Teflon AF, were obtained on a Thermo Scientific^{TM}Genesys 10S UV-Vis Spectrometer from Fisher Scientific GmbH (Schwerte, Germany) in a 10 mm precision cuvette made of Quartz SUPRASIL® by Hellma Analytics (Type 104-QS). The optode was cut to fit the size of the inside of the cuvette and placed to face the light source. Baseline correction of the spectra were acquired using a 1 M sodium hydroxide solution and a small piece of an uncoated PET foil.

Emission Spectra

Emission spectra of sensor foils were measured on a CLARIOstar Plus microplatereader from BMG Labtech (Ortenberg, Germany) in tissue culture test plates with 12 wells. The respective optodes were cut to fit the size of the wells, with the optical sensitive side of the optode facing down, which was fixated with PDMS (Silicone Elastomer), and the side with the proton impermeable PTFE Fluoropore membrane filter facing upwards. This way the change in emission intensity was measured upon different concentrations of ammonia were added into the wells. Baseline correction of the spectra were acquired using a 1 M sodium hydroxide solution.

6.2.2. Optical Measurements

Calibrations and Imaging set up

Calibrations as well as experiments were measured using a single-lens reflex (SLR) camerain combination with a macro objective lens and depending on the excitation source an appropriate filter was utilized. For excitation with a blue (470 nm) LED in combination with a short-pass filteran orange 530 nm longpass filter was chosen whereas for a 405 nm UV LED a yellow 455 nm long-pass filter was used. The LEDs were controlled by a trigger box(imaging.fish-n-chips-de). The software look@RGB (imaging.fish-n-chips-de) allowed

the gathering of the images and enabled the simultaneous control of the SLR camera and the LED light.
For the calibrations, sensor foils were mounted into a small (350 mL) or into a large aquarium (2 L), these were then filled with different buffer solutions or sodium hydroxide solutions.

Buffer and analyte solutions
Various buffer or analyte solutions were prepared for the respective calibrations dissolving adequate amounts of buffer salts or analyte salt in deionized water (Milli-Q, 18 MΩ cm). In order to set different pH values as requested NaOH and HCl standard solutions were utilized for adjustment.

6.2.3. Sensor foils

Sensor foil fabrication
Sensor foils were prepared via knife-coating sensor cocktails onto dust-free transparent polyethylene terephtalate (PET) foils. After applying the sensor chemistry in form of a cocktail onto the foil it can be distributed onto the foil by dragging a film applicator across the PET foil. Optical insulations as well as proton barriers were applied as will be discussed in section7.

7. Experimental

7.1. Ammonia Sensor with the pH Indicator Dye Ethyl Eosin (TM01& TM02)

The ratios and the fabrication steps for these sensor foils were derived from a prior study[61]. Implementations of a few deviations to the suggested sensor cocktail were the addition of a reference dye in order to conduct ratiometric imaging, the use of a different solvent due to the enhanced solubility of the indicator dye and varying insulation layers against pH and ionic strength. The sensor cocktails for each sensor foil consisted of 0.8 mg of the indicator dye ethyl eosin, 0.7 mg of the reference dye perylene, 2 g of 10 wt.% cellulose acetate propionate (CAP) in acetone, 2 mg of 4', 4''(5'')-Di-tert-butyldibenzo-18-crown-6 and 0.3 mg of methane sulfonic acid. This cocktail was knife coated onto a PET foil resulting in a layer with a thickness of ~12 µm after solvent evaporation. The subsequent steps were either applying a polytetrafluoroethylene (PTFE) Fluoropore membrane onto the wet sensor film or knife coating a 50 wt.% PDMS in hexane layer (30 µm) onto the dry sensor chemistry (see Table 5).

7.2. Ammonia Sensor with the pH Indicator Dye Bromophenol Blue (TM03 & TM06)

Additional sensor layers were fabricated according to a previous study[62]with different proton barriers applied. Therefore, each optode consisted of a cocktail of 1.3 mg Bromophenol Blue, which is the indicator dye, two fluorescent dyes, 2 mg Macrolex yellow and 0.2 mg Macrolex red, and 2 g of a mixture of 5 wt.% polymer, Hydromed D4, in THF. This was knife coated on top of a dust free PET foil and after the solvent evaporated a hydrogel layer of 6 µm remained. The various layers used as proton barriers were either a PTFE Fluoropore membrane, 90 wt.% PDMS in hexane or a 3.5 wt.% Teflon layer. The layer thicknesses as well as whether or not an additional layer containing diamond powder (DP) in order to increase the signal intensity was used can be obtained from Table 5. Only the PTFE Fluoropore membrane was applied instantly onto the still wet sensor cocktail whereas the other proton impermeable layers were applied using the film applicator. For further calibration measurements only the sensor foils TM03 and TM06 were used as TM04 turned out to show slow dynamics and hardly any reversibility in preliminary tests.

Table 5: Composition of proton barriers and film thicknesses of sensor foils TM01-TM06.

Sensor	Proton barrier	Additional layer containing DP	Wet film thickness [µm]	Resulting film thickness [µm]
TM01	PTFE Fluoropore membrane	-	-	75
TM02	50 wt.% PDMS in hexane	-	60	30
TM03	PTFE Fluoropore membrane	-	-	75
TM04	90 wt.% PDMS in hexane	-	60	54
TM06	3.5 wt.% Teflon layer + 1.1 wt.% DP	3.5 wt.% Teflon layer + 1.1 wt.% DP	240	22

7.3. Sensor Foils containing the pH Indicator Dye Oxazine 170 perchlorate (TM07-TM16)

Optodes containing the indicator dye Oxazin 170 perchlorate were prepared based on the work of a former study.[55]The difference made was the amount used for each sensor foil. For the first ones 120 µL of a 2 mg/mL dye stock in EtOH were mixed with 2.4 mL of a 10 wt.% ethyl cellulose in EtOH stock and a Fluoropore membrane placed onto the still wet cocktail, which had been knife coated (120 µm wet film) onto a PET foil beforehand. These sensor foils were then dried in a drying oven at 55 °C overnight. In subsequent sensor foils the amounts of the indicator dye and the polymers as well as the solvents were altered but the procedure remained the same. The used polymers were ethyl cellulose (EC), cellulose acetate propionate (CAP), hydromed D4 and the solvents ethanol, chloroform, toluene/ethanol (8/2), isopropanol/H_2O (9/1) and tetrahydrofuran (THF). The concentrations of the polymer in the polymer solvent cocktails were 5 wt.% or 10 wt.%. As ion impermeable filters either served a polytetrafluoroethylene (PTFE) Fluoropore membrane, which was attached onto the wet sensor layer, or a Teflon AF layer knife coated (120 µm wet film) on top of the dried sensor layer with a concentration of either 10 wt.% or 13.5 wt.% Teflon AF. The compositions can be seen in Table 6.

Table 6: Composition of all sensor foils containing pH indicator dye Oxazine 170 perchlorate

Sensor	Dye [mg]	Used Polymer	Polymer [wt.%]	Used Solvent	Polymer stock added	Used proton barrier
TM07	0.24	EC	10	EtOH	2.4 mL	FP membrane
TM08	0.3	EC	10	EtOH	3 mL	13.5 wt.% Teflon AF
TM09	0.3	EC	10	EtOH	3 mL	FP membrane
TM10	0.6	EC	5	EtOH	3 mL	-
TM11	0.8	EC	10	Toluene/EtOH	1.3 g	-
TM12	0.7	CAP	10	$CHCl_3$	1.2 g	-
TM13	0.5	D4	10	Isoprop/H_2O	1.2 g	-
TM14	1.2	D4	7.5	Isoprop/H_2O	1.7 g	10 wt.% Teflon AF
TM15	1.2	D4	7.5	Isoprop/H_2O	1.7 g	FP membrane
TM16	0.9	D4	5	THF	2 g	FP membrane

7.4. Sensor Foils containing Oxazine 170 Perchlorate and a Reference Dye (TM17-TM25)

The manufacturing of these optodes was analogously to the approach described in the methods section of the manuscript within this thesis and can be found in section 12.1. The only distinction is constituted by varying amounts of the sensor components and these are listed in Table 7.

Table 7: Composition of all sensor foils containing pH indicator dye Oxazine 170 perchlorate and reference dye Macrolex yellow.

Sensor	Dye [mg]	Reference Dye [mg]	Used Polymer	Polymer [wt.%]	Used Solvent	Polymer stock added	Used proton barrier
TM17	1.0	1.1	D4	5	THF	2.0	FP membrane
TM20	1.3	1.4	D4	5	THF	2.1 g	FP membrane
TM21	1.0	1.2	D4	5	THF	2.0 g	FP membrane
TM22	1.0	1.15	D4	5	THF	1.5 g	FP membrane
TM25	0.8	0.8	D4	5	THF	1.5 g	FP membrane

7.5. pH and O_2 Sensitive Sensor Foils

The fabrication of the sensor foils sensitive towards pH and oxygen as well the used amounts and the subsequent calibration steps can be found in section12under the methods part of the manuscript.

7.6. Calibrations and Cross-sensitivity Measurements

For the calibration of the sensor foils the appropriate amounts of ammonium chloride for addition to the aquarium filled with either a phosphate buffer solution or a sodium hydroxide solution were calculated with the Henderson-Hasselbalch equation (see equation 4.1.1.). TM01, TM02, TM03 and TM06 were measured in an aquarium filled with 2 L phosphate buffer (0.1 M, pH 7) and via addition of an ammonium chloride stock solution with a concentration of 225 g L^{-1}. The aquarium was not emptied after each concentration step

throughout a calibration. Hence, the already added NH_4Cl stock solution volumina were taken into consideration to reach the respective total volume for each calibration step. As an example, the calibration steps and calculated concentrations for TM03 and TM06 can be seen in Table 8. TM01 and TM02 were calibrated between 0-1000 ppb.

Table 8: Ammonium chloride amounts for calibration in 2 L. Total NH_4Cl volume represents the entire volume of NH_4Cl in the 2 L tank per concentration. Added NH_4Cl volume takes the already added NH_4Cl into consideration.

NH_3 [ppm]	NH_3 [mmol/L]	NH_4^+ [mmol/L]	NH_4Cl [ppm]	TotalNH_4ClVolume [mL]	NH_4Cl Volume added [mL]
0	0	0	0	0	0
0.03	0.002	0.306	16.375	0.146	0.146
0.1	0.006	1.02	54.584	0.485	0.340
0.3	0.018	3.061	163.750	1.456	0.970
1	0.059	10.204	545.841	4.852	3.396
3	0.176	30.613	1637.523	14.556	9.704
10	0.587	102.04	5458.410	48.519	33.963

Other calibrations were conducted in a small aquarium filled with 300 mL 0.5 M sodium hydroxide solution with pH > 12 and addition of an ammonium chloride solution with a concentration of 300 g L^{-1}(see Table 9). For all calibrations the chosen calibration steps were maintained for around 12-15 minutes and pictures taken every 3-5 minutes.

To investigate the response of the ammonia O17MY optode towards possible cross-sensitivities calibrations of TM17 and TM20 were conducted via addition of different quantities of ammonium chloride with a concentration of 300 g L^{-1} for ammonia calibration curves. The addition of various volumes of a 300 g L^{-1} trimethylamine hydrochloride stock solution lead to a TMA calibration curve. Table 9shows the calculated amounts of the two amines.

In order to measure towards hydrogen sulphide a small aquarium, with the optode TM20 attached to the inside, was filled with distilled water, made acidic by adjusting the pH to pH 4 by adding a 1 M HCl solution and saturated the water with nitrogen to make it oxygen free. A 0.01 M sodium sulphide solution was then added to obtain various concentrations.

Table 9: Ammonium chloride and trimethylamine hydrochloride amounts for 300 mL. Total NH_4Cl Volume added takes the already added NH_4Cl into consideration.

NH_3 [ppm]	NH_3 [mmol/L]	TMA [mmol/L]	NH_4Cl [ppm]	TMAHCl [ppm]	NH_4Cl / TMAHClTotal Volume added [mL]
5	0.249	0.085	15.7	8.08	0.016/ 0.008
10	0.587	0.169	31.4	16.2	0.016/ 0.008
20	1.174	0.338	62.8	32.3	0.031/ 0.016
30	1.762	0.508	94.2	48.5	0.031/ 0.016
40	2.349	0.677	125	64.7	0.031/ 0.016
60	3.523	1.015	188	97.0	0.063/ 0.032
80	4.698	1.35	251	129	0.063/ 0.032
100	5.872	1.69	314	162	0.063/ 0.032
160	9.395	2.71	502	259	0.188/ 0.097

7.7. Data analysis

The determination of the calibrations as well as the analysis of images from the experiments were conducted similarly to the steps mentioned in section 12.3 under the calibration and data analysis part of the manuscript as the utilization of the software ImageJ was consulted for all measurements.

7.8. Biological Applications

Sediment experiment

Sediment was collected from a lake in Vennelystparken, Aarhus (Denmark, 56°09’53.7"N, 10°12’28.7"E). The sediment was sieved with a sieve of a 1.78 mm^2mesh size before utilizing it for analysis and stored wrapped in plastic to prevent withering.

An aquarium able to hold 2 L was filled one third with the prepared sediment and on top of that with another third of water. Half of the ammonia sensitive optode (TM17) of interest was covered in sediment and the other half in the water phase.

For the first three hours images of the optode immerged in the sediment and water phase were taken every 30 minutes. Upon that, 25 mL of a 300 g L^{-1} ammonium chloride solution were added into the water phase. Images were gathered every five minutes for a total of 30 minutes. This was followed by another addition of 12.5 mL ammonium chloride solution and pictures taken for the same amount of time and also in an interval of five minutes. The last addition occurred via injecting 12 mL of the same NH_4Cl solution directly into the sediment right in front of the sensor. Again, recording times were chosen every five minutes for a total of 40 minutes for this last addition step.

Soil – pig manure experiment I

The soil sandwiches were fabricated as can be seen in Figure 11 and similar to the procedure described in section 12.4 within the manuscript. The only preliminary deviations to the sandwich that was built afterwards are the thickness of the sandwich as only two rows of microscope slides were glued to one of the glass plates with an UV curing glue resulting in an inner thickness of 2 mm of the soil sandwich. Also, the positioning of the optodes was different. A pH sensor foil and an ammonia sensitive optode (TM22) were fixated onto the glass plate with the microscope slides. Soil (m=72.93 g) was applied on top of these two optodes until the soil almost covered the entire sensors. The other glass plate was fitted with a big O_2 optode, which was placed a few mm lower compared to the optodes on the opposite side resulting in the oxygen sensor being covered completely in soil. This side was utilized to close and then seal the sandwich with isolation tape. The pig manure was introduced into the sandwich with the help of a syringe.

The soil was collected and treated according to the methods part in section 12.5 within the manuscript as the same soil was involved in both experiments. The pig manure was collected from Aarhus University and provided by Jesper Nørlem Kamp with features as follow: total-N: 3.93 kg/ton (NH4-N: 2.89 kg/ton; organic-N 1.04 kg/ton), phosphorus: 0.62 kg/ton and a dry matter content of 3.09%.

The imaging set up was similar to the one elucidated in the manuscript under the methods part (section 12.2). Therefore, one ratiometric RGB set-up per side was used with the only alteration lying in the choice of excitation light. For the side with the NH_3 and pH optode an UV LED (405 nm) paired with a yellow long-pass filter (455 nm) and for the other side with the O_2 optode facing the set-up a blue LED (470 nm) together with an orange long-pass filter (530 nm) were employed.

Firstly, an image with dry soil of all three optodes was recorded. Thereafter, 10 mL of water and after that another 5 mL were added on to the soil and images taken, respectively. This was followed by adding 7 mL of pig manure with a syringe to the soil surface. Images were then collected for the next 50 minutes with an interval of every five minutes. Moreover, about 3 mL of pig manure were injected in front of each optode (pH and ammonia) and this was tracked by taking images every five minutes again for a total of 50 minutes.

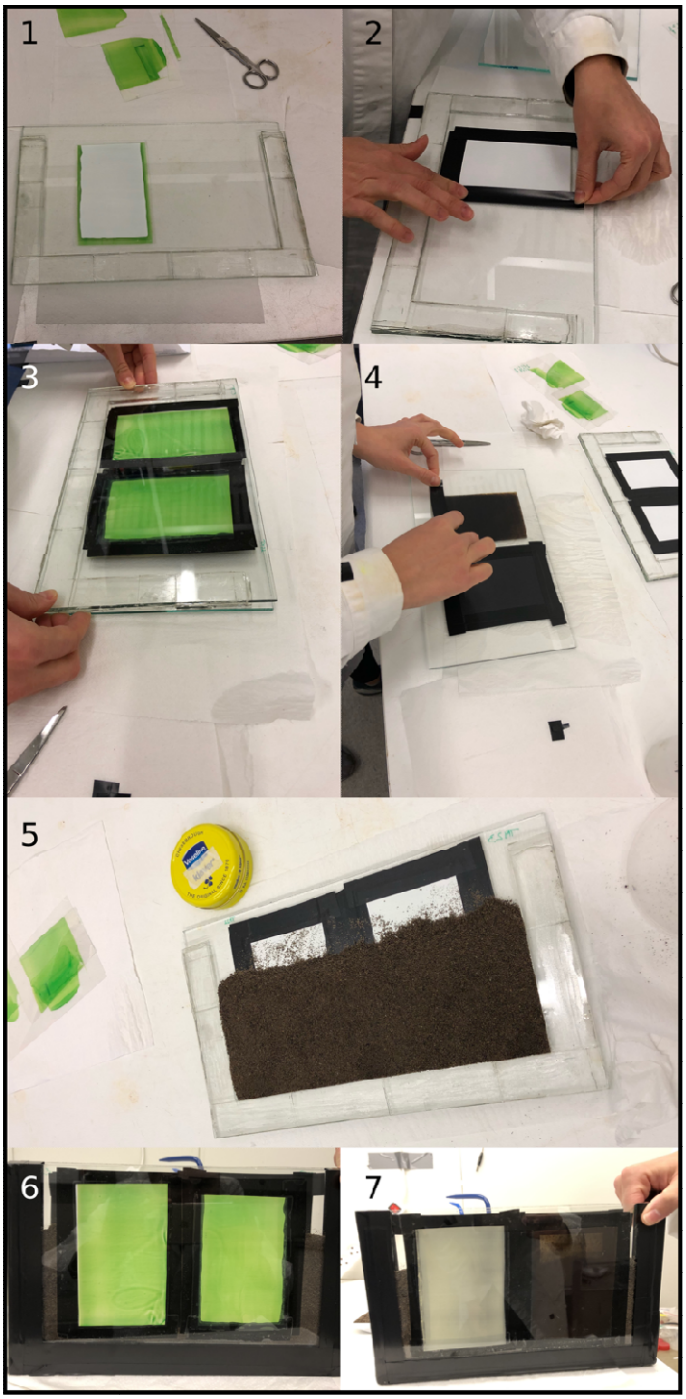

Figure 11: Fabrication of soil sandwich. 1) Glass slide one with the microscope slides attached and an ammonia optode positioned ready to be fixated. 2) Taping of the sensor foil onto the glass plate with the sensitive side of the optode facing upwards and the non-sensitive PET side being attached against the glass. 3) View of the readily prepared glass plate of the side facing the SLR camera and excitation light. 4) Fixation of the pH and O_2 optodes with isolation tape on the second glass plate. 5) Application of the soil before the sandwich is closed. 6) Closed soil sandwich with the ammonia optodes facing the camera. 7) Closed soil sandwich with the pH and O_2 optodes facing the camera.

7.9. Measurement Set-up

A general overview of the setup for the optical measurements. A single-lens reflex (SLR) camera was equipped with a macro objective lens and attached to that was a longpass filter (Filter 1), either an orange (530 nm) or a yellow (455 nm) one. Immediately after the first filter a second filter (Filter 2), a #10 medium yellow plastic filter, was mounted onto the lens hood. Various LED lights were used as excitation light and controlled by a trigger box, which was connected to the camera and to the light itself as well as to the computer in order to be managed via a software. The respective optodes were mounted into an aquarium for calibration purposes. For subsequent experiments the distance between the camera and the aquarium or the experiment setup was kept the same.

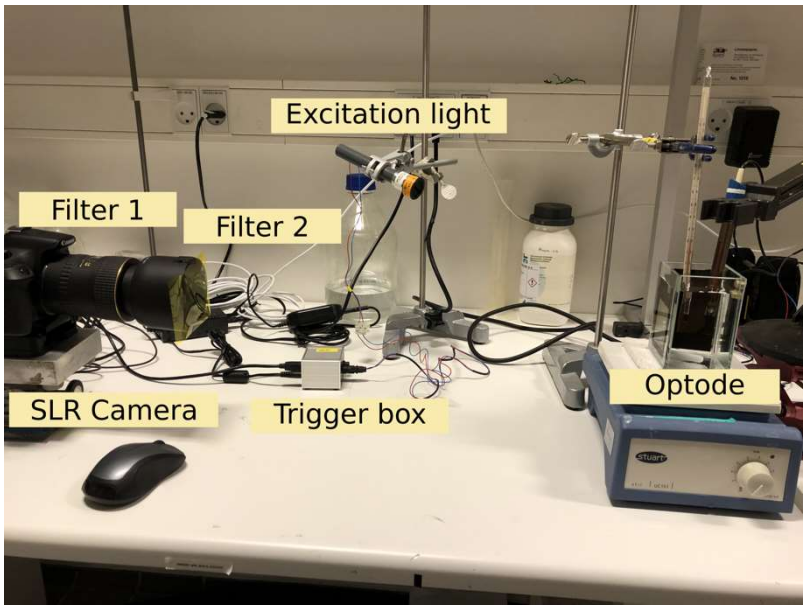

Figure 12: Measurement setup utilized for all calibrations and experiments showing the single-lens reflex camera, two different filters, a trigger box together with an excitation light and the optode to be measured.

8. Results and Discussion

8.1. Scope of this Thesis

This thesis aimed for the development of a novel optical ammonia sensor and the application of such in biological systems in order to gather better understanding of the nitrogen dynamics by visualizing NH_3 using an optode. There are great differences in ammonia concentrations that are present and therefore expected for detection within sediments and soils. Microbial processes within sediments show concentrations in a low ppb range, whereas in soils ammonia volatilization through fertilization results in concentrations of up to 200 ppm.[63,2] This demand for detecting different levels of ammonia and as there are a number of already existing ammonia sensors able to sense in the ppb range, the path of this thesis started with the reproduction of some of those optodes paired with the implementation of varying protective layers. Thereupon, the combination of a pH sensitive dye, which has previously been used for sensing ammonia from 0-60 ppm[55], with an inert reference dye and a proton impermeable layer in order to facilitate ratiometric based imaging of ammonia followed.

Hence, different sensor materials, cross-sensitivities, the response behaviour of the sensor foil, optical characterizations as well as the application of the optode into a biological system were studied and conducted. The biological system of choice was pig manure being applied onto soil and therefore the changing chemical microenvironment after this process and the headspace above the soil were of interest. The outcomes of this study amounted to a manuscript, which makes up part IV of this thesis. Thus, the exact design of the newly developed optode and the imaging approach can be found in section 11.1 (Results and Discussion in the manuscript).

The work leading towards the manuscript as well as the related additional experiments and results are shown and discussed within this section.

8.2. Characterization and Calibrations of Ammonia Sensitive Optodes at ppb Concentration Levels

8.2.1. Calibration of TM01, TM02, TM03 and TM06

The measurement of ammonia in a trace level range due to the toxicity of ammonia at concentrations from 25 ppb towards fish and organisms as well as the prevalence of NH_3 within sediments was pursued within the work of Waich *et al* , from which the sensors TM01 and TM02 are derived, and Abel *et al*, providing the ratios for sensors TM03 and TM06.[61,62] The possibility to implement a ratiometric two wavelength imaging approach with both sensors lead to the fabrication of such with some alterations but the utilization of the suggested general principles and chemicals.

Calibrations of the ammonia sensitive foils TM01, TM02, TM03 and TM06 were conducted with the optical measuring set up described in section 6.2.2 using an UV LED as excitation source and a yellow longpass filter but different ammonia concentrations.

The sensing principle of TM01 and TM02 consists of the deprotonation of the pH indicator dye (ethyl eosin), where the inert reference dye (perylene) does not change in emission intensity. Thus, the fluorescence of the TM01 and TM02 optodes increased when the sensors were exposed to ammonia and this can be detected and compared via a colour camera. This camera utilizes different colour channels (red, blue and green) in order to gather an image. Here, the altered fluorescence of the ethyl eosin is located in the green channel whereas the emission of perylene identifies with the blue one. This is why the green channel was divided by the blue channel in order to get an increasing ratio, which was plotted against the ammonia concentrations. The comparison of the calibration curves can be found inFigure 13 as well as the influence of the two different gas permeable membranes (a PTFE fluoropore membrane and a PDMS layer) that have been applied onto the planar optodes. It became apparent that the ratio of TM01 is enhanced compared to the ratio of TM02, which probably is a result of the white and reflecting fluoropore membrane increasing the intensity because of light scattering.[59]

Also, there is an increased difference in the change of the ratio within TM01 as the enhancement of intensity between 0-1000 ppb of ammonia is less pronounced in TM02. The

reason for this could be the altered dynamic properties due to the PDMS layer as the sensor cocktail remained the same for both optodes. In addition, formation of aggregates or inhomogeneous distribution of the dyes could be responsible for the initial decrease of the ratio for the first two calibration steps.

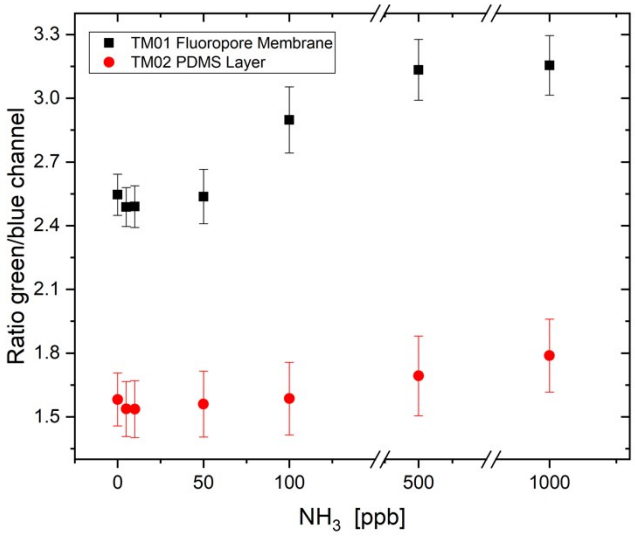

Figure 13: Calibration curve of TM01 (Fluoropore membrane) and TM02 (PDMS layer) in comparison illustrating the impact of the used layers.

Figure 14 shows the change in colour of the already discussed optodes TM01 and TM02 at 0 ppb NH_3 (protonated indicator dye) and at 1000 ppb NH_3 (deprotonated indicator dye). These photographic images emphasize the mentioned differences in intensities of the two sensor foils, where an increase in intensity is noticeable for TM01 but a rather weak enhancement for TM02 upon exposure towards ammonia.

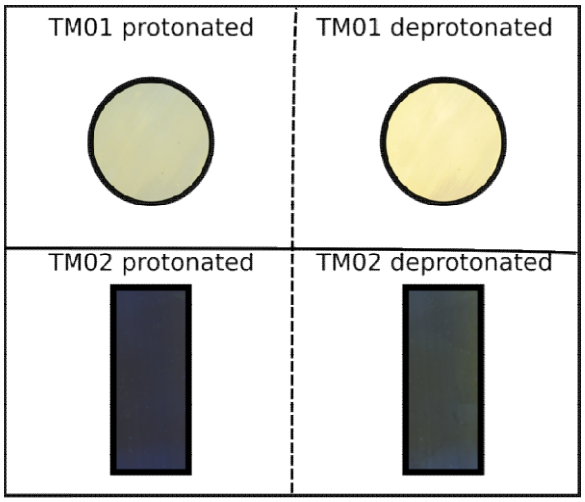

Figure 14: Photographic images of the optodes TM01 and TM02 in buffer solution while calibration under 405 nm LED excitation.

The calibration curves of the planar optodes TM03 and TM06 are shown in Figure 15 and illustrate the different responses to ammonia exposure between 0-10 ppm NH_3. In general, the sensing principle relies on a Förster resonance energy transfer (FRET) between the donor (Macrolex yellow) and the acceptor (Macrolex red), which is not affected by the non-fluorescent indicator dye (bromophenol blue) when protonated. As soon as the indicator dye gets deprotonated by ammonia the FRET cascade is quenched due to the changing absorbance behaviour of bromophenol blue.[62] This behaviour together with the signals of the fluorescent dyes can be detected again using a colour camera and is referenced by dividing the colour channels of interest. Here, the red channel was divided by the blue channel. The sensor foil with the fluoropolymer membrane (TM03) showcased a stepwise decrease of the ratio (red/blue) suggesting that the indicator dye is protonated at 0 ppm of ammonia and gets increasingly deprotonated, thus, quenching occurs with enhanced ammonia concentrations. In contrast, the optode with the Teflon AF membrane (TM06) had a diminished intensity and it seems that it got completely quenched at a lower NH_3 concentration already. There are two possible factors influencing these outcomes, one explaining the diminished ratio in general can be derived from the fact that the Teflon AF layer lacks in the ability of light scattering effects[59], which helps to generate higher intensities talking of the PTFE membrane. The other factor influencing the seemingly quick deprotonation can be attributed to a porous layer of Teflon AF leaving holes for the buffer solution to enter and therefore interactions of pH and ions with the sensor chemistry take place instead of providing an ammonia selectivity. This can also be seen in Figure 16 as TM03 is of an orange colour when protonated and no NH_3 diffused into the sensor and when deprotonated at the highest NH_3 concentration no colour

can be seen suggesting the quenching process took place. Whereas the intensity of TM06 showcased to be quenched at an earlier ammonia concentration already also illustrating some inhomogeneous spots.

Unfortunately, the requirements of measuring in a ppm range were not met by these optodes, which is not surprising due to the low pK_a values of both pH indicator dyes, Ethyl eosin has a pK_a of 3.8 and Bromophenol blue a pK_a of 4.1.[61,62]These low values enable ammonia sensing in the ppb range as the sensitivity of a pH indicator dye is dependent on the pK_a. Therefore, this led to the use of a different pH indicator able to operate in higher concentration levels, which will be further discussed in the next section.

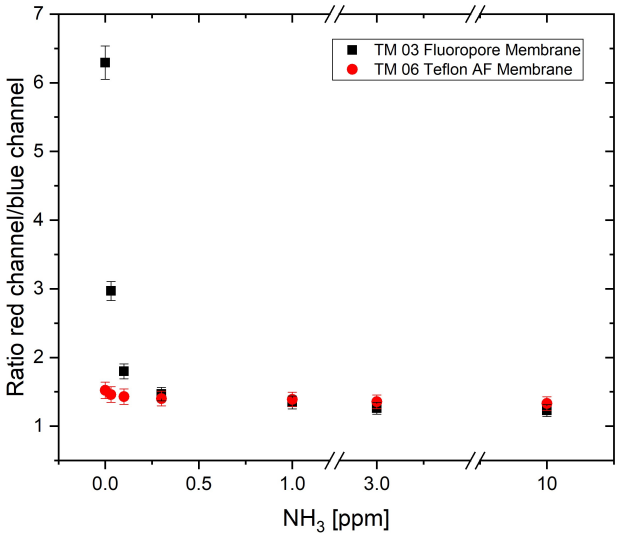

Figure 15: Calibration curve of TM03 (Fluoropore membrane) and TM06 (Teflon AF membrane) in comparison illustrating the effectiveness of the used layers.

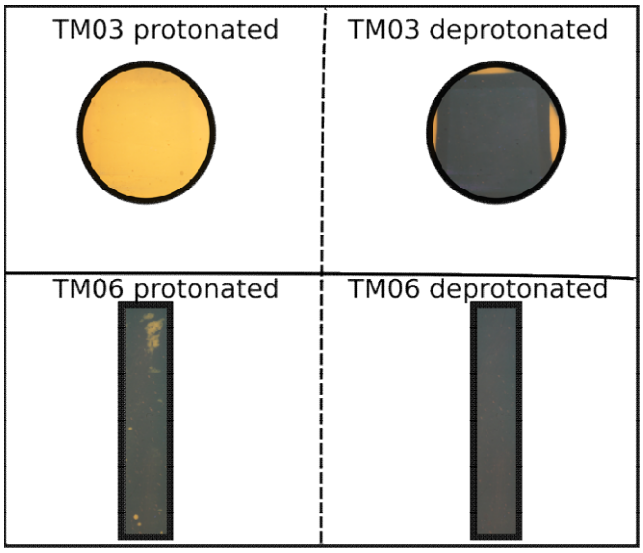

Figure 16: Photographic images of the optodes TM03 and TM06 in buffer solution while calibration under 405 nm LED excitation.

8.3. Characterization, Calibration and Screening of the new O17 Optodes at ppm Concentration Levels

The fluorescent pH sensitive dye Oxazine 170 perchlorate (O17) has already been utilized for sensing ammonia from 0 to 60 ppm in a previous study[55] where it was immobilised in the polymer ethyl cellulose (EC). When the dye is deprotonated a colour change from blue to pink occurs as the absorption and the emission properties change (Figure 20). As already mentioned in section7.3, where the exact amounts and materials of the prepared optodes are listed, the sensor foils TM07-TM10 were manufactured according to the literature with O17 and EC dissolved in ethanol. The materials were used in varying amounts as all optodes turned whitish instead of staying blue due to crystallisation of the polymer, which can be seen in Figure 17A. This did not lead to any improvement, thus, the choice of another solvent followed (TM11). Upon evaporation of the solvent mixture toluene/ethanol (8:2) the sensor turned purple instead of staying blue (Figure 17B), which could be due to the change in polarity.

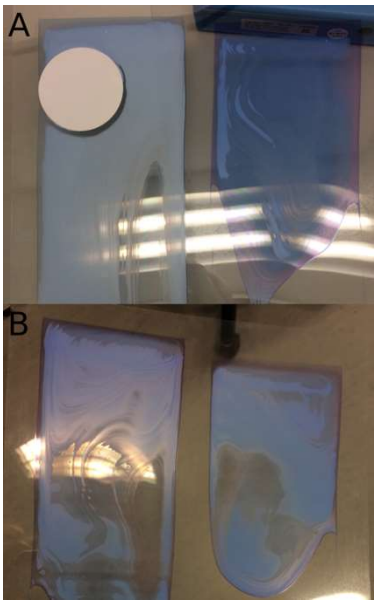

Figure 17: A) Image of the sensor foil upon ethanol evaporated and left a crystallized polymer (EC) in which the indicator dye was immersed. B) Image of the sensor foil upon evaporation of a different solvent mixture, toluene/ethanol (8:2), and EC, which turned purple.

Adjacently, cellulose acetate propionate (CAP) was mixed with the dye and chloroform (TM12) leading to a blue optode without signs of crystallisation. Unfortunately, no change in colour was observed upon addition of drops of HCl, NaOH or NH_4Cl solution. Therefore, the composition was altered once more to the polymer hydromed D4 and the solvent combination isopropanol/H_2O (9:1) (TM13, TM14, TM15) or the solvent tetrahydrofuran (TM16) together with the indicator dye yielding blue optodes. These showed a response when drops of the already mentioned base, ammonium chloride solution and then to reverse the colour change drops of an acid were applied onto the sensor chemistry.

These findings lead to the planar optodes TM14, TM15 and TM16 with the proton and ion impermeable layers Teflon AF and two fluoropore membrane PTFE filters, respectively. As can be seen in Figure 18, the calibration curves show diverse responses to various concentrations of ammonia. In terms of increased ratios, the optodes with the PTFE fluoropore membranes are advantageous over TM14 and, even though the sensor foil with the highest intensities turned out to be TM15, the composition of TM16 was selected for further steps. As it was observed that the sensor chemistry of TM15 diffused through the applied polytetrafluoroethylene filter and got augmented there whereas this was not the case for TM16, perhaps due to the lower boiling point of THF, hence a faster evaporation of such. Also, an easier application of the membrane was enabled using THF as solvent.

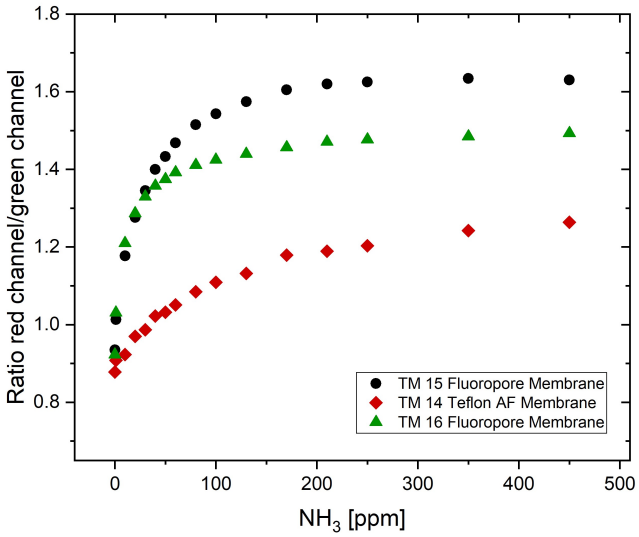

Figure 18: Calibration curve of TM15 (Fluoropore membrane, Isopropanol/H2O, D4), TM14 (Teflon AF membrane, Isopropanol/H2O, D4) and TM16 (Fluoropore membrane, THF, D4) in comparison illustrating the results of the different approaches.

However, the inert dye Macrolex yellow (MY) was introduced into the sensor chemistry of TM16 resulting in the optode TM17. A ratiometric two-wavelength imaging approach was already feasible before implementing the reference dye but as becoming apparent in Figure 19 the introduction of MY appears to result in an increase in emission of the planar optode upon excitation in the calibration and measuring set up and also the change in colour is easier to recognize. This alteration of the different colours dependant on the protonated or deprotonated state of the indicator dye is illustrated in Figure 20, where an optode with only containing Oxazine 170 perchlorate undergoes the transition from blue (protonated dye) to pink (deprotonated dye). In contrast, the sensor including MY together with O17 showcases a transition from green (protonated dye) to orange (deprotonated dye). Further details about the newly developed planar optode TM17 as well as the calibration curve can be found in section 11.1 within the manuscript.

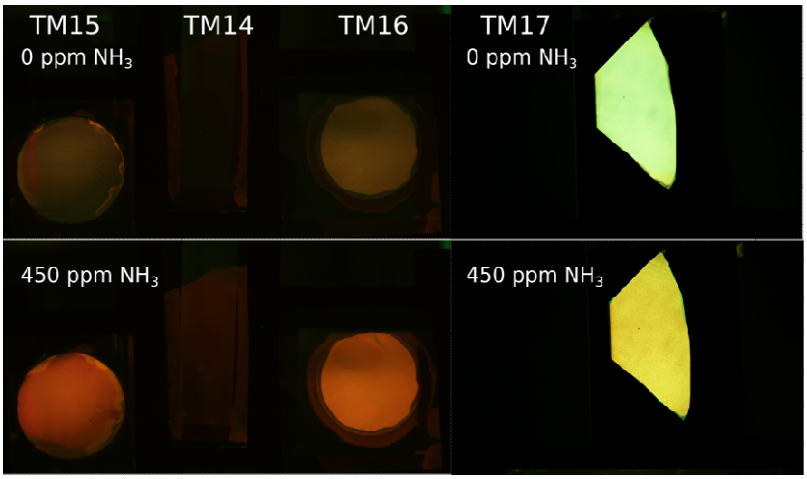

Figure 19: TM14-16 O17 optodes prepared with different solvents and membranes/layers-top: after excitation with a (470 nm) blue LED combined with an orange long-pass filter and no addition of ammonia. bottom: after excitation with blue LED and addition of 450 ppm NH_3. On the right: TM17 optode with O17 and MY and Fluoropore membrane - excitation with (405 nm) UV LED and a yellow longpass filter and also no addition of ammonia and at the bottom after adding 450 ppm NH_3.

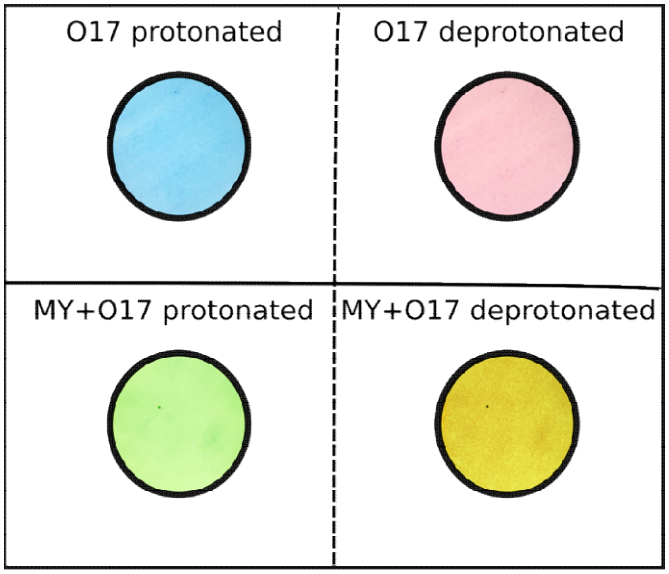

Figure 20: Top: Photographic images of the optode only containing the indicator dye Oxazine 170 perchlorate (O17) when it is protonated (blue) and deprotonated (pink). Bottom: Photographic images of the optode containing the indicator dye O17 in combination with the reference dye Macrolex yellow (MY) when it is protonated (green) and deprotonated (orange).

8.4. Optical Characterization

8.4.1. Absorption and Emission Spectra

The change in color, which is already mentioned and shown in section 8.3, indicates that a change of absorption and fluorescence properties takes place and this was further investigated by recording absorption and emission spectra.

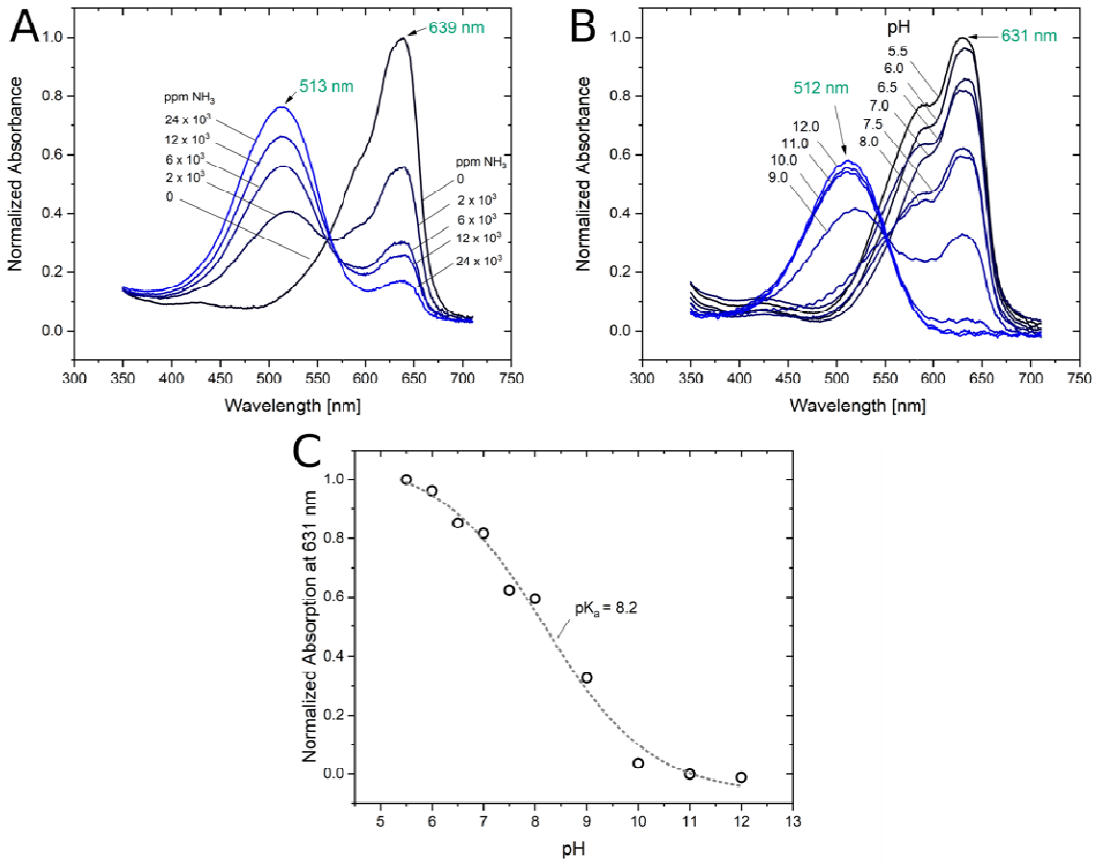

Figure 21: A: Changes of the absorption properties of Oxazine 170 perchlorate (O17) coated onto a PET foil and consisting of a transparent Teflon AF layer upon exposure to various concentrations of NH_3. B: Normalized absorption of another piece of the O17 optodewithout a Teflon layer exposed to different pH values. C: Normalized absorption at 631 nm as a function of pH to gather the pK_a.

Hence, in Figure 21A the absorption properties of an optode with just the O17 dye immobilized in Hydromed D4 and a Teflon AF membrane, which is transparent in order to enable absorption measurements, is depicted. There the alteration from the absorption maximum at 639 nm to the maximum at 513 nm with increasing ammonia concentration is

displayed, indicating a blue shift (hypsochromic shift). This behavior was further investigated in Figure 22B, which illustrates the emission spectra of another O17 optode with the only difference being the protective layer, a PTFE Fluoropore membrane. The fluorescence emission maximum at 662 nm declined when the dye got deprotonated and so did another, diminished emission peak at 502 nm. Contrary to that, the intensity at 602 nm rose with an enhancement of the level of ammonia. These observations of the alternating emission peaks are in accordance with literature but there are differences in the positions of the peaks. In there the rising emission peak lies at 565 nm when deprotonation of the O17 dye takes place and the declining peak at 630 nm.[55] These shifts of 37 nm and 32 nm, respectively, can be due to the different materials that were used for the optodes as well as the choice of fluorescence detection devices, which were not the same either. The involvement of the reference dye MY within the sensor is shown in Figure 22D, where the emission peak at 502 nm then showed higher intensities, which were still declining the more ammonia was introduced. In addition, the emission peak at 658 nm slightly shifted but also remained the same behavior of depletion due to deprotonation of the indicator dye. In connection with that the peak at 602 nm gained in intensity and as can be found in Figure S1 within the supporting information of the manuscript (sectionIV.13) this is the reason for the rising ratio when the ratiometric imaging approach via a color camera was conducted. The red channel got divided by the green channel and the declining emission peak at 502 nm of MY can be assigned to the green one. And even though the emission peak at 658 nm, which lies within the red color channel, lost in intensity, the surge in intensity of the peak at 602 nm also located within the red channel lead to a higher ratio.

Since the Oxazine 170 perchlorate is a pH indicator dye, absorption spectra at various pH values of an optode without a membrane were recorded. Hence, Figure 21B demonstrates the normalized absorbance spectrum and shows a similar course to the one shown Figure 21A of the peak alterations due to deprotonation of the dye. Moreover, in the attempt to find out about the pK_a of the used pH indicator dye the normalized absorbance at 631 nm was plotted against the pH values resulting in a pK_a of 8.2. The higher pK_a can be seen as an explanation for the potential of measuring in a higher ammonia concentration range.

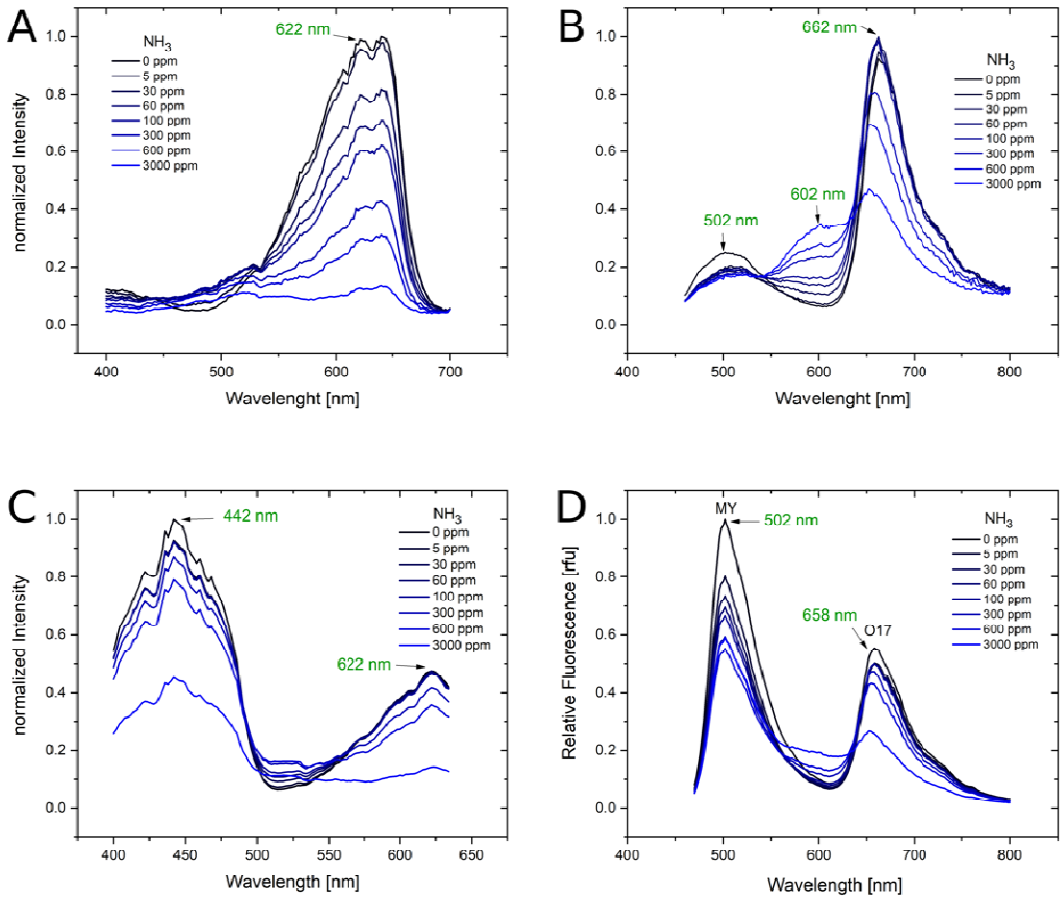

Figure 22: A: Excitation spectrum with normalized intensity of Oxazine 170 perchlorate (O17) immersed in hydromed D4 and doctorblated onto a PET foil with a PTFE fluoropore membrane applied on top. B: Emission spectra of the same O17 optode mentioned in A with an excitation of 440 nm. C: Excitation spectrum with normalized intensity of O17 together with the reference dye Macrolex yellow (MY) immersed in hydromed D4 and doctorblated onto a PET foil with a PTFE fluoropore membrane applied on top. D: Emission spectra of the same O17/MY optode mentioned in C with an excitation of 445 nm.

8.5. Cross-Sensitivity

There are several other amines with the potential to interfere with ammonia measurements due to their ability to also diffuse through the gas permeable protective layer and deprotonation of the indicator dye. As there is one amine in particular, which is trimethylamine, occurring within several organisms, cross sensitivity measurements of such and ammonia from 0 to 150 ppm were conducted. The diminished response of the sensor foil towards trimethylamine compared to the response to ammonia can be seen in the calibration curves in Figure 23. This enhanced response to ammonia over trimethylamine could be due to the bulky and hydrophobic properties of trimethylamine, which influence diffusion into the rather polar matrix of the sensor.[61]

In addition, hydrogen sulphide, which also occurs in sediments, is an acidic gas and is able to also diffuse through the gas permeable membrane.[64] Therefore, the investigated cross-sensitivity towards H_2S is depicted in Figure 24 where no response was demonstrated by the sensor system. In contrast, the same optode was calibrated towards ammonia as well showing the expected response.

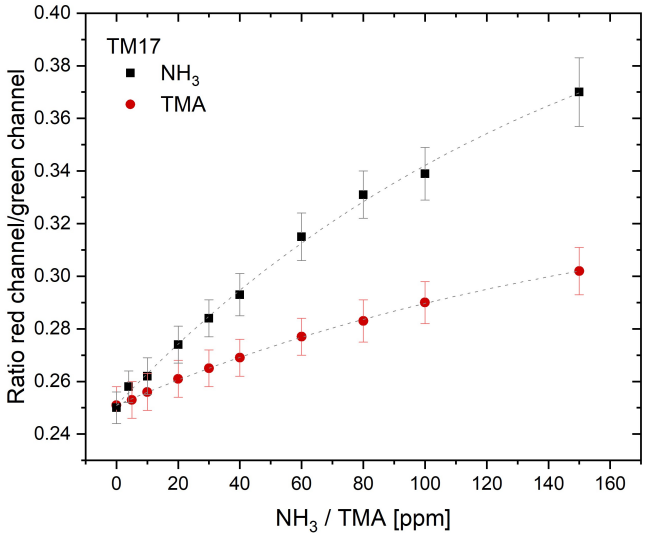

Figure 23: Calibration curves of TM17 for ammonia and trimethylamine showing a diminished response of the TM17 optode towards trimethylamine.

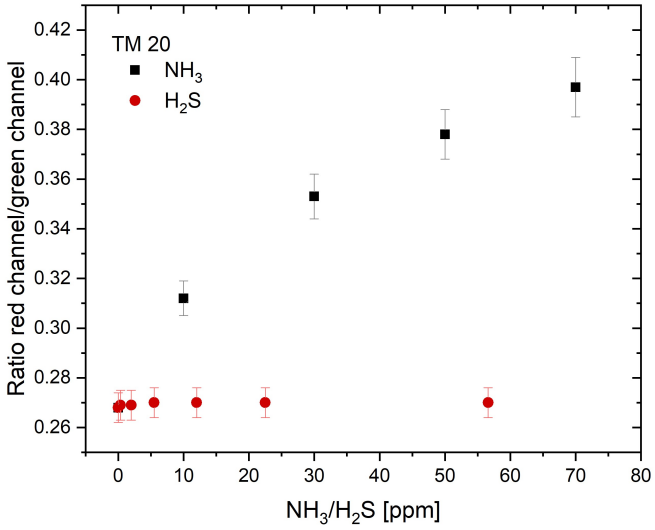

Figure 24: Calibration curve of TM20 for ammonia and H_2S – illustrating no response for H_2S.

8.6. Response curves

A response curve towards NH_3 concentrations from 0 to 800 ppm was recorded (Figure 25) together with the recovery of the sensor, which showed that the planar optode is fully reversible. However, a specific recovery time was not identified as the first image was taken 30 minutes after the aquarium was filled with tab water and air introduced with the help of an aquarium pump in order to eliminate remains of ammonia. Figure 26 demonstrates a close up outlining that the sensor response lies at around 90 seconds. These tests were carried out with the ammonia optode TM22 which was prepared according to the steps mentioned in section 7.4with the amounts listed in Table 7.

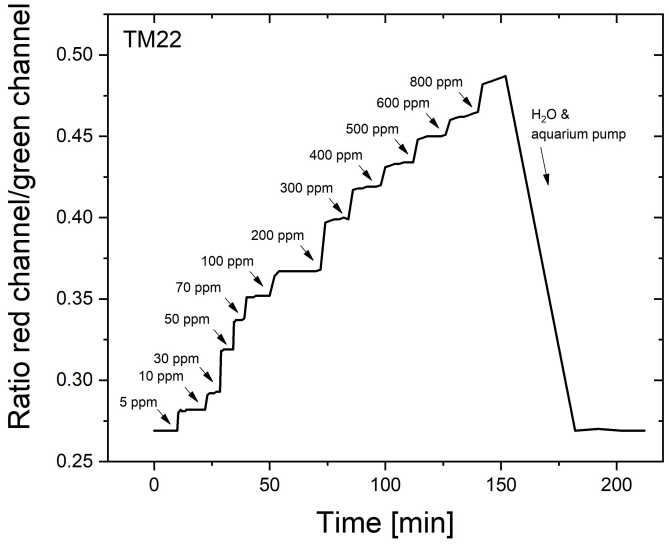

Figure 25: Response curve of an NH_3optode(TM22) at different ammonia concentrations and the recovery after 30 minutes due to the addition of H_2O and an aquarium pump.

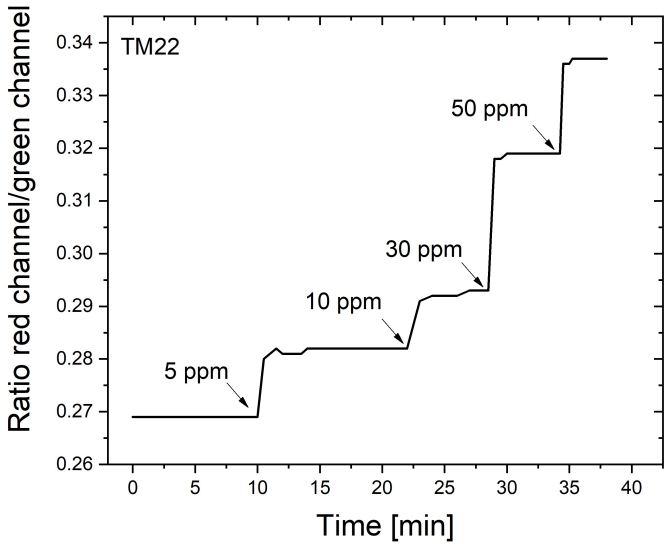

Figure 26: A close up of the same ammonia optode (TM22) to investigate the response time upon addition of various ammonia concentrations (0-50 ppm).

8.7. Measurement in Sediment

In order to test the planar optode and its ability to visualize ammonia within a water-locked biological system a sensor foil with the same composition as the in section 7.4 mentioned TM17 was attached to the inside of an aquarium. Half of that optode was covered in sediment and the other half in the water phase that was poured on top of the sediment layer (see Figure 27). The imaging set up remained the same as it was for the calibration, which is described within the manuscript together with the calibration curve of the sensor foil (section 11.1).

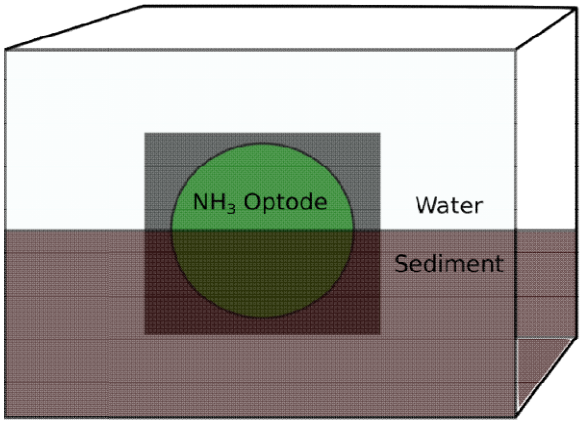

Figure 27: Set up of the aquarium, with an NH_3 optode mounted to the inside, filled with sediment and water. A SLR camera together with an UV LED lamp as excitation source were placed in front of the side with the optode attached to it.

Sediments are valuable parts of ecosystems for converting, eliminating or assimilating nitrogen.[65] This is possible because of aerobic as well as anaerobic processes within the nitrogen cycle. This way, sediments are capable of counterbalancing between assimilatory and dissimilatory actions on a spatially small-scale[65], making an optode a good choice of sensing tool. The consumption of ammonia or nitrate, helping certain species to grow, makes up the assimilatory part. Whereas dissimilatory pathways are nitrification or denitrification, where either NH_3 gets oxidized to nitrite and then to nitrate, which is an aerobic process, or under anoxic conditions where NO_3^- gets reduced to NO_2^- and then via several steps to nitrogen gases, such as NO and N_2O and subsequently resulting in N_2. Also, ammonia oxidation without the dependence on oxygen is called the anammox process. Within which NH_3 is oxidized with nitrite producing N_2. All of the described possibilities thus far entail a decrease in ammonia. In contrast, another possible course that can take place under anoxic conditions but implying an increase in NH_3 is the dissimilatory nitrate reduction to ammonia (DNRA).

This respiratory reduction, which can involve NO_3^- or NO_2^-, together with the other anoxic pathways mainly occur in surroundings lacking in oxygen, such as sediments. Other reasons for released ammonia are nitrogen fixation or ammonification. The latter is a common process within sediments as well and is realized via the mineralization of organic compounds. [65,66,67,1]

Another factor that needs to be taken into consideration is the pH dependent equilibrium between ammonia and ammonium, where ammonium is present in acidic to neutral conditions and ammonia under alkaline ones as the pK_a amounts to 9.25. Also, this optode only detects the gaseous base of these two, the NH_3. Additionally, temperature does of course play a role as well as it has an impact on the NH_3/NH_4^+ equilibrium.[68]

In this attempt to apply the sensor foil within a sediment, the opening of the aquarium was covered in order to minimize ammonia volatilization. The temperatures of the sediment and the water were gathered throughout this experiment and so was the pH. Images of this set up with half of the optode immerged in sediment were taken for the first three hours, the results of three chosen regions of interest (ROIs) plotted against the time can be found in Figure 28B. These regions of interest were picked to get a better insight into the varying concentrations at the specific locations. It can be seen that ammonia concentrations for the ROIs in the water phase remained constant whereas a slight rise in NH_3 concentration becomes apparent for ROI 2 within the sediment. This could be due to dissimilatory processes, such as the already mentioned DNRA or ammonification, which mainly takes place in the surface sediment layer.[63] Another reason could be due to the monitored increase in temperature especially seen in the sediment. Where a temperature change of 5°C within the first three hours was determined. After that the temperature stayed at 20°C throughout the rest of the experiment. The pH of the sediment resulted in pH 6.8 and the water phase above showed a pH of 7.2. However, it should be noted that the sensor was not temperature compensated and the measurement can be influenced by temperature fluctuations. This should be considered by interpretation of the data.

After the addition of 25 mL of a NH_4Cl in phosphate buffer solution (pH 7.5) on top of the sediment a sudden increase in ammonia levels of the ROIs in the water layer (ROIs 1 and 3) up to 18 and 30 ppm occurred. This together with selected images is depicted in Figure 28C and Figure 28A. A diminished rise in ammonia concentrations was deduced from the second addition of ammonium chloride solution, as only half of the first amount was poured into the water phase. And only after the third addition of NH_4Cl solution, which then was injected

directly in front of the optode and into the sediment, did the region of interest within the sediment show a significant spike in ammonia concentration reaching > 300 ppm.

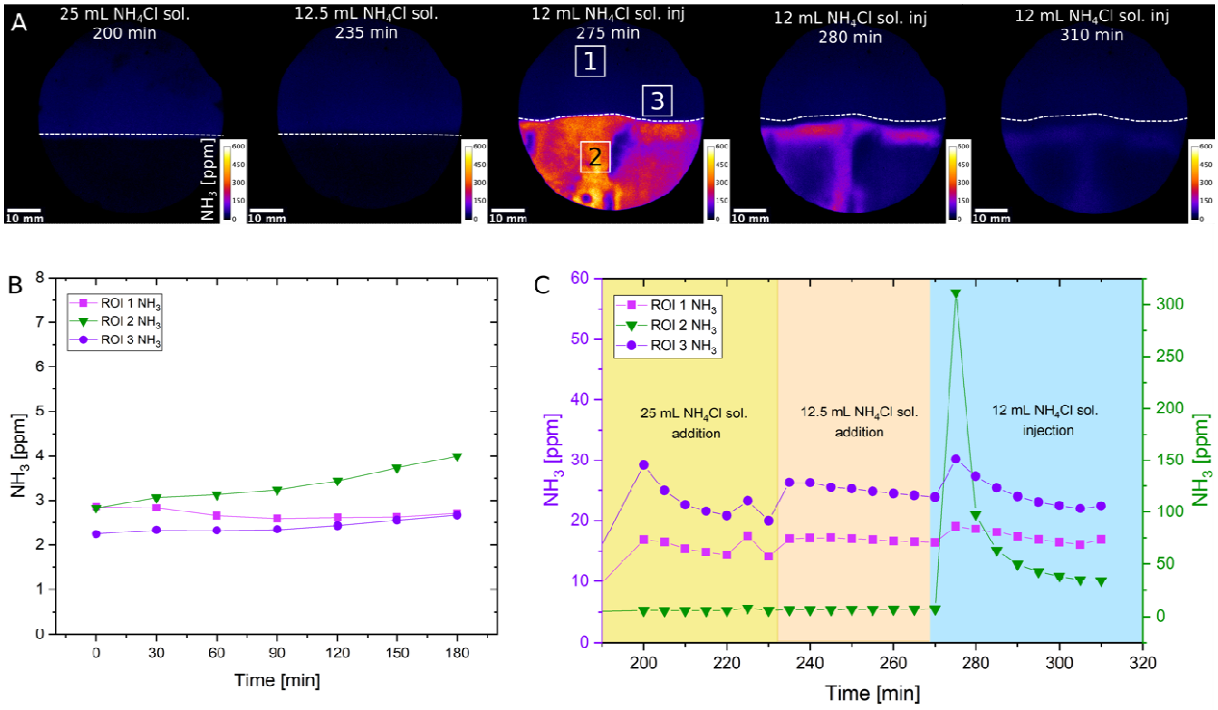

Figure 28: A: False colour images of the NH3 levels and their distribution in the sediment and in the overlaying water phase at various time points after applying and injecting an ammonium chloride solution. B: Ammonia level profile of the 3 regions of interest (ROIs 1-3) for the first 3 hours without any addition of NH_4Cl solution. C: Ammonia level profile of the 3 ROIs (1-3) for nearly 2 hours and throughout various additions of NH_4Cl solution.

Reasons for the decline of ammonia levels for all regions of interests could either be because of ammonia evaporation as the lid on top of the aquarium was not airtight or the turnover to ammonium due to the low pH of both media. Another reason, though mainly applicable for the sediment, could be the assimilation of ammonium.[65]

Either way, we were able to answer the main questions with this experiment whether or not this sensor foil can be utilized in a water locked system and if it is possible to make the dynamics within the sediment visible. Moreover, as low NH_3 concentrations within the ppb range usually can be found within sediments the addition of an ammonium chloride solution to assure higher ammonia concentration was chosen as an aid. To further investigate the exact processes that might take place, other planar optodes or sensors, such as pH or O_2 optodes, would be of great help to find the respective answers.

8.8. Soil – pig manure experiment I

As mentioned above, to get a better understanding of the processes taking place within a biological system more than one analyte needs to be investigated. Hence, together with the new NH_3 optode, also a pH and an O_2 optode were deployed. These three sensor foils were implemented into the first soil sandwich with a thickness of 2 mm. The ammonia and the pH planar optode were mounted onto one glass plate and on the opposite glass plate a fairly big O_2 sensor foil was attached. In between those glass plates a certain amount of soil was applied. This arrangement together with the imaging setup can be seen in Figure 29. As this was the preliminary soil sandwich to the one described in the manuscript (section 12.4) the optode design, imaging approach as well as the calibration curves are not illustrated again as they are elucidated within the manuscript. Only the differences to the subsequent setup are described such as the already mentioned diverging positioning of the sensor foils. Due to this, the excitation sources and the respective filters were altered as well. Thus, in contrast to the second soil sandwich, NH_3 and O_2 or pH and O_2 were analysed.

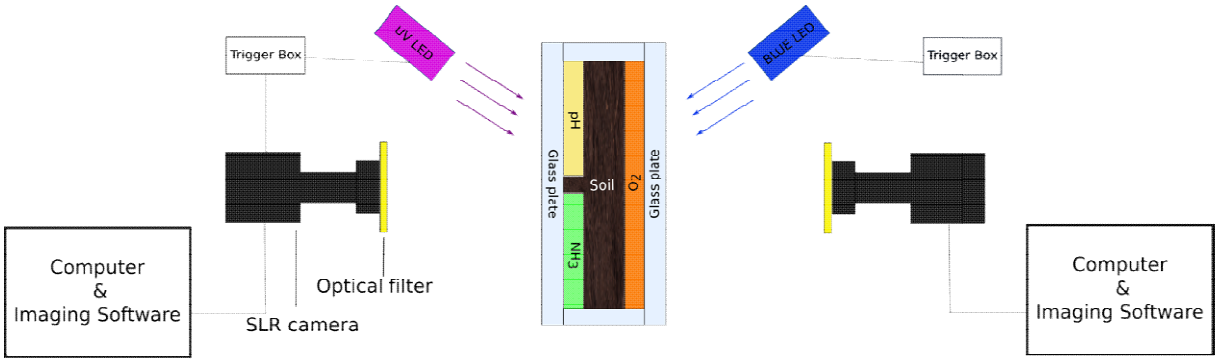

Figure 29: Experimental and imaging setup. The two glass plates build up a soil sandwich with a thickness of 2 mm. The used optodes (one NH_3, one pH and one big O_2) were mounted to the inside and soil was distributed in between. Two single-lens reflex (SLR) cameras together with an UV LED and a blue LED were placed facing the respective sides of the soil sandwich. Therefore, ratiometric and simultaneous imaging of the three parameters took place. The manure was introduced using a pipette and entering from the top.

The ammonia emission from soils resulting from agriculture, manure and ammonia-based fertilizers paired with processes going on within the soil upon manure application, were of interest. The various actions that can occur when something rich in organic matter and nitrogen comes in contact with a microorganism potent system is studied with this setup, as manure is added to the sandwiched soil. The roles both, pH and also O_2 play within the various interactions that can lead to either increasing or decreasing ammonia levels, were tried to illustrate and are discussed in more detail within the manuscript (section 11.3).

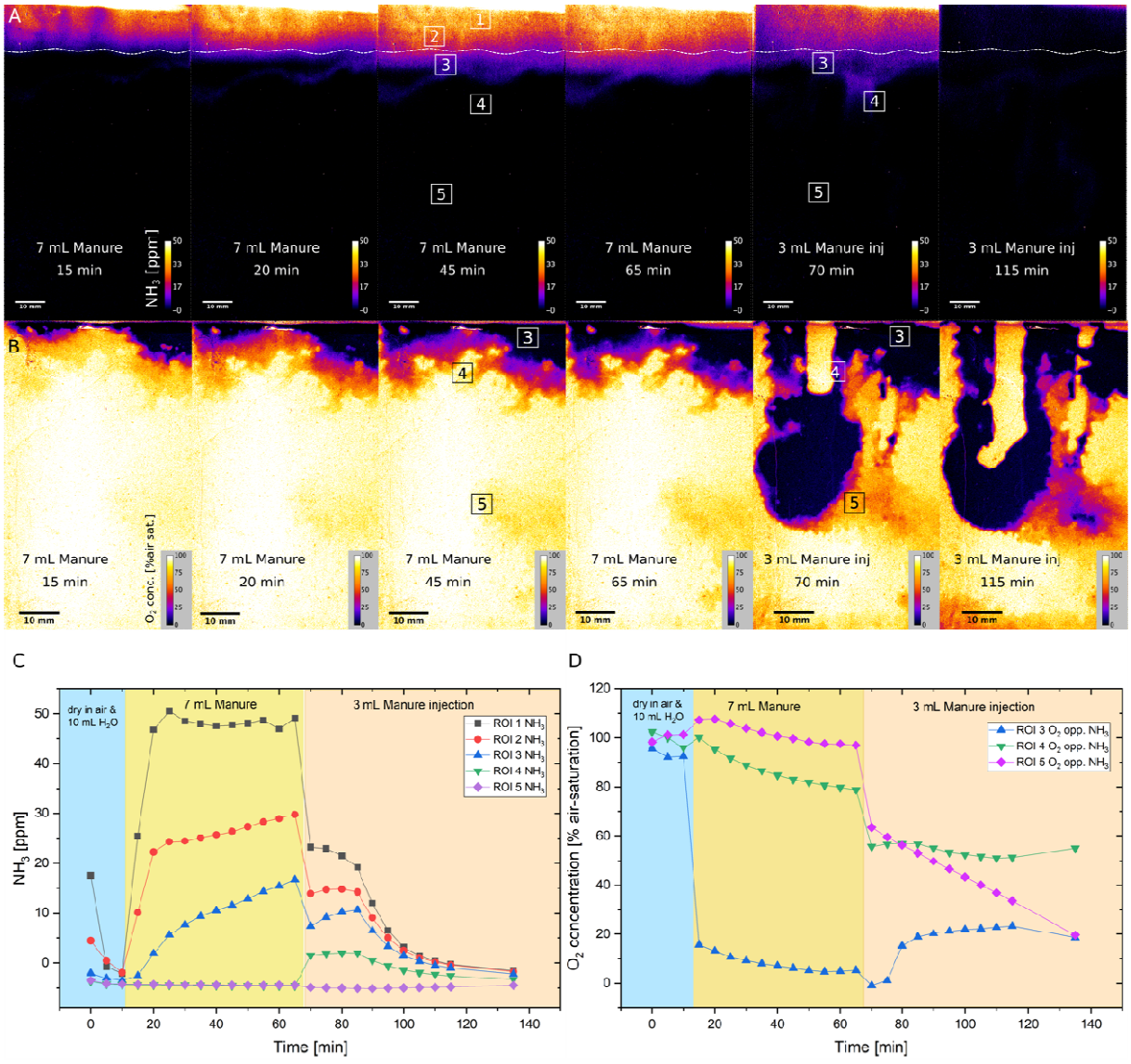

Figure 30: A: False color images of the ammonia level propagation in the headspace above the soil, around the soil/air interphase, where the dashed line alludes the soil surface, and within the soilat different time points after manure application and manure injection. B: False color images of the O_2 concentration opposite to the NH_3optode at the same time point mirroring the NH_3 images though without depicting the headspace above the soil. C: NH_3 concentration profile of the 5 regions of interest (ROIs 1-5) throughout the experiment. D: O_2 concentration profile of the 3 ROIs (3-5) throughout the experiment.

The first ten minutes within the time trace for specifically chosen regions of interest (ROIs) for the NH_3/O_2 combination (Figure 30) show the response when the dry soil and the subsequent addition of 10 mL and then another 5 mL of water were imaged. In Figure 31 the same initial

treatment is illustrated for the pH/O_2 combination, starting with pH 5 and rising to pH 6-6.5 with addition of water. The pH values for ROIs 1 and 2 stay low as they measure the headspace above the soil, which is not in an aqueous solution. This was followed by the addition of 7 mL manure, which lead to a steep rise in NH_3, up to 50 ppm, though this only was the case for the selected ROIs in the headspace of the air/soil interphase, indicating the immediate volatilization of the ammonia from the manure. The ROI located directly underneath the air/soil interphase, thus within the soil, suggested the diffusion of ammonia into the soil and also showed the progress of this with increasing ammonia levels with time. This course of ammonia proliferation is accompanied by a decrease in oxygen for the upper regions of interest within the soil.

It is worth mentioning that the O_2optode was attached in such a manner that only the soil could be analysed without the headspace above it. The already discussed addition of 7 mL of manure also entailed a surge in pH to pH 7-8.5. And also, the anoxic regions expanded on this side with time. Then after one hour 3 mL manure were injected in front of each optode (NH_3 and pH) and this time a sudden decline in ammonia levels occurred, at least for the top 3 ROIs. This could be due to the fact that the soil sandwich was closed with laboratory film and needed to be opened in order to conduct the second manure addition, leading to a loss of the gaseous headspace ammonia out of the sandwiched glass plates. Even though there is a significant decrease of ROIs 1-3 in the beginning and a rather insignificant increase for ROI 4, all of them result in a complete diminishment of ammonia after 135 minutes. In regard to the O_2 and pH levels lead the injection of manure to a further decrease in oxygen as manure extensively leached into the soil, with the exemption of ROI 3 opposite the NH_3optode, which underwent an increase due to seemingly heterogeneities. However, the pH in the headspace depicted hardly any change despite the regions where the injection took place resulting in an increase of pH to pH 7.25 and 6.5.

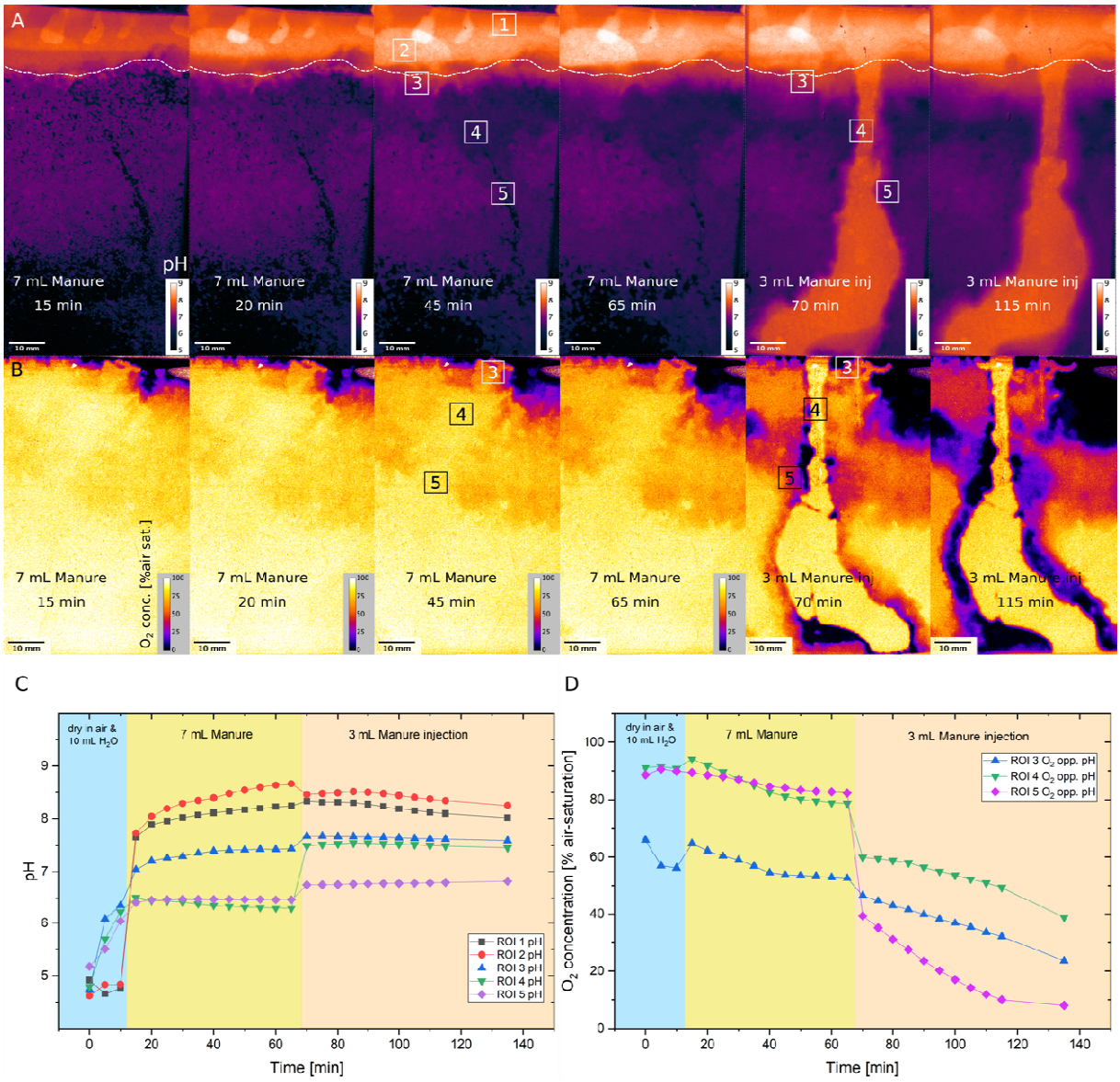

Figure 31: A: False color images of the pH level propagation in the headspace above the soil, around the soil/air interphase, where the dashed line alludes the soil surface, and within the soilat different time points after manure application and manure injection. B: False color images of the O_2 concentration opposite to the pH optode at the same time point mirroring the NH_3 images though without depicting the headspace above the soil. C: pH profile of the 5 ROIs (1-5) throughout the experiment. D:O_2 concentration profile of the 3 ROIs (3-5) throughout the experiment.

For an even better understanding of the interplay of the particular analytes, the alterations of the analyte levels over time can be gathered from so called rate images. Therefore, two images at two different times are subtracted from each other and then divided by the respective time.[69] Thus, inhomogeneous changes upon the first manure addition (Figure 32 A and B) affecting either emissions of ammonia or propagation of O_2 decrease can be seen in rates and this together with the uneven seepage of manure within the soil also becomes apparent in Figure 32 C and D after the injection of manure. This comparison shows that this irregular distribution takes place in both cases, when manure is added on top of the soil and also when injected. Unfortunately, the comparison between the various behaviours of the analytes was not that approachable due to the rather bad positioning of the O_2 optode as well as the lack in visible changes within the soil, which was the case for both, the NH_3 and the pH optode (Figure 33). However, injection of the manure brought a more impactful response as alterations of the respective analytes became more detectable and enabled to gather mirrored impacts within the soil environment.

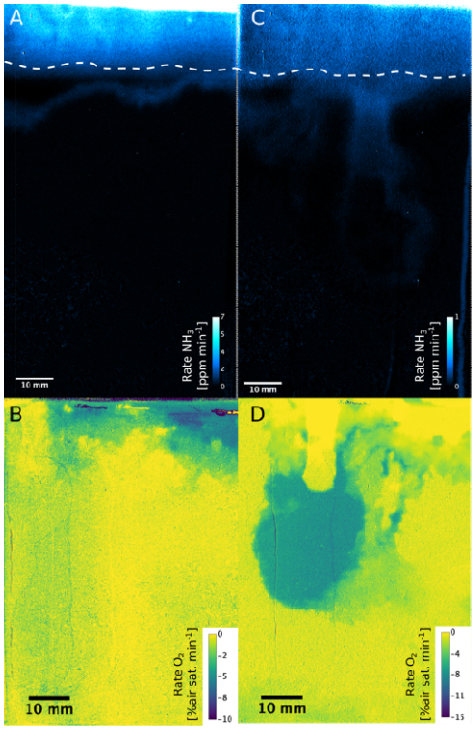

Figure 32: A: False color image of the rate of NH_3 emission in ppm min^{-1} directly upon the first manure addition on the wetted soil. B: False color image of the rate of O_2 depletion in % air sat. min^{-1} directly upon the first manure addition on the wetted soil. C: Similar to A rate of NH_3 emission in ppm min^{-1} after manure injection. D: Similar to B rate of O_2 depletion in % air sat. min^{-1} after manure injection.

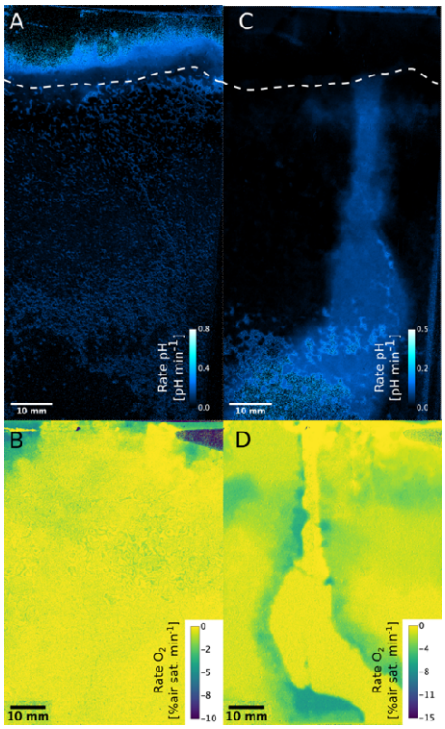

Figure 33: A: False color image of the rate of pH in pH min^{-1} directly upon the first manure addition on the wetted soil. B: False color image of the rate of O_2 depletion in % air sat. min^{-1} directly upon the first manure addition on the wetted soil. C: Similar to A rate of pH in pH min^{-1} after manure injection. D: Similar to B rate of O_2 depletion in % air sat. min^{-1} after manure injection.

Overall, this first soil sandwich was crucial in order to determine the possibility of such application and the improvements that need to be implemented such as the distance between the glass plates resulting in an increased thickness of the setup and a more constructive positioning of the sensor foils. Moreover, it was important to show that this experiment is reproduceable, thus the interpretations regarding the microbial and chemical processes within the microenvironment of the soil are further elucidated within the manuscript attached in the next chapter.

IV. Visualizing the NH_3 emission and the local O_2 and pH microenvironment of soil upon manure application

The manuscript within this chapter is accepted for publication in
Environment International

9. Abstract

The application of fertilizers and manure on fields is the largest source of ammonia (NH_3) in the atmosphere. NH_3 emission from agriculture has negative environmental consequences and is largely controlled by the chemical microenvironment and the respective biological activity of the soil. While gas phase and bulk measurements can describe the emission on a large scale, those measurements fail to unravel the local processes and spatial heterogeneity at the soil air interface. We report a two dimensional (2D) imaging approach capable of visualizing three of the most important chemical parameters associated with NH_3 emission from soil. Besides the released NH_3 itself also O_2 and pH microenvironments are imaged using reversible optodes in real-time with a spatial resolution of < 100 µm. This combined optode approach utilizes a specifically developed NH_3 optode with a limit of detection of 2.11 ppm and a large working range (0 – 1800 ppm) ideally suited for studying NH_3 volatilization from soil. This NH_3 optode will contribute to a better understanding of the driving factors for NH_3 emission on a microscale and has the potential to become a valuable tool in studying NH_3 dynamics.

10. Introduction

The application of livestock manure and synthetic fertilizers ensures high crop yield and sustains production in agriculture. Nevertheless, extensive use of fertilizers is expensive and harms the environment globally, as access nutrients leach into waterbodies and greenhouse gasses are emitted [70]. Gas emission from agricultural fields is a strong contributor to climate change [71]. One of those gasses is ammonia (NH_3)[72,73]. While less in the public focus than greenhouse gasses, NH_3 emission is linked to various processes concerning the environmental and public health. NH_3 contributes to the formation of atmospheric particulate matter, decreases visibility, accelerates global warming, shows toxicity at elevated concentrations and can act as a source of nitrogen to sensitive ecosystems due to atmospheric deposition[68]. On a global scale livestock production with the associated manure management and the application of synthetic fertilizers contribute each to around 30-40% of the global NH_3 emission [68]. This, therefore, makes agriculture the biggest source of NH_3 emission[74].

While globally NH_3 emission happens on a large scale [3,75], the underlying chemical and biological processes are controlled by small-scale (µm to mm) chemical gradients within the soil and soil/air interface [76]. Kim and Or recently showed that the pH microenvironment has a critical role in controlling the emission of NH_3 and nitrous acid (HONO) from drying soils and biocrusts [77]. As the pH determines the speciation between the volatile NH_3 and the non-volatile ionic NH_4^+ the local pH regulates the emission of NH_3 directly [78]. Similarly, the bacteria catalyzed transformation of NH_3 is affected by the local oxygen microenvironment [5,79]. Ammonia oxidizing bacteria for example consume O_2 to convert NH_3 to nitrite, so the local O_2 availability has a direct impact on this bacterial NH_3 sink. In addition, the uptake of NH_4^+ by plants as well as microbes within the soil is an essential process contributing to the depletion of free NH_3. It is thus clear that the chemical microenvironment plays a crucial role in NH_3 emission and that considering the local microenvironment is essential for a deeper understanding of NH_3 emission dynamics and the underlying processes [76]. While gas phase measurements of NH_3 are technically easy to realize using sensors [2] as well as other methods[80], such approaches only provide bulk measures and do not account for the local chemical conditions at the relevant scale. So far, no study was able to visualize and quantify the spatial and temporal heterogeneity of NH_3 at the soil/air interface at below 1 mm resolution. This certainly is the case due to the lack of an appropriate method, like an optode for NH_3.

Planar optical sensors, so called optodes [81], are among the best tools to visualize complex chemical microenvironments [17] in two dimensions (2D). Optodes for O_2 [23,82,83] and pH [84] have been applied extensively in marine and terrestrial systems [18,85] and greatly improved our understanding of the biogeochemical processes involving those analytes [86,87] in particular for structurally complex systems. For example, studies using optodes have shown that the local O_2 availability within the soil affects the emission of N_2O and other greenhouse gases [23,83]. While optodes for O_2 and pH are rather well established, optodes for other important species (like H_2S [64], NH_4^+ [26,88] and CO_2 [89–91]) are sparse, often based on in house synthesized specialized indicators and therefore less well established and used within environmental sciences. This limits our ability to investigate chemical transformations in heterogeneous natural systems. So far, to the best of our knowledge, no dedicated NH_3 optode was developed to study NH_3 emission. Currently most NH_3 optodes aim at monitoring low (ppb) levels of dissolved NH_3 in aquatic systems [54,57,92] due to the toxic effects NH_3 has to aquatic organisms even at those low levels [6]. Such optodes working in the ppb range are unsuited for studying NH_3 emissions from soil where concentrations up to 200 ppm can be reached [2].

In here, we present a dedicated NH_3 optode capable of imaging $NH_3$and demonstrate that this optode can be a valuable tool to study the processes at the soil/air interface in 2D. We also combine the NH_3 optode with other optodes sensitive to either pH or O_2 to quantify the chemical microenvironment at the soil air interface upon manure application. This study is the first 2D visualization of NH_3 emission from a soil surface and the first application of chemical imaging within a terrestrial system showing the temporal and spatial heterogeneity of the chemical microenvironment for three critical parameters related to NH_3 emission.

11. Results and Discussion

11.1. Optode design and imaging approach

Our newly developed optode (Figure 1) enables measurements of NH_3 in the ppm range with a limit of detection (LOD) of 2.11 ppm and a large dynamic range up to 1800 ppm. The sensing principle of this planar optode is based on the fluorescent pH indicator Oxazine 170 perchlorate, which is immobilized in a hydrogel. The indicator dye was combined with an inert reference dye (Macrolex yellow) enabling a ratiometric approach to reference intensity-based signals (see supporting Figure S1 for spectra) [93,94]. Cross-sensitivity towards pH and interferences with all other ionic species were overcome by using agas permeable and ion

impermeable fluoropolymer membrane on top of the sensing layer[59]. Hence, the indicator dye is deprotonated by gaseous NH_3 that diffuses through the hydrophobic membrane. Upon deprotonation, the indicator changes its fluorescence properties (see supporting Figure S1) which can be detected using a color camera. The optode enables imaging of NH_3 over a broad range (0-1800 ppm) with a linear response from 0-60 ppm (see Figure 1). The ratiometric imaging approach allows using a regular single-lens reflex (SLR) camera taking advantage of the red, green and blue channels that are used to assemble an image [93]. All optical components used as well as the utilized trigger box to analyze the NH_3 optode are commercially available and similar to the equipment, which is widely applied for O_2 and pH optodes [84,93,95], making it possible to combine those optodes within a single setup. Thus, we combined the here developed NH_3 optode with optodes for O_2 and pH to study the chemical microenvironment at the soil/air interface in detail.

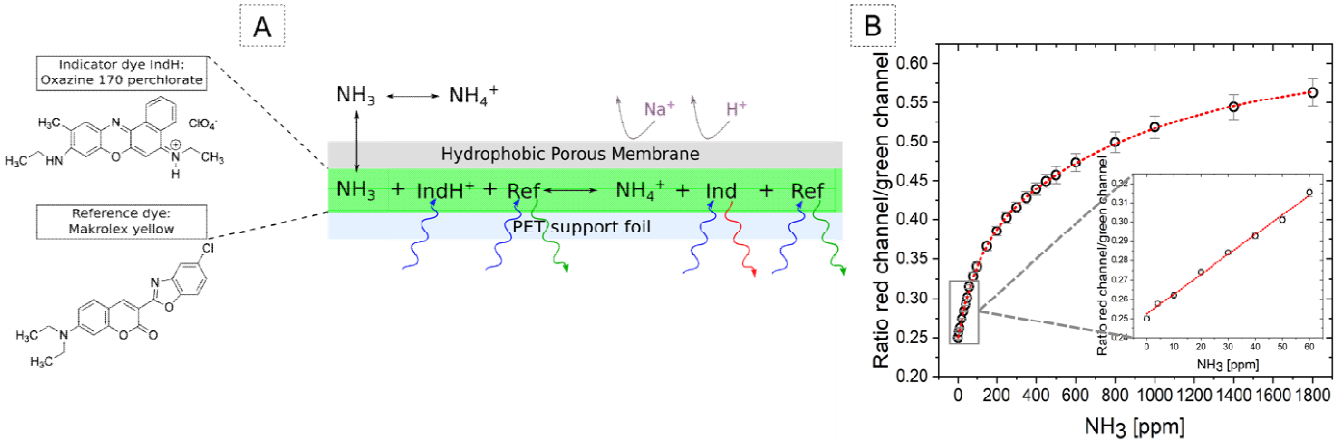

Figure 1: A: Composition of the planar NH_3 optode and the interaction with ammonia that leads to a changed emission of the indicator dye. B: Calibration curve of the NH_3 optode (data fitted with an exponential decay function; $R^2 > 0.996$) and a close up of the linear range (linear fit; $R^2 > 0.993$). The NH_3 optode has an LOD of 2.11 ppm.

11.2. Setup for combined O_2, pH and NH_3 visualization

All three optodes were integrated into a thin (4 mm) soil sandwich [96,97]. This means that a volume of soil was sandwiched between two glass plates equipped with optodes. Two NH_3 optodes were placed on one side and one O_2 and one pH optode on the other side (see Figure 2). In combination with two opposing cameras and excitation sources, this enabled the parallel imaging of three parameters. Given the spatial arrangement of the optodes, it was possible to analyze either NH_3 and O_2 or NH_3 and pH together. The calibration curves of the O_2 and pH

optodes (see supporting Figure S2) as well as the response curves of the developed NH_3 optode at different ammonia concentrations (see supporting Figure S3) are available.

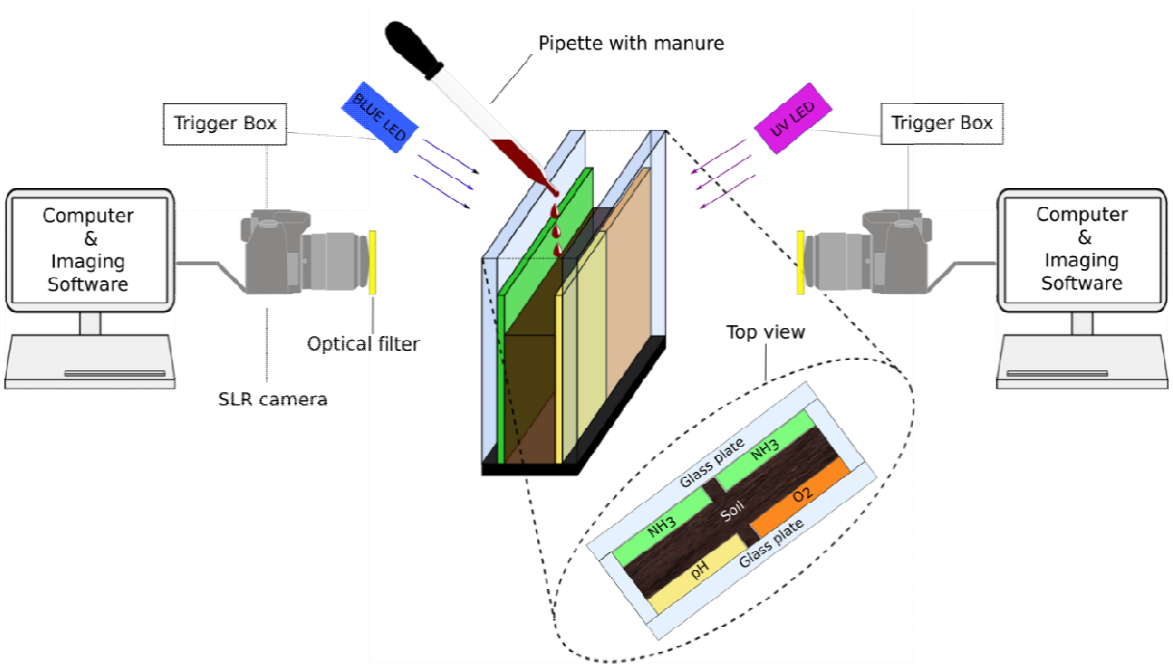

Figure 2: Experimental setup. Two transparent glass plates formed a so-called soil sandwich with an internal thickness of 4 mm. Optodes (one O_2, one pH and two NH_3) were attached to the insides as shown. Soil was filled in between the slides and the optodes leaving a headspace. Two single-lens reflex cameras as well as a blue LED and an UV LED were positioned at the respective sides of the soil sandwich. This enabled simultaneous imaging of the three parameters. Manure was applied on the soil surface from the top using a pipette.

11.3. The chemical microenvironment and its impact on NH_3 emission

With the described setup at hand, we were able to visualize what happens to the chemical microenvironment of soil upon manure application. As mentioned, manure and synthetic fertilizers are the main sources of NH_3 emission into the atmosphere. Manure contains substantial amounts of dissolved organic carbon, mineral nitrogen and water. In short, an ideal mixture to stimulate a variety of chemical and microbial processes within the soil. In terms of NH_3 emission, the following processes need to be considered. The degradation of urea, uric acid or undigested proteins are the main processes producing NH_3 within manure. It is clear that local pH and O_2 availability affects the catalytic performance of the enzymes used to degrade the respective precursors [68]. Take for example the enzyme uricase that uses O_2 and water to convert uric acid into CO_2 and NH_3. Due to the common storage of manure most of the fast degradation processes already happened within the manure tank, resulting in a readily

available NH_3. Besides NH_3 sources there are also several processes including nitrification and assimilation that decrease the local NH_3 concentration. Nitrifying microorganisms (e.g. ammonia oxidizers) oxidize NH_4^+ consuming O_2[79] which again demonstrates the interconnection between those analytes. Additionally, it is essential to remember that NH_3 is in a pH dependent equilibrium with ammonium (NH_4^+), the sum of both forms is called total ammonia nitrogen (TAN). Only NH_3 can be emitted from the soil surface into the air and only this form can be detected by the optode. Several theoretical models exist that account for those as well as other chemical and physical processes, but they still fall short of fully predicting the emission of NH_3[98–100]; likely due to the problem of accurately modeling local heterogeneities.

In the system presented here, we combine a specially developed NH_3 optode with optodes for two of the main chemical parameters governing the faith of NH_3 within soil, namely O_2 and pH. We chose to use a rather thin sieved soil sample and sandwiched the soil between the respective optodes for this proof of concept study. By doing so, it was possible to correlate the obtained quantitative images for NH_3 and O_2 or NH_3 and pH directly, as the sample is only 4 mm thin, heterogeneity within the width of the soil slice was kept to a minimum, while still allowing the addition of manure from the top. This limits the sample volume, but this approach enables a rather direct correlation of the obtained images from the respective sides of the soil sandwich.

The dry soil was first exposed to 10 mL of water to humidify the soil before 7mL of manure were added. The headspace of the soil sandwich was sealed with laboratory film, and chemical imaging started immediately before the water addition. Selected images and a time trace for selected regions of interest (ROIs) are shown in Figure 3 for the NH_3/O_2 optode combination and in Figure 4 for the NH_3/pH optode combination. It is evident that the addition of manure had an immediate effect on the chemical microenvironment of the soil. While the just wetted soil was well oxygenated and showed an acid pH of 4-5, manure addition resulted in the formation of an anoxic layer on the top soil and a sudden pH increase up to pH 7.5 to 8. A sudden spike in the NH_3 emission accompanied this. Ammonia in the gas phase above the soil reached levels > 150 ppm.

To illustrate the differences in local concentration and dynamics we selected ROIs representing the gas phase on top of the soil sample as well as ROIs at the air/soil interphase. The initial emission of NH_3 was instantaneous, this indicates that the application released the NH_3 already present within the manure. Due to the increased surface area upon application, dissolved NH_3 within the manure can reach the gas phase quickly. Also, the alkaline manure

pH favors NH_3 emission [101]. The observed emission profile is largely in agreement with previously obtained gas phase measurements [102] and can be explained with a transport-reaction model taking also into account the role of CO_2 emission and surface pH [78]. Microbial transformation reactions within the soil play likely no role in this initial very fast emission.

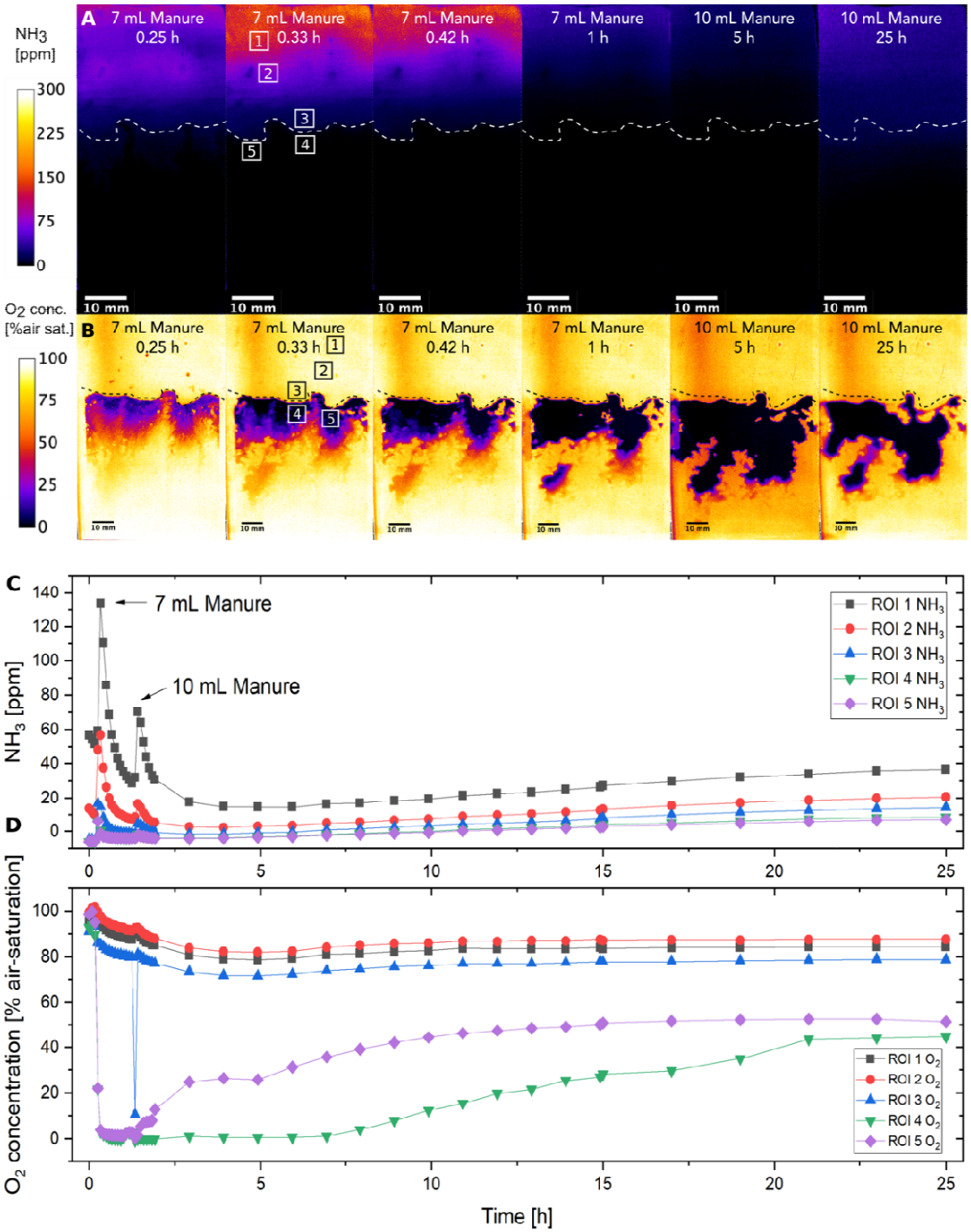

Figure 3: A: False color images of the NH_3 concentration distribution within the soil, around the soil/air interphase (dashed line indicates the soil surface) and in the headspace above the soil at different time points after manure application. B: False color images of the O_2

concentration opposite to the NH_3 optode at the same time point mirroring the NH_3 images. C: NH_3 concentration profile of the 5 regions of interest (ROIs 1-5) throughout the 24 hour manure application experiment. D: O_2 concentration profile of the 5 ROIs (1-5) throughout the 24 hour manure application experiment.

After the initial peak NH_3 levels within the headspace and at the air/soil interface decreased. As the soil sandwich is not airtight NH_3 can leave the headspace and/or be consumed via e.g. nitrification. The expansion of the anoxic zone within the soil could result from O_2 consumption during active nitrification, but this process is generally considered slow and not supposed to contribute to a significant reduction of TAN within the first 24 h [76]. After one hour an additional 10 mL of manure were added on top of the soil. Again, NH_3 emission spiked, but reaching lower peak concentrations. This is likely, because the soil surface was already covered by a thin manure film at that point and therefore the increase in surface area was less pronounced. The peak was again followed by a decline in headspace and interface NH_3 levels. The second addition of manure had minimal effect on the surface pH as well as on the O_2 levels within the soil. Soil pH remained at around 7.75 to 8.25 and the anoxic zone within the soil continued to expand with manure seeping into the soil. Ammonia levels in both the gas phase and interface decreased then for around 5 hours. In this period between it is likely that aerobic microbial respiration (ammonia oxidation) and NH_4^+ assimilation [103] contributed to the decrease in NH_3 levels, as both O_2 and pH decrease. Aerobic respiration consumes O_2 and results in the formation of acidic CO_2. The apparent change in the signal from the pH optode above the soil surface indicates that increased levels of acidic gasses like CO_2 are released from the soil at this point [78]. Afterwards NH_3 emission gradually increased again. Degradation processes of organic procurers (like urea, or proteins) or desorption of previously absorbed NH_4^+ from soil particles can explain the observed slow increase of NH_3 at this point. A general slight increase in the soil pH (see zoom in Figure 4) accompanies the increasing emission and further supports a slow release of NH_3fuelled either by biological production or desorption.

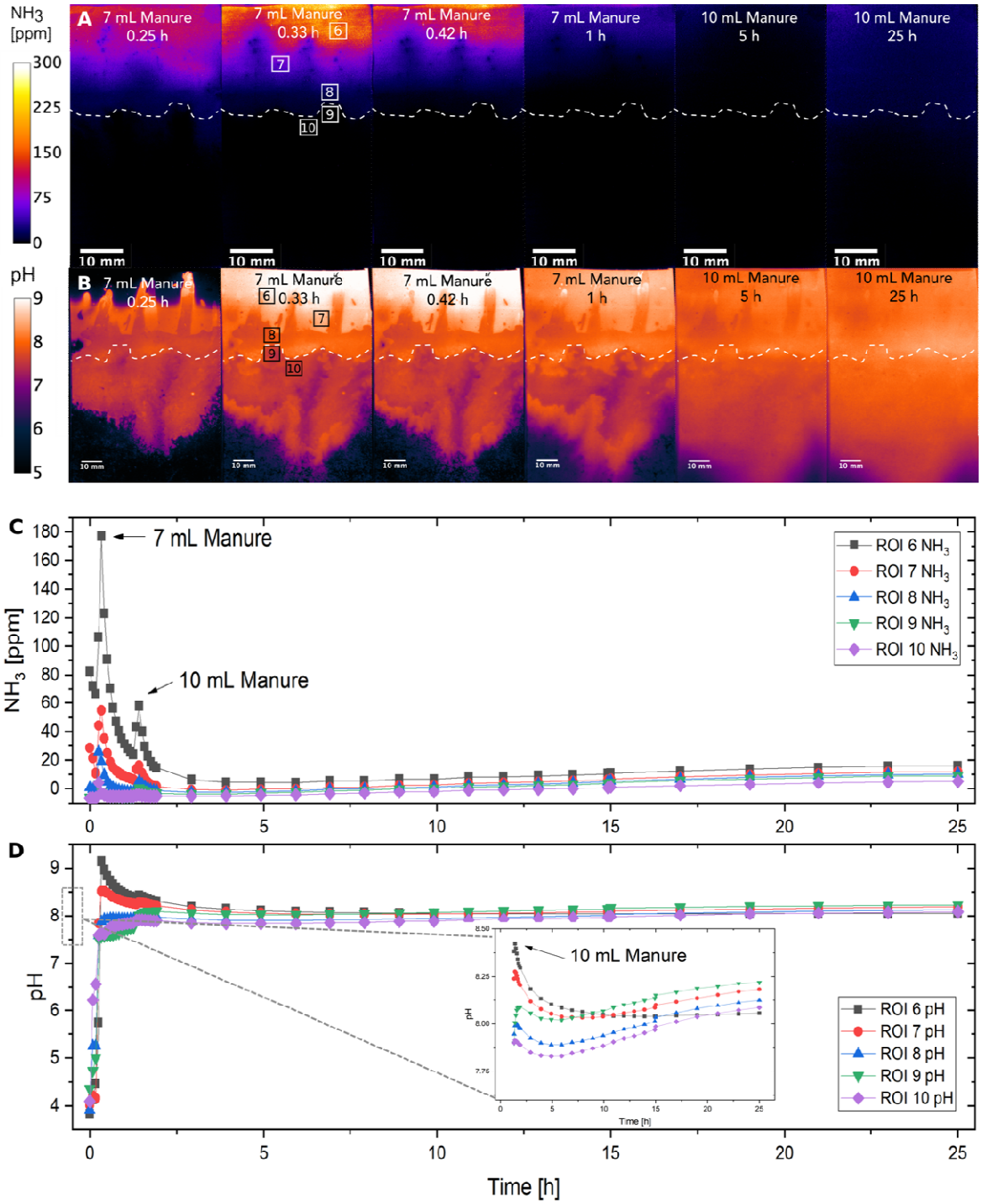

Figure 4: A: False color images of the NH_3 concentration distribution within the soil, around the soil/air interphase (dashed line indicates the soil surface) and in the headspace above the soil at different time points after manure application. B: False color images of the pH opposite to the NH_3 optode at the same time points mirroring the NH_3 images. C: NH_3 concentration profile of the 5 regions of interest (ROIs 6-10) throughout the 24 hour manure application experiment. D: pH profile of the 5 ROIs (6-10) throughout the 24 hour manure application experiment with a zoom showing the pH region between 7.75 and 8.50.

Furthermore, line profiles obtained at the air/soil interface show the change in the microenvironment and enable a direct alignment of O_2 and NH_3 (Figure 5) or pH and NH_3 (supporting Figure S4). Extracting concentration profiles from the chemical images allows for the in depth analysis of the chemical and biological processes as shown otherwise by microsensors [19,104–106]. With as resolution of around 100 µm per pixel the chemical images generated in this study can provide high-resolution profiles of three important analytes related to the emission of NH_3. The high nutrient content of manure results in a very active respiration within the manure layer as seen by a rapid O_2 consumption at the air/soil interface (Figure 5C and D). The respective NH_3 profiles also show a consumption of NH_3 that aligned with the O_2 consumption. Directly after manure addition the consumption happen just underneath the soil surface, where the biggest O_2 consumption is observed. This could indicate active nitrification, but one has to keep in mind only the gaseous NH_3 and not the total ammonia nitrogen (TAN) is measured here. The concentration of TAN can be obtained via using the simultaneous pH measurement to calculate the estimated NH_4^+ that exists in equilibrium to the measured NH_3 at a given pH using the Henderson–Hasselbalch equation (see supporting figures S4 for a calculated TAN profile). While for those TAN profiles the respective O_2 profile at the same location is not available, it appears that TAN consumption happens a few mm underneath the soil/air interface at the initial manure application and deeper with the soil (at the bottom of the anoxic front) at the end of the experiment. A slight NH_3 and TAN production can be observed at the soil surface at the end of the experiment, which is in line with the observed overall increase in NH_3 emission. While outside the scope of this study, further analysis of the profiles could be used to look at the biological and chemical processes involved as shown previously using microsensor based approaches [107,108].

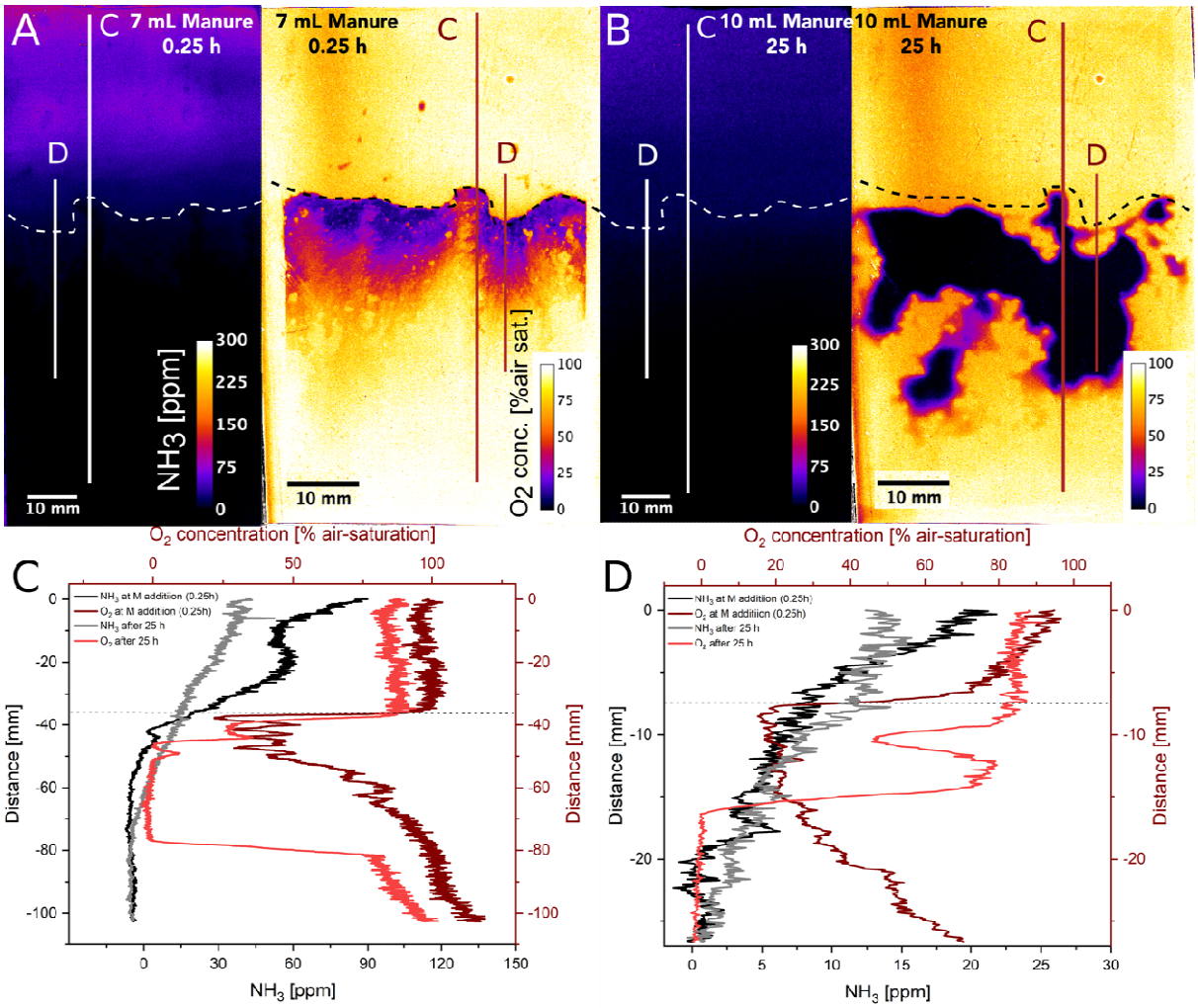

Figure 5: A and B: False color images of NH_3 and O_2 concentrations at different time points. Panel A shows the images directly after manure addition and B at the end of the experiment (25 hours). C: O_2 and NH_3 concentration profiles extracted at the two depicted time points along the longer line shown in panels A and B. D: O_2 and NH_3 concentration profiles extracted at two depicted time points along the shorter line shown in panels A and B.

While the extraction of line profiles is an excellent way to study concentration gradients and to determine e.g. fluxes in a similar manner done by using microsensors [109], the possibility of using the 2D information from the images is not exploited. Therefore, changes in the analyte concentration over time can be depicted as rate images by simply subtracting two images from subsequent time points with each other and taking into consideration the time between the images [69]. This enables a close look on the 2D heterogeneity of the O_2 depletion and NH_3 emission, as shown in Figure 6 for the first addition of manure on the wet soil. It is clear that the rates of NH_3 release and O_2 depletion show a heterogeneous pattern that can be associated with the infiltration of manure being non-uniformly on a soil surface. Structural features like

the small elevation visible in the two images leads to a concentration of liquid manure in the valleys besides the elevation. This further results in a heterogeneous infiltration and consequently in a matching pattern of local O_2 depletion and NH_3 emission. While the structural features here are just bumps of a few mm they already result in a distinct shift in soil chemistry. In non-sieved natural soils containing also stones and plant roots a way more heterogeneous chemical microenvironment can be expected. As demonstrated already for other analytes than NH_3, optodes are ideal tools to look at such complex microenvironments [84,89,97].

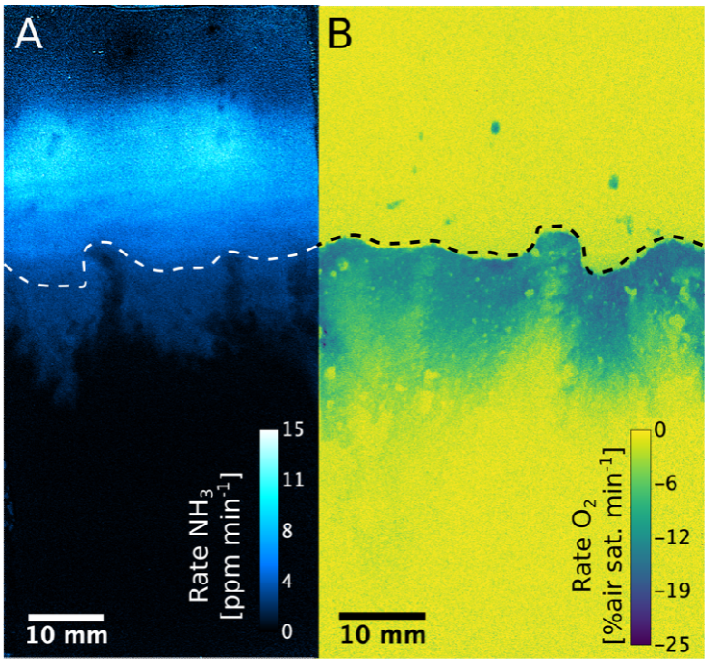

Figure 6: A: False color image of the rate of NH_3emission in ppm min^{-1} directly upon the first manure addition on the wetted soil. B: False color image of the rate of O_2depletion in % air sat. min^{-1} directly upon the first manure addition on the wetted soil.

In conclusion, we developed and applied the first NH_3 optode dedicated to visualizing the volatilization of NH_3 from a soil surface, together with the main driving factors, O_2 and pH. The novel optode consists of commercially available compounds enabling reproduction without the need of e.g. indicator synthesis. We believe that this is a great advantage, as this will enable other researchers to readily use this optode. In addition, the used imaging and calibration method only requires a standard single-lens camera, an excitation light source, optical filters and a trigger box. The entire setup is available at low costs [93]; again hoping to facilitate a widespread use of this method. We demonstrated the potential of the system by

imaging NH_3 emission from soil upon manure application. It was not the aim of this study to elucidate the entire soil biogeochemistry, but it is evident that the optode and combination approach presented here enables studying biological and chemical processes related to NH_3 in detail. The use of NH_3, O_2 and pH optodes allows analysis of all three parameters in real-time with a sub-mm (<100 μm) resolution. As pH and a variety of microbial processes, like the oxygen consuming nitrification, affect the availability of free NH_3, this combinatory imaging approach gives more detailed insides into those processes than pure gas phase measurements. The hope is that in the future even additional optodes; e.g. CO_2 [89,90] or multianalyte optodes [110], could be included, to visualize even more of the complex chemical microenvironment of soil. While in this study a rather thin soil sample was analyzed, the optode could in the future be included into other setups like rhizotrons [28] or even fitted on equipment that could be installed in-situ at a field [111]. As soil is a heterogeneous and complex matrix, results from optode based studies are needed to better understand the chemical microenvironment at a fine scale and to provide essential data to help improve our understanding [77] and current models on NH_3 emission [99,100]. The presented optode has the potential to become a valuable tool in environmental monitoring related to NH_3 emission from not only soil, but also other important sources where the chemical microenvironment matters (e.g. biofilters).

12. Materials and Methods

12.1. Optode fabrication

The NH_3 optode used was prepared by knife-coating a sensor cocktail onto a transparent dust-free polyethylene terephthalate (PET) foil (PuetzFolien, Taunusstein, Germany) using a film applicator (Byk-Gardner GmbH). The cocktail consisted of 0.8 mg of the indicator dye Oxazin 170 perchlorate (Sigma Aldrich), 0.8 mg of the reference dye MY (Macrolex® fluorescence yellow 10GN, Lanxess, Köln, Germany) and 1.5 g of a mixture of 5% wt. polymer (Hydromed D4, AdvanSource Biomaterials) dissolved in THF (Tetrahydrofuran, Sigma Aldrich). Instantly after the coating a PTFE Fluoropore membrane filter (purchased from Advantec, Japan) was placed onto the still wet sensor film and carefully applied with a soft painting brush. As the THF evaporates through the filter a thin (~6 μm) hydrogel layer, which acts as a matrix for the dyes, is enclosed between the membrane filter and the PET foil. In order to ensure complete proton impermeability, the edges of the filter were sealed with PDMS, a mixture of 10:1 Silicone elastomer base and Silicone elastomer curing agent (Sylgard 184 Silicone Elastomer Kit, DOW Europe GmbH).

The preparation of the O_2 and the pH optodes were conducted similar to a previous study [84] and to the ammonia optode though using different dyes, solvents and ratios of such. Therefore, for the O_2 optical sensor film 1.3 mg MY, 1.3 mg PtTFPP (Platinum(II)-meso(2,3,4,5,6-pentafluoro)phenyl-porphyrin, Frontier Scientific), 100 mg PS (Polystyrene, MW 192,000 g mol^{-1}, Sigma Aldrich) were dissolved in 1 g of $CHCl_3$ (Merck KGaA, Darmstadt, Germany). This cocktail was spread on a PET foil and a layer of ~10µm was obtained after the chloroform evaporated. For different reasons as reaching high resolution and minimizing the impact of background light an optical isolation needed to be applied on top of the sensor layer. This cocktail consisted of 4% wt. (40 mg) of carbon black dispensed in 1 g 20% wt. solution of silicone glue (Elastosil E43, Wacker Chemie AG, Germany) in hexane (Merck KGaA, Darmstadt, Germany). After applying this layer with the help of a knife coater the optical isolation had a thickness of ~24 µm.

The pH optode cocktail consisted of 1.5 mg of the lipophilic pH indicator HPTS (1-Hydroxypyrene-3,6,8- tris-bis(2-ethylhexyl)sulfonamide, provided by Dr. Sergey Borisov, Graz University of Technology, Austria) [112], 1.5 mg Perylene (Sigma Aldrich), 75 mg D4 and 75 mg diamond powder (Monocrystalline diamond powder, Microdiamant AG) dissolved/dispersed in 1.5 g THF and subsequently knife coated onto a PET foil resulting in a layer thickness of ~10 µm due to solvent evaporation. The necessity of an isolation layer met the same requirements for the pH optode as for the O_2 optode. It contained 1.5 mg HPTS, 1.5 mg Perylene, 75 mg D4 and 24 mg carbon black dissolved in 1.5 g THF. Since this isolation layer was coated on top of the sensor layer and thereafter the solvent evaporated a layer thickness of ~8 µm was achieved.

12.2. Imaging setup

The imaging setup consisted of two ratiometric RGB setups per side, as two NH_3 optodes were imaged on one side and a pH and an O_2 optode on the opposite side. The imaging of the NH_3 optodes was conducted with a SLR camera (EOS 1300D, Canon, Japan) in combination with a macro objective lens (Macro 100 F2.8 D, Tokina, Japan), an orange 530 nm longpass filter (OG530 SCHOTT, 52 mm x 2 mm) with another plastic filter (#10 medium yellow; LEEfilters.com) attached in front of the long-pass filter in order to minimize background fluorescence. For excitation of the NH_3 optode a blue (470 nm) LED (r-s components, Copenhagen, Denmark) together with a short-pass filter was used. The LED was controlled by a trigger box, which is a USB-controlled LED driver unit (imaging.fish-n-chips-de). The

software look@RGB (imaging.fish-n-chips-de) allowed the gathering of the images and to control of the SLR and LED.

The pH and O_2 optode imaging set up was similar to the one of the NH_3 optodes with certain exceptions. A yellow 455 nm long-pass filter (GG455 SCHOTT, 52 mm x 2 mm) and a 405 nm UV LED (r-s components, Copenhagen, Denmark) were used instead of the filter and excitation light mentioned above.

12.3. Calibration and data analysis

A calibration curve for the ammonia optode (Figure 1) was obtained as follows. A small piece of the optode used in the experiment was mounted into a small aquarium (350 mL) which was filled with 300 mL of a 0.5 M sodium hydroxide solution (pH > 12). Different ammonia concentrations (0, 5, 10, 30, 50, 70, 100, 200, 300, 400, … , 1800 ppm) were facilitated through subsequent addition of a stock solution of ammonium chloride (NH_4^+Cl from Bie&Bernsten A-S, Denmark) with a concentration of 300 g L^{-1}. Due to the high pH in the experimental chamber the equilibrium between NH_3 and NH_4^+ was on the side of NH_3 (pK_a 9.25) at all times. After every addition, each calibration step was held for at least 12 minutes and images were taken every 3 minutes. In order to determine the calibration, images were analyzed using the software ImageJ (imagej.nih.gov/ij/). For the NH_3 optode, the red channel (analyte sensitive emission of the indicator dye) was divided by the green channel (emission of the inert reference dye) utilizing the ImageJ plugin Ratio Plus. This ratio was correlated to the NH_3 concentration (see Figure S1). For the soil experiments also the red/green ratios were obtained and fitted to the calibration curve with the help of the Calibrate tool of ImageJ (function: exponential with offset). The limit of detection (LOD) was determined from the mean of measured ratios of the blank plus three times the measured standard deviation (0.250 ± 0.00141). This resulted in the LOD of 2.11 ppm.

O_2 and pH optode calibration and data analysis were conducted similar to a previous study [84] with a few differences as follows. For the determination of a calibration curve for the O_2 optode a small piece of the sensor foil was positioned and fixed on the inside of a small aquarium. The water inside the aquarium was titrated with a 2% sodium dithionite solution (Sigma Aldrich) to obtain different O_2 levels up until a fully deoxygenized state of the water. These O_2 levels were controlled via an optical O_2 microsensor (FireSting GO_2, PyroScience GmbH, Aachen, Germany; calibrated by 2- point calibration with 0 % and 100 % air saturated water). Similar to the steps mentioned above the calibration curve was obtained by using the

red/green image ratios and plotting them against the titrated and measured O_2 levels. Furthermore, a macro (programmed for ImageJ) was used to apply the calibration to the soil experiment images for O_2. Therefore, the red/green ratios of the calibration were normalized (ratio at zero Oxygen divided by the ratio) and fitted using a modified Stern-Volmer fit as shown in equation 1 (see Figure S2 for the data). This fit gives the parameters (*Ksv* and *f*) needed for the macro in addition to R_0. This approach is well established and further information on O_2 imaging can be found within literature [93,97,113].

$$\frac{R_0}{R} = \frac{1}{\frac{f_1}{1+K_{SV}^1*[O_2]}+(1-f_1)} \qquad (equation\ 1)$$

For the pH optode calibration a pH sensor foil was placed inside a small glass tank (350 mL) and filled with a 0.1 M phosphate buffer solution (pH 7; ionic strength = 0.377 M adjusted with NaCl). Different calibration points (pH 2, 5, 5.5, 6, 6.5, 7, 7.5, 8, 8.5, 9, 12) were adjusted by using a 1 M NaOH solution and 1 M HCl solution. A pH meter (PHM210 Meterlab, Radiometer Analytical, Lyon, France) facilitated the monitoring of the pH throughout the calibration. Images were taken every five minutes for a total of 15 minutes at each pH to ensure that equilibrium was achieved. Here, ratio images were generated dividing the blue channel by the red channel and the gathered ratios were opposed to the measured pH points to receive a calibration curve. A different macro was created to ensure a more precise use of the calibration curve for the target experimental images received from the soil sandwich set up. For this a Sigmoidal fit was utilized again generating parameters (A, B, x_0 and d_x) needed to put into the macro (see data and fit in Figure S2) and by adjusting the formula pursuant to the already mentioned study [93].

12.4. Soil sandwiches

The soil sandwiches were assembled according to the rhizo-sandwiches in an earlier study [96] with a few alterations. A total of four rows of microscope slides (Hounisen, Denmark) were glued to three of the edges of a glass plate (29 x 17 cm^2) with an UV curing glue (Loctite 3494, Henkel-Adhesives). Two ammonia optodes were taped on the inside of the glass plate. Soil (m= 96.95 g) was spread out, distributed evenly and covered two thirds of the optodes. A second glass plate equipped with one pH and one O_2 optode next to each other was used to close the sandwich, sealing it with modeling clay and isolation tape (Super 33+ Vinyl electrical tape, Scotch ^{TM} Brand, USA). The sandwich then had an inner thickness of 4 mm, which left just enough space to apply the pig manure using a volumetric pipette.

12.5. Biological application

Soil (loamy sand; 87% sand, 10% slit, 3% clay with a soil pH of around 6) was collected at a garden close to Aarhus (Denmark). The soil was sieved (1.78 mm^2 mesh size) prior to analysis and stored dry and in darkness. The soil had a water content of 15% when filled into the soil sandwich. The pig manure used in this study was generously provided and had the following characteristics: total-N: 3.11 kg/ton (NH_4-N: 2.72 kg/ton; organic-N 0.38 kg/ton), phosphorus: 0.13 kg/ton and a dry matter content of 1.3%. Soil was filled into the soil sandwich as described above.

At first, images of the optodes with dry soil were taken. After that, 10 mL of water were applied evenly, and two images were acquired in an interval of five minutes. Thereupon, 7 mL of pig manure were applied again with an attempt of even distribution and images taken every five minutes for a total of 60 minutes. After every manure addition the soil sandwich was sealed with PARAFILM®. Another 10 mL of manure were added with recording times of every 5 minutes for 35 minutes in the beginning, then migrating to one image per hour for 14 hours to in the end changing it to an image taken every two hours, which mounts up to 24 hours. The subsequent additions increased the soil water content from initial 15% to final of approximately 43%.

Acknowledgement

This study was supported by research grants from the Poul Due Jensen Foundation (KK) and a Sapere Aude grant from the Independent Research Fund Denmark (IRFD): DFF-8048-00057B (KK). An ERASMUS+ internship grant enabled TM to conduct this study at Aarhus University.

The authors want to thank Lars Borregaard Pedersen, Mette L. G. Nikolajsen and Ronny Mario Baaske for excellent technical support. Fabian Steininger and Dr. Silvia E. Zieger are thanked for constructive discussions and support. Jesper Nørlem Kamp (Aarhus University) is thanked for providing access to the manure used in this study. Vincent Valentin Scholz is acknowledged for helping with the initial preparation of the soil sandwich. The authors wish to state their gratitude toPhD Sasha D. Hafner (Aarhus University) and Prof. Andreas Schramm (Aarhus University) for valuable feedback on the manuscript and to Prof. Sergey Borisov (Graz University of Technology, Austria) for constructive feedback and for supporting the mobility of TM.

Author Contributions

KK and TM designed the research. TM conducted the experiments. KK assisted TM with data analyzes. KK wrote the manuscript with editorial help from TM. All authors have given approval to the final version of the manuscript.

Conflict of Interest Disclosure

The authors have no conflict of interest related to the presented work. All research was performed free of any commercial interest.

13. Supporting Information

Supporting figures:

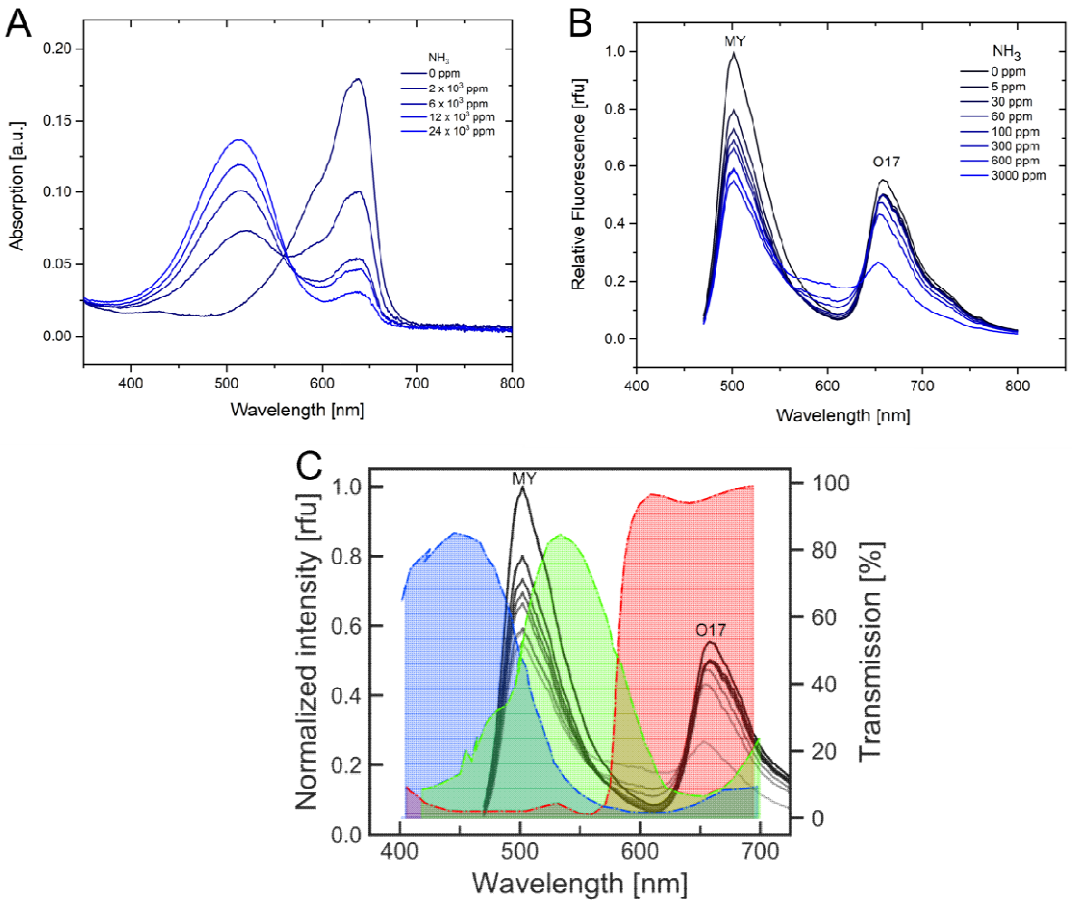

S1: Spectral change of the NH_3 optode when exposed to the analyte. A: absorption spectra of an optode only consisting of oxazin 170 perchlorate (O17) exposed to different levels of NH_3. Note that in this optode a transparent Teflon membrane (Teflon AF solution from Sigma-Aldrich was coated on top of the sensing layer) was used instead of the previously used hydrophobic fluoropore membrane. As this membrane showed an impact on the dynamic properties of the sensor the used concentrations of NH_3 are substantially higher. B: changes in the emission spectra of the NH_3 optode, here consisting of the indicator dye (O17) and the reference dye (MY), exposed to the analyte at different concentrations. C: Same emission spectra as in B with the spectral properties of the respective color channels of the camera in the background. While in fact the peak emission of both dyes (indicator and reference) decreases the increase observed at around 600 nm leads to the measured overall increase in the ratio of the red/green channel seen in the calibration curve in Figure 1. At the same time, this explains why the calibration curve is linear at first and then flattens.

Note: Absorption Spectra of the Oxazine perchlorate 170 dye (A), were measured on a

Thermo Scientific™Genesys 10S UV-Vis Spectrometer from Fisher Scientific GmbH (Schwerte, Germany) in a 10 mm precision. The optode was cut to fit the size of the inside of the cuvette and placed to face the light source. Baseline correction of the spectra were acquired using a 0.5 M sodium hydroxide solution and a small piece of an uncoated PET foil. Emission spectra of the optodes (B) were measured on a CLARIOstar Plus microplatereader from BMG Labtech (Ortenberg, Germany) in tissue culture test plates with 12 wells by TPP Techno Plastic Products AG (Trasadingen, Schwitzerland). The respective optodes were cut to fit the size of the wells, with the proton impermeable PTFE Fluoropore membrane facing upwards and were fixated with PDMS on the edge.

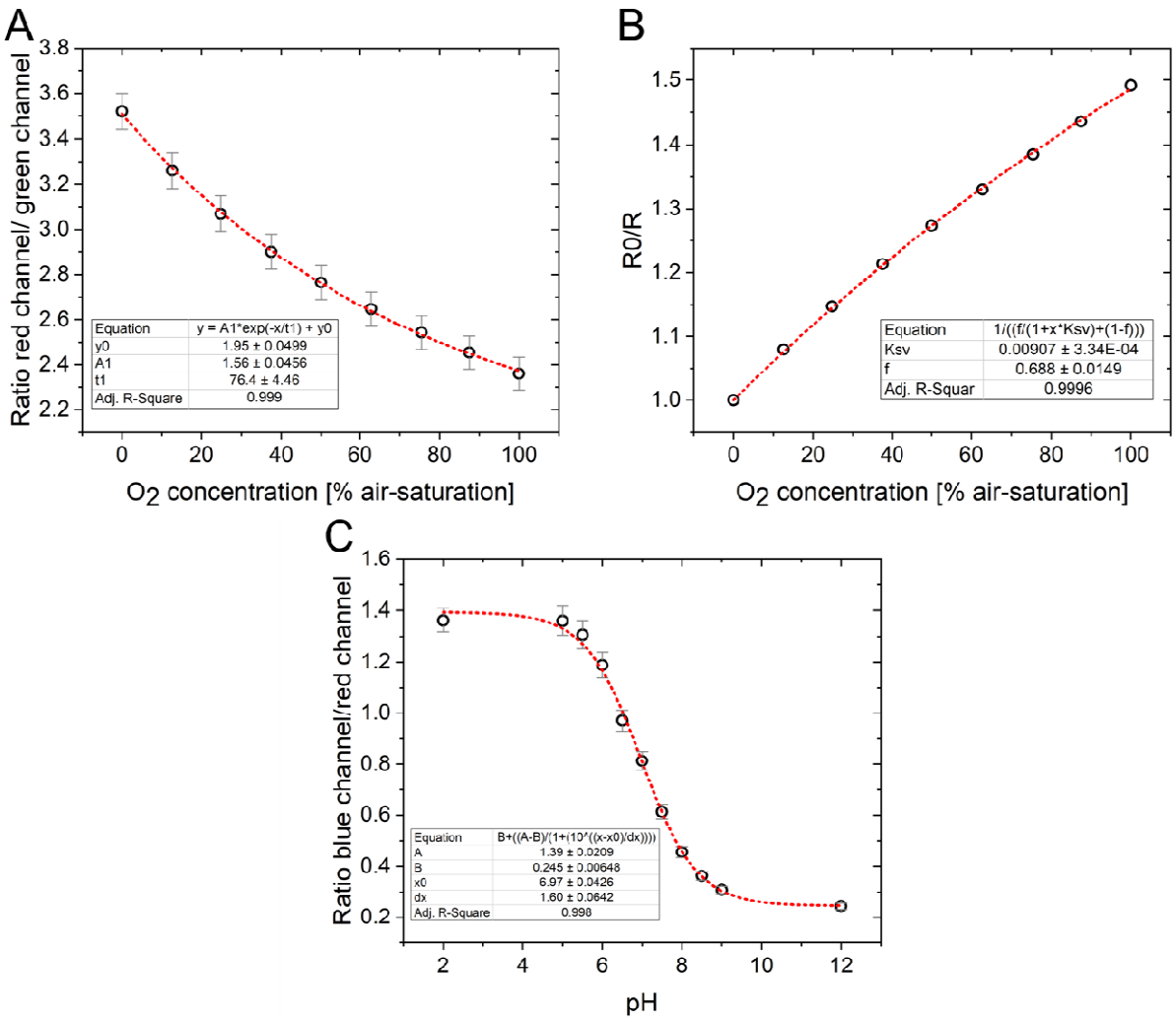

S2: Calibration plots of the O_2 and pH optode. A: the values of the red/green ratios plotted against the O_2 levels fitted with an exponential decay function, $R^2 > 0.999$. B: the normalized ratio (R_0/R) plotted against the O_2 levels fitted with a modified Stern-Volmer equation (equation 1), $R^2 > 0.999$).C: the blue/red channel ratios versus the pH values fitted with a Sigmoidal function, $R^2 > 0.998$.

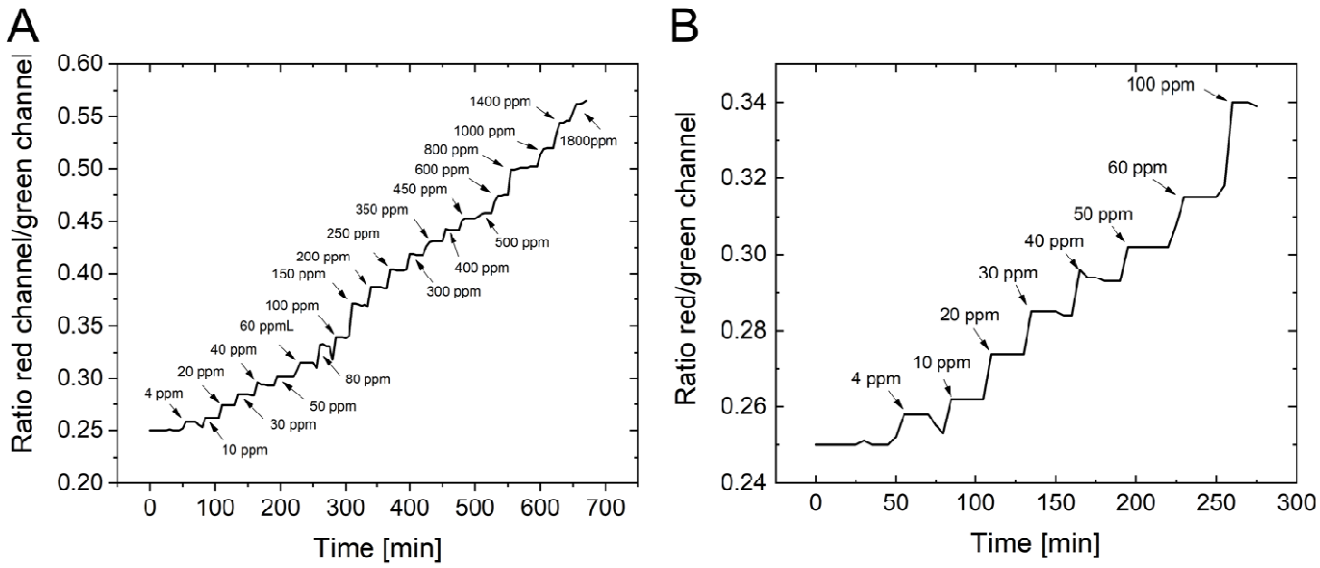

S3: Response curves of an NH_3 optode at various ammonia concentrations. A: response curve at the ammonia concentrations of the calibration points. B: close up of ammonia concentration from 0 to 100 ppm.

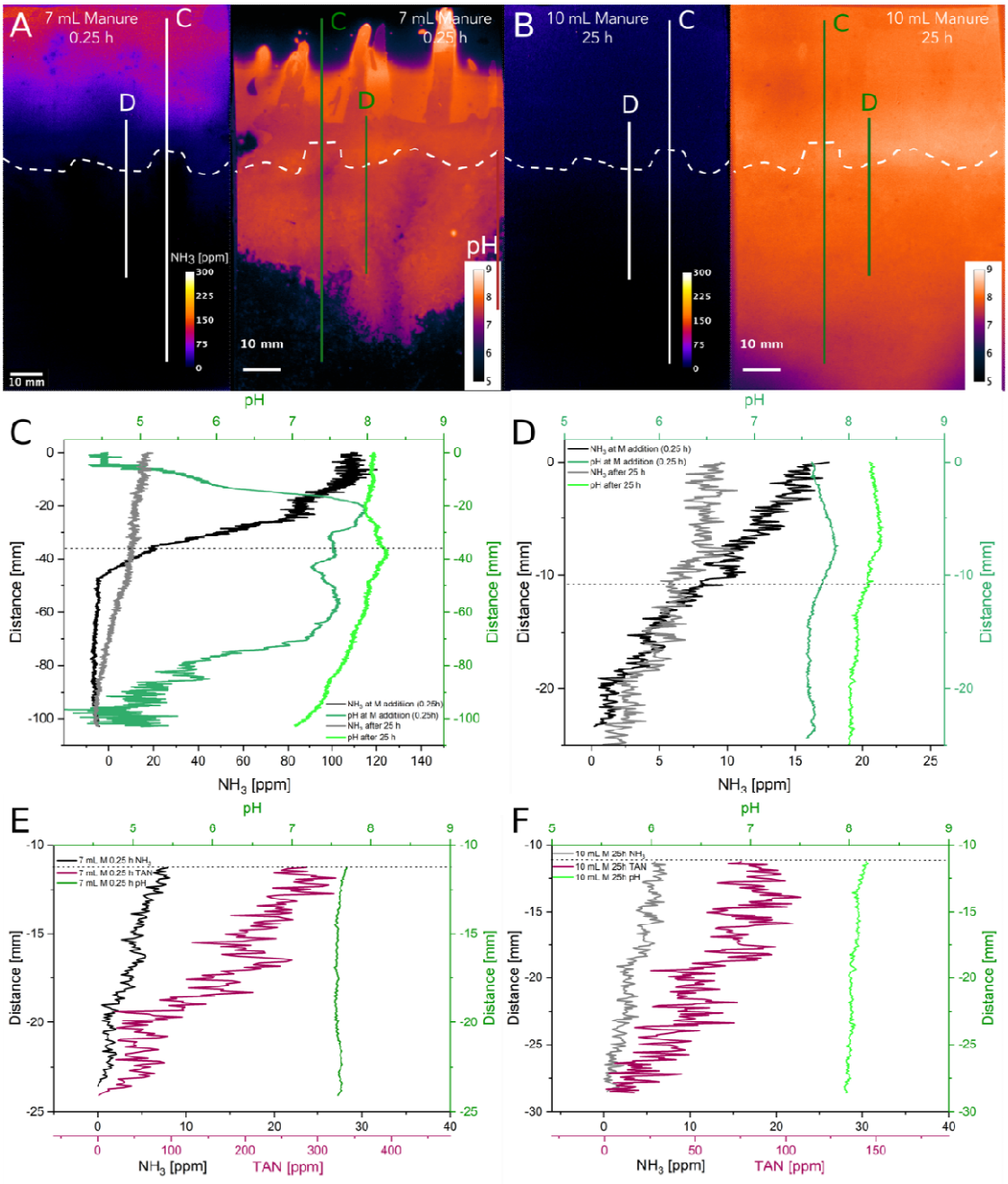

S4: A and B: False color images of NH_3 concentrationand pH at different time points. Panel A shows the images directly after manure addition and B at the end of the experiment (25 hours). C: pH and NH_3 concentration profiles extracted at the two depicted time points along the longer line shown in panels A and B. D: pH and NH_3 concentration profiles extracted at two depicted time points along the shorter line shown in panels A and B. E+F: Calculated TAN profiles using the respective pH and NH3 profiles in combination for the respective time points (E directly after manure addition and F after 25 hours).

V. Conclusion and Outlook

In this thesis a novel ammonia optode was developed, characterized and applied in order to monitor the NH_3 emission from a soil surface upon application of manure. In addition, two other parameters, pH and O_2, which have an impact on these emissions and the microenvironment within the soil were visualized as well. All this was done utilizing optical sensors and a ratiometric imaging approach. The measurement set-up for that was kept fairly simple as standard single-lens cameras, optical filters, LED lights as excitation light sources and trigger boxes were sufficient to conduct the calibrations and the subsequent measurements. Moreover, the newly developed NH_3 optode does only comprise materials that are commercially available, through which laborious synthesis of an indicator has been ruled out.

The underlying principle of this optode is based on the deprotonation of a pH sensitive indicator dye (Oxazine 170 perchlorate), which is immersed in a polymer matrix, hydrogel D4, together with a reference dye (Macrolexyellow). The use of a proton impermeable membrane, PTFE Fluoropore membrane, protecting the sensing chemistry enables ammonia diffusion without interferences of pH or ions. Ammonia induces the deprotonation of the pH fluorophore that then experiences a shift in its absorption and emission bands, which provides the signal that can be translated into the desired information. The optode shows fast response times, full reversibility, a detection limit of 2.11 ppm and a broad dynamic range up to 1800 ppm.

The concentration range in which the sensor foil can operate in enables to receive a better understanding of biological systems with NH_3 concentrations of higher levels. As most of the ammonia optodes developed so far work in lower concentration levels, mainly within the ppb range, these optodes are more commonly found in literature. Hence, this thesis started with manufacturing some of the low concentration ammonia optical sensors allowing to test various polymer materials and proton impermeable layers. These investigations and the demand for a NH_3 optode able to measure within the ppm range led to the novel, already presented optode.

The application of this new optode within various set ups shows that it is possible to conduct measurements in waterlogged systems, such as sediments, as well as in soil. Also, the offered

combination approach of NH_3, pH and O_2 optodes facilitates analysis of these parameters in real time with a sub-mm (< 100 µm) resolution. This simultaneous and two-dimensional monitoring of the three parameters not only enables to gather more information about the biological and chemical processes linked to ammonia within the microenvironment but also allows to improve the gathered information through line profiles and rate images. This supplements currently performed gas phase and microsensor measurements help to gain a better understanding of the local microenvironment and its role in NH_3 emission.

However, there still is room for improvement in both, the sensor design and the application of such. For instance, the selectivity is one of the desired optimisations. So far cross-sensitivity towards trimethylamine, one of many volatile amines able to also diffuse through the gas permeable membrane, was obtained. This could be diminished by incorporating ionophores, which would then bind the resulting ammonium ion upon deprotonation of the pH indicator. Other alterations of desire concerning the sensor design would be to implement pH sensitive dyes with lower pK_a values as this value is decisive for the sensor sensitivity. Hence, pH sensitive fluorophores with values between pK_a 4 to ~7 could pave the way for ammonia optodes able to measure in a concentration range from high ppb to low or medium ppm, which is of great interest for further chemical and biological process investigations.

While in this thesis combined optode imaging already took place, the addition of optodes sensitive towards other parameters could help to expand the understanding of the complexity of microenvironments. Furthermore, better planned and more sophisticated set ups and optode positionings will lead to an increased exploitation of the potential of this novel ammonia optode, especially in ammonia emission studies from and within soils. One example for future studies is to monitor the efficiency of nitrification inhibitors to reduce the fertilizer loss of agricultural fields.

VI. References

1. Madigan, M. T., Martinko, J. M., Bender, K. S., Buckley, D. H. & Stahl, D. A. *Brock Biology of Microorganisms*. (Pearson, 2015).
2. Timmer, B., Olthuis, W. & Berg, A. van den. Ammonia sensors and their applications—a review. *Sensors Actuators B Chem.***107**, 666–677 (2005).
3. Van Vuuren, D. P., Bouwman, L. F., Smith, S. J. & Dentener, F. Global projections for anthropogenic reactive nitrogen emissions to the atmosphere: An assessment of scenarios in the scientific literature. *Current Opinion in Environmental Sustainability***3**, 359–369 (2011).
4. Hafner, S. D., Montes, F. & Alan Rotz, C. The role of carbon dioxide in emission of ammonia from manure. *Atmos. Environ.***66**, 63–71 (2013).
5. Kuypers, M. M. M., Marchant, H. K. & Kartal, B. The microbial nitrogen-cycling network. *Nat. Rev. Microbiol.***16**, 263–276 (2018).
6. Randall, D. . & Tsui, T. K. . Ammonia toxicity in fish. *Mar. Pollut. Bull.***45**, 17–23 (2002).
7. Giannadaki, D., Giannakis, E., Pozzer, A. & Lelieveld, J. Estimating health and economic benefits of reductions in air pollution from agriculture. *Sci. Total Environ.***622**–**623**, 1304–1316 (2018).
8. Baek, B. H., Aneja, V. P. & Tong, Q. Chemical coupling between ammonia, acid gases, and fine particles. *Environ. Pollut.***129**, 89–98 (2004).
9. Mount, G. H. *et al.* Measurement of atmospheric ammonia at a dairy using differential optical absorption spectroscopy in the mid-ultraviolet. *Atmos. Environ.***36**, 1799–1810 (2002).
10. Erisman, J. W. *et al.* Instrument development and application in studies and monitoring of ambient ammonia. *Atmos. Environ.***35**, 1913–1922 (2001).
11. Rigoni, F. *et al.* Environmental monitoring of low-ppb ammonia concentrations based on single-wall carbon nanotube chemiresistor gas sensors: Detection limits, response dynamics, and moisture effects. *Procedia Eng.***87**, 716–719 (2014).
12. Moos, R. *et al.* Selective ammonia exhaust gas sensor for automotive applications. *Sensors Actuators, B Chem.***83**, 181–189 (2002).
13. Bayrakli, I., Turkmen, A., Akman, H., Sezer, M. T. & Kutluhan, S. Applications of external cavity diode laser-based technique to noninvasive clinical diagnosis using expired breath ammonia analysis: chronic kidney disease, epilepsy. *J. Biomed. Opt.***21**, 087004 (2016).
14. Smith, A. F. *et al.* Bioelectronic protein nanowire sensors for ammonia detection. *Nano Res.***13**, 1479–1484 (2020).
15. Davies, S., Spanel, P. & Smith, D. Quantitative analysis of ammonia on the breath of patients in end-stage renal failure. *Kidney Int.***52**, 223–228 (1997).

16. Close, L. G., Catlin, F. I. & Cohn, A. M. Acute and Chronic Effects of Ammonia Burns of the Respiratory Tract. *Arch. Otolaryngol.***106**, 151–158 (1980).

17. Li, C. *et al.* Planar optode: A two-dimensional imaging technique for studying spatial-temporal dynamics of solutes in sediment and soil. *Earth-Science Rev.***197**, 102916 (2019).

18. Santner, J., Larsen, M., Kreuzeder, A. & Glud, R. N. Two decades of chemical imaging of solutes in sediments and soils - a review. *Anal. Chim. Acta***878**, 9–42 (2015).

19. Peter Revsbech, N. Analysis of Microbial Communities with Electrochemical Microsensors and Microscale Biosensors. in *Methods in enzymology***397**, 147–166 (2005).

20. Bottrell, S. H. *et al.* Insights into redox cycling of sulfur and iron in peatlands using high-resolution diffusive equilibrium thin film (DET) gel probe sampling. *Chem. Geol.***244**, 409–420 (2007).

21. Robertson, D., Welsh, D. T. & Teasdale, P. R. Investigating biogenic heterogeneity in coastal sediments with two-dimensional measurements of iron(II) and sulfide. *Environ. Chem.***6**, 60–69 (2009).

22. Sochaczewski, Ł., Davison, W., Zhang, H. & Tych, W. Understanding small-scale features in DGT measurements in sediments. *Environ. Chem.***6**, 477–485 (2009).

23. Zhu, K., Bruun, S., Larsen, M., Glud, R. N. & Jensen, L. S. Heterogeneity of O2 dynamics in soil amended with animal manure and implications for greenhouse gas emissions. *Soil Biol. Biochem.***84**, 96–106 (2015).

24. Brodersen, K. E. *et al.* Seagrass-Mediated Phosphorus and Iron Solubilization in Tropical Sediments. *Environ. Sci. Technol.***51**, 14155–14163 (2017).

25. Yin, H., Zhu, Q. & Aller, R. C. An irreversible planar optical sensor for multi-dimensional measurements of sedimentary H2S. *Mar. Chem.***195**, 143–152 (2017).

26. Delin, S. & Strömberg, N. Imaging-optode measurements of ammonium distribution in soil after different manure amendments. *Eur. J. Soil Sci.***62**, 295–304 (2011).

27. Meier, R. J. *et al.* Simultaneous photographing of oxygen and pH in vivo using sensor films. *Angew. Chemie - Int. Ed.***50**, 10893–10896 (2011).

28. Williams, P. N. *et al.* Localized flux maxima of arsenic, lead, and iron around root apices in flooded lowland rice. *Environ. Sci. Technol.***48**, 8498–8506 (2014).

29. Stahl, H. *et al.* A combined sensor for simultaneous high resolution 2-D imaging of oxygen and trace metals fluxes. *Limnol. Oceanogr. Methods***10**, 389–401 (2012).

30. Wolfbeis, O. S. Chemical sensors - survey and trends. *Fresenius. J. Anal. Chem.***337**, 522–527 (1990).

31. Gründler, P. *Chemische Sensoren - Eine Einführung für Naturwissenschaftler und Ingenieure*. *Springer Verlag* (Springer Verlag, 2004).

32. Banica, F.-G. *Chemical Sensors and Biosensors*. *Chemical Sensors and Biosensors* (John Wiley & Sons, Ltd, 2012). doi:10.1002/9780470511305

33. McDonagh, C., Burke, C. S. & MacCraith, B. D. Optical chemical sensors. *Chem. Rev.***108**, 400–422 (2008).

34. Hulanicki, A., Glab, S. & Ingman, F. Chemical sensors definitions and classification. *Pure Appl. Chem.***63**, 1247–1250 (1991).

35. Zakrzewska, K. Mixed oxides as gas sensors. *Thin Solid Films***391**, 229–238 (2001).

36. Xu, C. N., Miura, N., Ishida, Y., Matsuda, K. & Yamazoe, N. Selective detection of NH3 over NO in combustion exhausts by using Au and MoO3 doubly promoted WO3 element. *Sensors Actuators, B Chem.***65**, 163–165 (2000).

37. Tomchenko, A. A., Harmer, G. P., Marquis, B. T. & Allen, J. W. Semiconducting metal oxide sensor array for the selective detection of combustion gases. *Sensors Actuators, B Chem.***93**, 126–134 (2003).

38. Jerger, A., Kohler, H., Becker, F., Keller, H. B. & Seifert, R. New applications of tin oxide gas sensors: II. Intelligent sensor system for reliable monitoring of ammonia leakages. *Sensors Actuators, B Chem.***81**, 301–307 (2002).

39. Lundström, I., Spetz, A., Winquist, F., Ackelid, U. & Sundgren, H. Catalytic metals and field-effect devices-a useful combination. *Sensors Actuators B. Chem.***1**, 15–20 (1990).

40. Meyerhoff, M. E. *et al.* Polymer-Membrane Electrode-Based Potentiometric Sensing of Ammonia and Carbon Dioxide in Physiological Fluids. *Clin. Chem.***28**, 1973–1978 (1982).

41. Bühlmann, P., Pretsch, E. & Bakker, E. Carrier-based ion-selective electrodes and bulk optodes. 2. Ionophores for potentiometric and optical sensors. *Chem. Rev.***98**, 1593–1687 (1998).

42. Crespo, G. A. Recent Advances in Ion-selective membrane electrodes for in situ environmental water analysis. *Electrochim. Acta***245**, 1023–1034 (2017).

43. Lähdesmäki, I., Lewenstam, A. & Ivaska, A. A polypyrrole-based amperometric ammonia sensor. *Talanta***43**, 125–134 (1996).

44. Lähdesmäki, I., Kubiak, W. W., Lewenstam, A. & Ivaska, A. Interferences in a polypyrrole-based amperometric ammonia sensor. *Talanta***52**, 269–275 (2000).

45. Kukla, A. L., Shirshov, Y. M. & Piletsky, S. A. Ammonia sensors based on sensitive polyaniline films. *Sensors Actuators, B Chem.***37**, 135–140 (1996).

46. Krug, F. J., Růžička, J. & Hansen, E. H. Determination of ammonia in low concentrations with Nessler's reagent by flow injection analysis. *Analyst***104**, 47–54 (1979).

47. Searle, P. L. The berthelot or indophenol reaction and its use in the analytical chemistry of nitrogen: A review. *Analyst***109**, 549–568 (1984).

48. Daridon, A. *et al.* Chemical sensing using an integrated microfluidic system based on the Berthelot reaction. *Sensors Actuators, B Chem.***76**, 235–243 (2001).

49. Valeur, B. *Molecular Fluorescence*. **1**, (Wiley-VCH Verlag GmbH, 2001).

50. Valeur, B. & Brochon, J.-C. *New trends in fluorescence spectroscopy : applications to chemical and life science*. *Springer series on fluorescence* (2001).

51. Borisov, S. M., Würth, C., Resch-Genger, U. & Klimant, I. New life of ancient pigments: Application in high-performance optical sensing materials. *Anal. Chem.***85**,

9371–9377 (2013).

52. Wolfbeis, O. S. Materials for fluorescence-based optical chemical sensors. *J. Mater. Chem.***15**, 2657–2669 (2005).

53. Rhines, T. D. & Arnold, M. A. Determination of ammonia in untreated serum with a fiber-optic ammonia gas ensor. *Anal. Chim. Acta***231**, 231–235 (1990).

54. Strobl, M., Walcher, A., Mayr, T., Klimant, I. & Borisov, S. M. Trace Ammonia Sensors Based on Fluorescent Near-Infrared-Emitting aza-BODIPY Dyes. *Anal. Chem.***89**, 2859–2865 (2017).

55. Duong, H. D. & Rhee, J. Il. A ratiometric fluorescence sensor for the detection of ammonia in water. *Sensors Actuators, B Chem.***190**, 768–774 (2014).

56. Waich, K., Borisov, S., Mayr, T. & Klimant, I. Dual lifetime referenced trace ammonia sensors. *Sensors Actuators, B Chem.***139**, 132–138 (2009).

57. Waich, K., Mayr, T. & Klimant, I. Microsensors for detection of ammonia at ppb-concentration levels. *Meas. Sci. Technol.***18**, 3195–3201 (2007).

58. West, S. J., Ozawa, S., Seiler, K., Tan, S. S. S. & Simon, W. Selective Ionophore-Based Optical Sensors for Ammonia Measurement in Air. *Anal. Chem.***64**, 533–540 (1992).

59. Müller, B. J., Steinmann, N., Borisov, S. M. & Klimant, I. Ammonia sensing with fluoroionophores – A promising way to minimize interferences caused by volatile amines. *Sensors Actuators, B Chem.***255**, 1897–1901 (2018).

60. Lakowicz, J. R. *Principles of fluorescence spectroscopy, 3rd Edition, Joseph R. Lakowicz, editor*. *Principles of fluorescence spectroscopy, Springer, New York, USA, 3rd edn, 2006.* (2006). doi:10.1007/978-0-387-46312-4

61. Waich, K., Mayr, T. & Klimant, I. Microsensors for detection of ammonia at ppb-concentration levels. *Meas. Sci. Technol.***18**, 3195–3201 (2007).

62. Abel, T., Ungerböck, B., Klimant, I. & Mayr, T. Fast responsive, optical trace level ammonia sensor for environmental monitoring. *Chem. Cent. J.***6**, 1–9 (2012).

63. Bolałek, J. & Graca, B. Ammonia nitrogen at the water-sediment interface in Puck Bay (Baltic Sea). *Estuar. Coast. Shelf Sci.***43**, 767–779 (1996).

64. Zhu, Q. & Aller, R. C. Planar fluorescence sensors for two-dimensional measurements of H2S distributions and dynamics in sedimentary deposits. *Mar. Chem.***157**, 49–58 (2013).

65. Dähnke, K., Moneta, A., Veuger, B., Soetaert, K. & Middelburg, J. J. Balance of assimilative and dissimilative nitrogen processes in a diatom-rich tidal flat sediment. *Biogeosciences***9**, 4059–4070 (2012).

66. Brunet, R. C. & Garcia-Gil, L. J. Sulfide-induced dissimilatory nitrate reduction to ammonia in anaerobic freshwater sediments. *FEMS Microbiol. Ecol.***21**, 131–138 (1996).

67. Koike, I. & Hattori, A. Denitrification and ammonia formation in anaerobic coastal sediments. *Appl. Environ. Microbiol.***35**, 278–282 (1978).

68. Behera, S. N., Sharma, M., Aneja, V. P. & Balasubramanian, R. Ammonia in the

atmosphere: a review on emission sources, atmospheric chemistry and deposition on terrestrial bodies. *Environ. Sci. Pollut. Res.***20**, 8092–8131 (2013).

69. Kühl, M. *et al.* Substantial near-infrared radiation-driven photosynthesis of chlorophyll f-containing cyanobacteria in a natural habitat. *Elife***9**, 1–15 (2020).

70. Aneja, V. P., Schlesinger, W. H. & Erisman, J. W. Farming pollution. *Nature Geoscience***1**, 409–411 (2008).

71. Gruber, N. & Galloway, J. N. An Earth-system perspective of the global nitrogen cycle. *Nature***451**, 293–296 (2008).

72. Saggar, S., Bolan, N. S., Bhandral, R., Hedley, C. B. & Luo, J. A review of emissions of methane, ammonia, and nitrous oxide from animal excreta deposition and farm effluent application in grazed pastures. *New Zeal. J. Agric. Res.***47**, 513–544 (2004).

73. Webb, J., Pain, B., Bittman, S. & Morgan, J. The impacts of manure application methods on emissions of ammonia, nitrous oxide and on crop response-A review. *Agriculture, Ecosystems and Environment***137**, 39–46 (2010).

74. Bouwman, A. F., Boumans, L. J. M. & Batjes, N. H. Estimation of global NH 3 volatilization loss from synthetic fertilizers and animal manure applied to arable lands and grasslands . *Global Biogeochem. Cycles***16**, 8-1-8–14 (2002).

75. Galloway, J. N. *et al.* Transformation of the nitrogen cycle: Recent trends, questions, and potential solutions. *Science***320**, 889–892 (2008).

76. Sommer, S. G. *et al.* Processes controlling ammonia emission from livestock slurry in the field. *Eur. J. Agron.***19**, 465–486 (2003).

77. Kim, M. & Or, D. Microscale pH variations during drying of soils and desert biocrusts affect HONO and NH3 emissions. *Nat. Commun.***10**, 1–12 (2019).

78. Hafner, S. D., Montes, F. & Alan Rotz, C. The role of carbon dioxide in emission of ammonia from manure. *Atmos. Environ.***66**, 63–71 (2013).

79. Stein, L. Y. & Klotz, M. G. The nitrogen cycle. *Current Biology* (2016). doi:10.1016/j.cub.2015.12.021

80. Hafner, S. D., Meisinger, J. J., Mulbry, W. & Ingram, S. K. A pH-based method for measuring gaseous ammonia. *Nutr. Cycl. Agroecosystems***92**, 195–205 (2012).

81. Schäferling, M. The art of fluorescence imaging with chemical sensors. *Angew. Chemie - Int. Ed.***51**, 3532–3554 (2012).

82. Glud, R., Ramsing, N., Gundersen, J. & Klimant, I. Planar optrodes:a new tool for fine scale measurements of two-dimensional O2 distribution in benthic communities. *Mar. Ecol. Prog. Ser.***140**, 217–226 (1996).

83. Zhu, K., Bruun, S., Larsen, M., Glud, R. N. & Jensen, L. S. Spatial Oxygen Distribution and Nitrous Oxide Emissions from Soil after Manure Application: A Novel Approach Using Planar Optodes. *J. Environ. Qual.***43**, 1809–1812 (2014).

84. Brodersen, K. E. *et al.* Seagrass-Mediated Phosphorus and Iron Solubilization in Tropical Sediments. *Environ. Sci. Technol.***51**, 14155–14163 (2017).

85. Kühl, M. & Polerecky, L. Functional and structural imaging of phototrophic microbial communities and symbioses. *Aquat. Microb. Ecol.***53**, 99–118 (2008).

86. Glud, R. N. Oxygen dynamics of marine sediments. *Mar. Biol. Res.***4**, 243–289 (2008).

87. Precht, E., Franke, U., Polerecky, L. & Huettel, M. Oxygen dynamics in permeable sediments with wave-driven pore water exchange. *Limnol. Ocean.***49**, 693–705 (2004).

88. Strömberg, N. & Hulth, S. An ammonium selective fluorosensor based on the principles of coextraction. *Anal. Chim. Acta***443**, 215–225 (2001).

89. Koop-Jakobsen, K., Mueller, P., Meier, R. J., Liebsch, G. & Jensen, K. Plant-sediment interactions in salt marshes – An optode imaging study of O2, pH, and CO2 gradients in the rhizosphere. *Front. Plant Sci.***9**, 541 (2018).

90. Lenzewski, N. *et al.* Dynamics of oxygen and carbon dioxide in rhizospheres of Lobelia dortmanna – a planar optode study of belowground gas exchange between plants and sediment. *New Phytol.***218**, 131–141 (2018).

91. Schutting, S., Klimant, I., de Beer, D. & Borisov, S. M. New highly fluorescent pH indicator for ratiometric RGB imaging of pCO 2. *Methods Appl. Fluoresc.***2**, 024001 (2014).

92. Abel, T., Ungerböck, B., Klimant, I. & Mayr, T. Fast responsive, optical trace level ammonia sensor for environmental monitoring. *Chem. Cent. J.***6**, 124 (2012).

93. Larsen, M., Borisov, S. M., Grunwald, B., Klimant, I. & Glud, R. N. A simple and inexpensive high resolution color ratiometric planar optode imaging approach: Application to oxygen and pH sensing. *Limnol. Oceanogr. Methods***9**, 348–360 (2011).

94. Koren, K., Jakobsen, S. L. & Kühl, M. In-vivo imaging of O2 dynamics on coral surfaces spray-painted with sensor nanoparticles. *Sensors Actuators B Chem.* 19–21 (2016). doi:10.1016/j.snb.2016.05.147

95. Nielsen, S. D. *et al.* Optical sensing of ph and o2 in the evaluation of bioactive self-healing cement. *ACS Omega***4**, 20237–20243 (2019).

96. Scholz, V. V, Müller, H., Koren, K., Nielsen, L. P. & Meckenstock, R. U. The rhizosphere of aquatic plants is a habitat for cable bacteria. *FEMS Microbiol. Ecol.***95**, 1–9 (2019).

97. Koren, K. *et al.* Luminescence Lifetime Imaging of Chemical Sensors - A Comparison between Time-Domain and Frequency-Domain Based Camera Systems. *Anal. Chem.***91**, 3233–3238 (2019).

98. Sommer, S. G. & Olesen, J. E. Modelling ammonia volatilization from animal slurry applied with trail hoses to cereals. *Atmos. Environ.***34**, 2361–2372 (2000).

99. Hafner, S. D. *et al.* A flexible semi-empirical model for estimating ammonia volatilization from field-applied slurry. *Atmos. Environ.***199**, 474–484 (2019).

100. Ni, J. Mechanistic models of ammonia release from liquid manure: A review. *J. Agric. Eng. Res.***72**, 1–17 (1999).

101. Bussink, D. W., Huijsmans, J. F. & Ketelaars, J. J. Ammonia volatilization from nitric-acid-treated cattle slurry surface applied to grassland. *Netherlands Journal of Agricultural Science***42**, 293–309 (1994).

102. Chaoui, H., Montes, F., Rotz, C. A. & Richard, T. L. Volatile ammonia fraction and flux from thin layers of buffered ammonium solution and dairy cattle manure. *Trans. ASABE***52**, 1695–1706 (2009).

103. Morvan, T., Leterme, P., Arsene, G. G. & Mary, B. Nitrogen transformations after the spreading of pig slurry on bare soil and ryegrass using 15N-labelled ammonium. in *European Journal of Agronomy* (1997). doi:10.1016/S1161-0301(97)00044-0

104. Sexstone, A. J., Revsbech, N. P., Parkin, T. B. & Tiedje, J. M. Direct Measurement of Oxygen Profiles and Denitrification Rates in Soil Aggregates. *Soil Sci. Soc. Am. J.* (1985). doi:10.2136/sssaj1985.03615995004900030024x

105. Markfoged, R., Nielsen, L. P., Nyord, T., Ottosen, L. D. M. & Revsbech, N. P. Transient N2O accumulation and emission caused by O2 depletion in soil after liquid manure injection. *Eur. J. Soil Sci.* (2011). doi:10.1111/j.1365-2389.2010.01345.x

106. Meyer, R. L., Kjaer, T. & Revsbech, N. P. Nitrification and Denitrification near a Soil-Manure Interface Studied with a Nitrate-Nitrite Biosensor. *Soil Sci. Soc. Am. J.* (2002). doi:10.2136/sssaj2002.4980

107. Schramm, A., De Beer, D., Wagner, M. & Amann, R. Identification and activities in situ of Nitrosospira and Nitrospira spp. as dominant populations in a nitrifying fluidized bed reactor. *Appl. Environ. Microbiol.***64**, 3480–3485 (1998).

108. De Beer, D., Schramm, A., Santegoeds, C. M. & Kuhl, M. A nitrite microsensor for profiling environmental biofilms. *Appl. Environ. Microbiol.***63**, 973–7 (1997).

109. Berg, P., Risgaard-Petersen, N. & Rysgaard, S. Interpretation of measured concentration profiles in sediment pore water. *Limnol. Oceanogr.* (1998). doi:10.4319/lo.1998.43.7.1500

110. Moßhammer, M. *et al.* Design and Application of an Optical Sensor for Simultaneous Imaging of pH and Dissolved O2 with Low Cross-Talk. *ACS Sensors***1**, 681–687 (2016).

111. Glud, R. N. *et al.* Distribution of oxygen in surface sediments from central Sagami Bay, Japan: In situ measurements by microelectrodes and planar optodes. *Deep Sea Res. Part I Oceanogr. Res. Pap.***52**, 1974–1987 (2005).

112. Borisov, S. M., Herrod, D. L. & Klimant, I. Fluorescent poly(styrene-block-vinylpyrrolidone) nanobeads for optical sensing of pH. *Sensors Actuators, B Chem.***139**, 52–58 (2009).

113. Wang, X.-D. & Wolfbeis, O. S. Optical methods for sensing and imaging oxygen: materials, spectroscopies and applications. *Chem. Soc. Rev.***43**, 3666–3761 (2014).

VII. Figures

VIII. List of Tables